accepted by ApJS

The Origins of Fluorescent H_2 Emission From T Tauri Stars

Gregory J. Herczeg[1,2], Jeffrey L. Linsky[1], Frederick M. Walter[3], Gösta F. Gahm[4], Christopher M. Johns-Krull[5]

ABSTRACT

We survey fluorescent H_2 emission in *HST*/STIS spectra of the classical T Tauri stars (CTTSs) TW Hya, DF Tau, RU Lupi, T Tau, and DG Tau, and the weak-lined T Tauri star (WTTS) V836 Tau. From each of those sources we detect between 41–209 narrow H_2 emission lines, most of which are pumped by strong Lyα emission. H_2 emission is not detected from the WTTS V410 Tau. The fluorescent H_2 emission appears to be common to circumstellar environments around all CTTSs, but high spectral and spatial resolution STIS observations reveal diverse phenomenon. Blueshifted H_2 emission detected from RU Lupi, T Tau, and DG Tau is consistent with an origin in an outflow. The H_2 emission from TW Hya, DF Tau, and V836 Tau is centered at the radial velocity of the star and is consistent with an origin in a warm disk surface. The H_2 lines from RU Lupi, DF Tau, and T Tau also have excess blueshifted H_2 emission that extends to as much as -100 km s^{-1}. The strength of this blueshifted component from DF Tau and T Tau depends on the upper level of the transition. In all cases, the small aperture and attenuation of H_2 emission by stellar winds restricts the H_2 emission to be formed close to the star. The Lyα and the H_2 emission blueshifted by 15 km s^{-1} relative to RU Lupi are extended to the SW by $\sim 0\farcs07$, although the faster H_2 gas that extends to $\sim$ 100 km s^{-1} is not spatially extended. We also find a small reservoir of H_2 emission from TW Hya and DF Tau consistent with an excitation temperature of $\sim 2.5 \times 10^4$ K.

[1]JILA, University of Colorado and NIST, Boulder, CO 80309-0440; gregoryh@astro.caltech.edu, jlinsky@jila.colorado.edu

[2]Current address Caltech, MC105-24, 1200 E. California Blvd., Pasadena, CA 91125

[3]Department of Physics and Astronomy, Stony Brook University, Stony Brook NY 11794-3800; fwalter@astro.sunysb.edu, msimon@astro.sunysb.edu

[4]Stockholm Observatory, AlbaNova, SE - 106 91 Stockholm, Sweden; gahm@astro.su.se

[5]Department of Physics & Astronomy, Rice University, Houston TX 77005-1892; cmj@rice.edu

Subject headings: accretion, accretion disks — circumstellar matter — line: identification — stars: pre-main sequence — ultraviolet: stars

1. INTRODUCTION

Molecular hydrogen is prevalent in both circumstellar disks and nebulosity around young stars. Observationally discriminating between these two sources of H_2 gas could provide a valuable probe of the physical characteristics and evolution of gas in protoplanetary disks. While other probes of this gas, such as CO and H_2O, have yielded powerful insights into the physical conditions of the disk (e.g., Najita et al. 2003; Brittain et al. 2003; Carr et al. 2004), identifying H_2 emission from the disk has been difficult because IR rovibrational transitions are weak, cold H_2 does not radiate, and diagnostics of H_2 gas in the disk can be contaminated by H_2 in surrounding molecular gas.

A variety of methods involving H_2 emission have been used to probe the circumstellar environments around young stars. H_2 emission was first detected around a young star in IR observations of the 1-0 S(1) line at 2.1218 μm from T Tau by Beckwith et al. (1978). Brown et al. (1981) used *IUE* to detect far-ultraviolet (FUV, $\lambda < 2000$ Å) H_2 emission from T Tau. IR maps of emission in the 1-0 S(1) line and long-slit FUV spectra of H_2 fluorescence reveal that the hot gas extends to 20″ from T Tau and is most likely heated by stellar outflows that shock molecular material near the stars (van Langevelde et al. 1994; Walter et al. 2003; Saucedo et al. 2003).

Valenti et al. (2000) detected Lyman-band H_2 emission in 13 of 32 classical T Tauri stars (CTTSs) observed in low-resolution ($R \equiv \frac{\lambda}{\Delta\lambda} \sim 200$) FUV spectra obtained with *IUE* and suggested that most of the non-detections resulted from inadequate sensitivity. Ardila et al. (2002) found in *HST*/GHRS spectra ($R = 20,000$) of eight CTTSs that the H_2 lines are blueshifted by 0–20 km s^{-1} relative to the radial velocity of the star. They note that systematic uncertainties in the wavelength calibration of GHRS could be as large as 20 km s^{-1} for several of their observations that occurred before COSTAR was installed on *HST*. However, they use the absence of any stars with redshifted H_2 emission to suggest that, for some sources, the blueshift may be significant. This H_2 emission would therefore be produced by stellar outflows. The limited spectral coverage and large ($\sim 2''$) aperture used in the GHRS observations prevented a thorough analysis of the H_2 lines, but Ardila et al. (2002) confirmed that these lines are pumped by Lyα. Fluorescent H_2 emission is also found from the accreting brown dwarf 2MASS J1207334-393254 (Gizis et al. 2005). Bary et al. (2003) detected warm H_2 in emission in the 1-0 S(1) line at 2.1218 μm from three of five CTTSs and one of 11 weak-lined T Tauri star (WTTSs). Based on kinematics, they

suggested that this H_2 emission is produced in the disk within 30 AU of the central star.

Emission in the 2.1218 μm line and the FUV lines is produced by warm (1000–3000 K) gas but not by the cold gas that comprises the bulk of the mass in circumstellar disks. Although H_2 does not radiate at temperatures of $\sim$ 10 K, emission from 50–100 K gas can be detected in pure rotational H_2 lines. Thi et al. (2001) used *ISO* to detect emission in the pure rotational H_2 S(1) and S(0) lines at 17 and 28 μm, respectively. However, Richter et al. (2002), Sheret et al. (2003), and Sako et al. (2005) did not detect emission in the S(2) 12 μm line or the S(1) 17 μm line from many young stars in their ground-based observations that used much smaller apertures than *ISO*. Several of these sources had claimed *ISO* detections of H_2, even though the ground-based non-detections were more sensitive to H_2 in a disk than *ISO*. Midway into the analysis of a larger sample, Richter et al. (2004) reported detections of these lines from several young stars including T Tau. If the *ISO* detections are real, then this H_2 emission is produced in a molecular cloud or an envelope extended beyond the circumstellar disk.

Cold H_2 gas can also be observed in absorption from the ground vibrational level at $\lambda < 1120$ Å. However, the detection of H_2 absorption through a disk requires that the disk be viewed nearly edge-on yet also be optically thin to FUV emission. The prevalence of H_2 absorption toward Herbig AeBe (HAeBe) stars observed with *FUSE* (Roberge et al. 2001; Lecavelier des Etangs et al. 2003; Bouret et al. 2003; Grady et al. 2004; Martin et al. 2004; Martin-Zaïdi et al. 2005) suggests that the H_2 absorption toward these more massive stars occurs in a molecular cloud or remnant molecular envelope rather than in a disk. For example, based on the observed radial velocity Martin-Zaïdi et al. (2005) suggest that the H_2 absorption from HD141569 is related to the nearby dark cloud L134N. Lecavelier des Etangs et al. (2001) and Roberge et al. (2005) use the absence of any H_2 absorption in *FUSE* spectra to place strong upper limits on the molecular gas mass in the evolved, optically thin disks of β Pic and AU Mic, respectively, which are both observed nearly edge-on.

The E140M echelle spectrograph on *HST*/STIS provides high resolution spectra covering a large wavelength range, permiting a detailed analysis of fluorescent H_2 emission in the FUV. In a STIS spectrum of TW Hya, Herczeg et al. (2002) detected over 140 H_2 lines from 19 distinct upper levels, demonstrating that the Lyα emission that pumps this H_2 emission is broad. The characteristics of this emission and the lack of any other molecular gas near TW Hya suggest that the emission was produced at the disk surface, in a thin layer heated to $T \sim 2500$ K (Herczeg et al. 2002, 2004). Although current models of gas in the disk suggest that neither FUV nor X-ray irradiation alone can produce temperatures of 2500 K (Glassgold et al. 2004; Nomura & Millar 2005), together they may sufficiently heat the gas to explain the FUV H_2 emission.

In contrast, long-slit *HST*/STIS spectra of T Tau reveal extended H_2 emission from only two upper levels that are pumped close to Lyα line center (Walter et al. 2003; Saucedo et al. 2003), which is similar to the H_2 fluorescence detected toward HH43 and HH47 (Schwartz 1983; Curiel et al. 1995). The on-source spectrum of T Tau shows a much richer H_2 spectrum, similar to that observed toward TW Hya, than is observed off-source (Walter et al. 2003).

The observed FUV spectra of CTTSs are dominated by strong emission in lines of C IV, Si IV, C II, O I, and many Lyα-pumped H_2 lines. Strong Lyα emission is observed if the small H I column density in our line of sight to the star is small. In addition to these lines, the FUV continuum emission from TW Hya rises at $\lambda < 1650$ Å and is significantly enhanced above the accretion continuum that dominates the NUV emission from CTTSs (Herczeg et al. 2004; Bergin et al. 2004). Bergin et al. (2004) also detected this emission from DM Tau, GM Aur, and LkCa15. They identify this continuum or pseudo-continuum emission as H_2, probably produced by collisions with energetic electrons, as may be seen from HH1/2 (Raymond et al. 1997). Bergin et al. (2004) speculate that this FUV continuum may be related to a deficiency of disk emission at $\lambda < 10$ μm, which is caused by the absence of optically thick micron-sized dust within a few AU of the central star (Calvet et al. 2000; D'Alessio et al. 2005). The ongoing accretion requires that the gas in the disk near the star is still present. The source of this H_2 continuum emission could be the disk surface but this remains to be explored. Herczeg et al. (2005) found that the FUV continuum is weak or not present from RU Lupi, even though RU Lupi is a source of strong fluorescent H_2 emission.

In this paper, we survey and analyze H_2 emission in the FUV spectra of five CTTSs and one weakly accreting WTTS. We report non-detections of H_2 emission in the spectra of two WTTSs, only one of which is marginally significant. In §2 we describe our observations and in §3 we describe our targets. In §4 we present an overview of FUV H_2 emission from each source, including line fluxes and pumping mechanisms. In §5 and §6 we analyze the properties of the H_2 emission, including spectral and spatial emission profiles, and consider the origin of this emission. §7 summarizes our conclusions. The H_2 emission from some sources is consistent with a disk origin, but from other sources is consistent with an outflow origin. High spectral and spatial resolution is essential to understanding H_2 emission from young stars.

2. OBSERVATIONS

We observed the T Tauri stars DF Tau, RU Lupi, T Tau, DG Tau, V836 Tau, V410 Tau, and V819 Tau with *HST*/STIS as part of *HST* program GO-8157. Each FUV observation consists of 4–5 orbits using the E140M echelle spectrograph, spanning 1170–1710 Å, with

the $0\farcs2 \times 0\farcs06$ aperture to isolate on-source emission. Each visit includes a brief long-slit optical spectrum with the G430L grating, spanning 2850–5750 Å. This program also included several long-slit STIS FUV spectra of T Tau, which were analyzed by Walter et al. (2003). We obtained FUV, NUV, and optical STIS spectra of DF Tau as part of *HST* program GTO-7718. This FUV observation of DF Tau used the unsupported $0\farcs5 \times 0\farcs5$ aperture, which reduces the spectral resolution but provides more spatial information. We also include and further analyze the *HST*/STIS FUV spectrum of TW Hya (Herczeg et al. 2002) that was obtained as program GTO-8041. Details of these observations are listed in Table 1.

The stars observed with the $0\farcs2 \times 0\farcs06$ aperture were acquired in a 1s exposure using the F28x50LP optical long pass filter that includes 5500–10000 Å, with a peak sensitivity at 6000 Å. We then peaked up on the sources using an optical white-light mirror and the CCD with the $0\farcs2 \times 0\farcs06$ aperture. For our observations of TW Hya and DF Tau that used the $0\farcs5 \times 0\farcs5$ aperture, the stars were acquired with a narrowband filter ($\sim$ 90 Å) centered on the [O II] 3727 Å line. For both TW Hya and DF Tau, the emission in this bandpass consists of the accretion continuum, high Balmer lines also produced by accreting gas, and weak photospheric emission. No peakup was necessary for these observations.

The pixel size of the FUV MAMA detectors in the E140M echelle mode is $0\farcs036$ ($\sim$ 3.3 km s^{-1}) in the dispersion direction and $0\farcs029$ (1.7 AU at the 57 pc distance of TW Hya and 4 AU at the $\sim$ 140 pc distance of the other stars in our sample) in the cross-dispersion direction.

We reduced the spectra using the *calSTIS* pipeline written in *IDL* (Lindler 1999). We corrected the FUV echelle spectra for scattered light using the *echelle_scat* routine in *IDL*. Several steps described below required manual processing.

The automated pipeline processing did not successfully extract the weak spectrum from our observation of DG Tau. We found the spectrum on the detector by searching for the maximum flux in several H_2 lines in the extraction window. Our extraction window is large enough to include any stellar emission, even if the H_2 emission is extended only to one side of DG Tau.

As the telescope breathes, the thermal focus changes can modulate the count rate when the point-spread function is larger than the aperture. The observations of RU Lupi and T Tau obtained with the $0\farcs2 \times 0\farcs06$ aperture both exhibit increasing count rates during each orbit that correlate with the improving telescope focus. We calibrate the flux of T Tau following the method Herczeg et al. (2005) developed for RU Lup. They noted a similar flux increase in E140M observations of the continuum FUV source V471 Tau (*HST* programs GO-7735 and GO-9283, P.I. F. Walter), which were observed through the same small aperture. The

0.″06 slit width is comparable to the width of the PSF, and Herczeg et al. (2005) showed that the flux correlates well with the instantaneous FWHM of the target in the cross-dispersion direction. We measured the flux and FWHM of emission in the cross-dispersion direction for several spectral regions in 300 s intervals. These spectral regions are dominated by strong lines of C II and C IV that are produced by accreting gas and are not extended beyond a point source. The spectral regions do not include a significant contribution from H_2 emission, which may be extended (see §5.2). Figure 1 compares the flux and FWHM in four regions of the T Tau spectrum with those from V471 Tau. We calculate a flux from T Tau of 1.82×10^{-12} erg cm^{-2} s^{-1} in the 1230–1650 Å region, and 2.54×10^{-13} erg cm^{-2} s^{-1} in the C IV doublet region (1545–1555 Å). We estimate that the flux calibrations for RU Lupi and T Tau are accurate to $\sim 15\%$. Since the telescope breathing was not significant during the observations of DF Tau and TW Hya, these spectra are flux-calibrated with an error of at most 10%. Models of the telescope breating[1] accurately predict the presence or absence of the thermal focus changes for the observations described above. The low count rates in the observations of DG Tau, V836 Tau, V410 Tau, and V819 Tau prevent us from determining whether they also suffered from the same thermal focus variations as RU Lupi and T Tau. Based on the telescopic breathing models[1] we do not expect any significant variations in the point spread function during those observations, and estimate that the flux in those observations is accurate to better than 15%.

The Doppler correction in the *calSTIS* data reduction pipeline was in error by a factor of 1.6[2]. We corrected for this problem in the observations of DF Tau, T Tau, and RU Lupi by cross-correlating the spectra obtained within the first 1500 s of each orbit, then subdividing and coadding each 300–500 s interval over each observation. We then applied this correction to the entire integration for each observation. This method results in a spectral resolution of about 45,000. The low S/N in our observations of DG Tau, V836 Tau, V819 Tau, and V410 Tau prevent the application of this method to correct for the erroneous wavelength shift. Those observations have $R \sim 25,000$. The $0.''5 \times 0.''5$ aperture that we used to observe DF Tau and TW Hya is an unsupported mode of STIS. By comparing the H_2 spectral profiles in our STIS E140M observations of TW Hya to the STIS E140H ($R \sim 100,000$) observations of TW Hya (Johns-Krull et al., in preparation), we find that the use of the $0.''5 \times 0.''5$ degrades the resolution of E140M spectra to $\sim 25,000$.

The initial wavelength calibration was performed using the on-board Pt/Cr-Ne lamps. We subsequently re-calibrated the wavelengths by shifting the measured wavelength of the

[1]see http://www-int.stsci.edu/instruments/observatory/focus/ephem.html

[2]see http://www.stsci.edu/hst/stis/calibration/pipe_soft_hist/update215c.html

geocoronal Lyα emission line to the predicted location. The relative wavelength calibration within an exposure is accurate to < 0.5 pixels, or < 1.5 km s^{-1}, and the absolute calibration across exposures is accurate to < 1 pixel, or < 3 km s^{-1} (Leitherer et al. 2001). The measured wavelengths of H_2 lines from the two DF Tau observations differ by 4 km s^{-1}, which is most likely an artifact from our wavelength calibration. We shift the wavelength scale in these two spectra by 0.25 pixels so that the heliocentric velocities of narrow interstellar O I 1302 Å, C II 1335 Å, and C II 1336 Å absorption lines are equal.

To complement our *HST* observations we obtained echelle spectra of T Tau, DF Tau, V819 Tau, and V410 Tau, with the SOFIN spectrograph at the *Nordic Optical Telescope* (*NOT*), covering the entire optical range at $R = 45,000$. We derive the projected rotational velocities and heliocentric radial velocities with an accuracy of ~ 1.5 km s^{-1} from these spectra and spectra of template stars. Because V410 Tau is a spotted, rapidly rotating star with broad and complex absorption lines, its radial velocity is measured less precisely. Our velocity measurements are similar to previous estimates (e.g., Herbig & Bell 1988).

3. SOURCES

Our sample consists of five CTTSs and 3 WTTSs. The CTTSs were selected because they are among the brightest CTTSs observed by *IUE* and have a range of disk inclinations, mass accretion rates, and circumstellar environments. The three WTTSs were selected to represent varying stages of disk evolution. One WTTS, V836 Tau, retains a disk and is weakly accreting. Two of the three WTTSs, V410 Tau and V819 Tau, show no H_2 emission and are only briefly discussed.

The known properties for each of our sources, including the radial velocity (v_r), the rotational velocity ($v \sin i$), inclination, and multiplicity are listed in Table 2. The stellar mass, radius, and temperatures for the Taurus stars may be found in Kenyon & Hartmann (1995). The properties of TW Hya and RU Lupi are listed in Webb et al. (1999) and Herczeg et al. (2005), respectively. We calculated the accretion luminosity (L_{acc}) and mass accretion rates ($\dot{M}_{acc}$) at the time of each observation using optical and, for DF Tau and TW Hya, NUV spectra, obtained nearly simultaneously with the FUV observation. For TW Hya, RU Lupi, T Tau, and DF Tau, we use extinctions (A_V) calculated from the neutral hydrogen column density in the line of sight to each star, measured from H I absorption against Lyα emission and H_2 absorption detected in *FUSE* spectra of the stars (cf. Walter et al. 2003; Herczeg et al. 2004). If dust grains in our line of sight to these sources are larger than the average interstellar grain, then A_V would be underestimated by $R_V/3.1$, where R_V is the total-to-selective extinction with an average interstellar value of 3.1 (Cardelli et al. 1989).

3.1. T Tau

As the archetype of the entire class of stars, T Tau is one of the most studied CTTSs. Walter et al. (2003) and Beck et al. (2004) present an overview of T Tau, which is comprised of the optically bright T Tau N separated by 0.″7 from the IR companion T Tau Sab.

T Tau N contributes all of the flux in the FUV because T Tau Sab is heavily obscured (Koresko et al. 1997; Duchene et al. 2005). Most previous estimates of the extinction to T Tau N are $A_V \sim 1.5$ mag (Kenyon & Hartmann 1995; Gullbring et al. 2000; White & Ghez 2001). Calvet et al. (2004) estimated $A_V = 1.8$ mag by fitting the accretion continuum and photospheric emission from T Tau, although the anomalously complex NUV continuum is poorly fit with standard accretion continuum models. An extinction of $A_V \sim 1.5$ mag would severely attenuate FUV emission, but emission in the C III 977 Å and O VI 1032 Å lines was detected by *FUSE* (Wilkinson et al. 2002). Walter et al. (2003) used the total hydrogen column density in the line of sight to T Tau N to calculate $A_V = 0.3$ mag, which we adopt here.

Various studies suggest an inclination of the disk axis from our line of sight of $8-23^\circ$ from our line of sight (Herbst et al. 1986, 1997; Eislöffel & Mundt 1998). IR H_2 emission imaged by van Langevelde et al. (1994) and Herbst et al. (1997), and long-slit *HST*/STIS FUV spectra obtained by Walter et al. (2003) and Saucedo et al. (2003) show spatially extended H_2 emission. Images of shock tracers such as [Fe II] and the extended H_2 emission reveal an extensive network of nebulosity, including Burnham's nebula and HH 155, produced by outflows interacting with ambient molecular material (e.g., Herbst et al. 1996, 1997; Stapelfeldt et al. 1998; Solf & Böhm 1999).

The nominal distance to T Tau and to the other stars in the Taurus molecular cloud is ~ 140 pc. Loinard et al. (2005) calculated a distance of 141 ± 2.8 pc to T Tau by measuring the parallax in high precision astrometric observations of non-thermal radio emission from T Tau S.

3.2. DF Tau

DF Tau is a binary system with a separation of 0.″09 and a position angle of $\sim 270^\circ$ at the time of our observations (White & Ghez 2001; Hartigan & Kenyon 2003; Schaefer et al. 2003; Hartigan et al. 2004). Schaefer et al. (2003) used the decreasing position angle of the pair (300° in 1994 to 262° in 2002) to study the orbital motion of the stars. They suggest that the optically bright component, DF Tau A, is the dimmer component in the near-IR. Schaefer et al. (2003) also find that the V-band emission from the primary star varies by 1.5

mag, while the secondary varies by less than 0.2 mag. They find that the two stars have a similar temperature, mass, and luminosity, but mass accretion rates of $\sim 10^{-8}$ and $\sim 10^{-9}$ $M_\odot$ yr^{-1} for DF Tau A and DF Tau B, respectively. As a result, DF Tau A dominates the U-band emission. Although these characteristics are all consistent with DF Tau A having a higher mass accretion rate than DF Tau B, they could also be explained by invoking a larger extinction to DF Tau B. Furlan et al. (2005) do not find any evidence for disk evolution, either by dust settling or a clearing of the inner disk, from *Spitzer* IRS spectra of DF Tau.

The disk is inclined to our line of sight by 60–85°, based on measurements of $v \sin i$ and a rotation period of 8.5 d (Hartmann & Stauffer 1989; Johns-Krull & Valenti 2001). Previous extinction estimates range between $A_V = 0.15$ and 0.45 mag. (Kenyon & Hartmann 1995; Gullbring et al. 1998; White & Ghez 2001). Following Herczeg et al. (2004), we measure $\log N$(H I)=20.75 from the absorption against the red side of the Lyα emission line. We also estimate $\log N(\mathrm{H_2}) = 20.2^{+0.3}_{-0.5}$ from the H_2 absoprtion against the O VI and C III emission lines in the *FUSE* spectrum of DF Tau. The uncertainty in this measurement is large because the measurement is inferred indirectly from the weak emission in the O VI 1038 Å line relative to the emission in the O VI 1032 Å line. The H_2 excitation temperature is also uncertain. The total hydrogen column density $\log N$(H)$\sim$ 20.95 corresponds to $A_V = 0.5^{+0.15}_{-0.2}$ mag assuming the standard interstellar gas-to-dust ratio (Bohlin et al. 1978). Our line of sight to the star may intercept the flared disk, which could have dust grains larger than is typical for the ISM. Any grain growth in our line of sight, either in a disk or the Taurus molecular cloud, will increase the gas-to-extinction ratio and cause us to underestimate the extinction. On the other hand, the flared disk may be deficient in grains if they have settled, relative to the gaseous disk.

In the long-pass optical acquisition image obtained prior to our small-aperture STIS observation of DF Tau, the pair are resolved with a separation of 96 mas and a position angle of 266°, with DF Tau A being about 13% brighter than DF Tau B in this band. This separation and position angle are consistent with the relative positions of DF Tau A and B measured by Schaefer et al. (2003) for the same epoch. The peak-up image and the echelle spectra, both obtained with the $0\farcs2 \times 0\farcs06$ aperture, have position angles offset by $\sim 48°$ from the dispersion direction, and only include one star. The peak-up presumably found DF Tau A, the brighter of the pair in the CCD.

Only one star is apparant in the acquisition [O II] image prior to the large-aperture observation of DF Tau. Both stars are included in our $0\farcs5 \times 0\farcs5$ observation of DF Tau with a position angle offset by 51° from the dispersion direction. The pair may not be resolvable and the secondary is not detected in the FUV. Assuming that DF Tau A dominates emission in the [O II] filter and in the FUV, then the fainter DF Tau B is located at +6 km s^{-1} in the

dispersion direction. Because the two observations were obtained with a PA that differed by 180°, any spectroscopically resolveable emission contributed by DF Tau B would appear slightly blueshifted in one observation and redshifted in the other observation.

We estimate a mass accretion rate of about 3×10^{-8} $M_\odot$ yr^{-1} based on the NUV-optical spectrum obtained just before our observation of DF Tau with the large aperture. During our small aperture observation, we measured an accretion luminosity about 15 times lower based on the emission in the G430L spectra shortward of the Balmer jump. The optical emission longward of the Balmer jump was about 5 times fainter during the small aperture observation than in the large aperture observation. The N(H I) and therefore the extinction does not change between the two observations.

The FUV spectrum obtained with the smaller aperture is about three times fainter than that obtained with the larger aperture, either because of variability in the mass accretion rate, the different aperture size, or the pointing being slightly offset from DF Tau A. These two observations, obtained with different apertures at different epochs, are analyzed separately.

3.3. RU Lupi

RU Lupi was discussed in detail by Giovannelli et al. (1995) and Herczeg et al. (2005). Although most previous studies have assumed that RU Lupi is a single star, Gahm et al. (2005) detected periodic radial velocity changes of 2.5 km s^{-1} in photospheric absorption lines, which may indicate the presence of a spectroscopic companion. Indirect evidence indicates that the disk and magnetosphere of RU Lupi are probably observed close to pole-on (Giovannelli et al. 1995; Herczeg et al. 2005). Stempels et al. (2005) derive an inclination of $\sim 23°$ based on the 3.7 d period and $v \sin i = 9.0$ km s^{-1}.

RU Lupi is one of the most heavily veiled CTTSs with a variable Hα equivalent width that peaks at 210 Å. Herczeg et al. (2005) described the *HST*/STIS observations of RU Lupi analyzed here. The mass accretion rate onto RU Lupi of 3×10^{-8} at the time of our observation is high for a K7 CTTS. The outflow from RU Lupi is also very strong, as seen in P Cygni line profiles of neutral, singly-ionized, and doubly-ionized species. The extinction to RU Lupi is $A_V \sim 0.07$ mag, based on the $\log N$(H)= 20.1 to the star (Herczeg et al. 2005). Like Taurus, the Lupus molecular cloud is probably located at 140 pc (de Zeeuw et al. 1999; Bertout et al. 1999).

3.4. DG Tau

DG Tau is a binary CTTS characterized by strong accretion and a powerful bipolar outflow. *HST*/WFPC2 images of DG Tau reveal an edge-on disk that obscures the star (Krist et al. 1995). The well-studied jets from DG Tau have provided powerful insights into the production of slow and fast winds from CTTSs (e.g., Bacciotti et al. 2002; Anderson et al. 2003; Hartigan et al. 2004). The jet has a position angle of 226° and an inclination to our line of sight of 38° (Bacciotti et al. 2002). In §5 we argue that the FUV H_2 emission from DG Tau is produced in an outflow. The FUV spectrum includes very little emission in lines other than H_2. The long-slit optical spectrum obtained with the $52'' \times 0\farcs2$ aperture included the star. The star was acquired with a long-pass optical filter and the optical peak-up succeeded in centering the optical emission. At least some of the X-ray emission from DG Tau is extended beyond the star and likely produced by outflows (Güdel et al. 2005). The FUV emission from DG Tau may also be significantly extended beyond the star. We estimate $L_{acc} = 0.22\ L_\odot$, which corresponds to $\dot{M} \sim 3 \times 10^{-8}\ M_\odot\ \mathrm{yr}^{-1}$.

We adopt an extinction of $A_V = 1.6$ mag to DG Tau, based on models of the NUV and U-band continuum by Gullbring et al. (2000). However, this extinction may apply only to the star itself but not to the warm molecular gas, because the star is viewed through its edge-on disk.

3.5. TW Hya

The namesake of the sparsely populated TW Hya association (Kastner et al. 1997; Webb et al. 1999), TW Hya is the closest (56 pc) and UV-brightest known CTTS. Even though it is ~ 10 Myr old (Webb et al. 1999), TW Hya is still weakly accreting, with $\dot{M}_{acc} = 2 \times 10^{-9}$ $M_\odot\ \mathrm{yr}^{-1}$ at the time of our observations (Herczeg et al. 2004). Since TW Hya is isolated from molecular clouds that are typically associated with CTTSs, the extinction is negligible (Herczeg et al. 2004). Images of the disk reveal that it is observed nearly face-on (Wilner et al. 2000; Krist et al. 2000; Trilling et al. 2001; Weinberger et al. 2002). Qi et al. (2004) used submillimeter observations of the CO $J = 3 - 2$ and $J = 2 - 1$ lines to measure an inclination of $7 \pm 1°$. From a lack of near-IR excess emission from the disk, Calvet et al. (2000) inferred that the warm micron-sized dust in the disk within 4 AU of the central star is optically thin.

The FUV spectrum of TW Hya was described by Herczeg et al. (2002) and the fluorescent H_2 emission was modelled by Herczeg et al. (2004). Weintraub et al. (2000) measured a flux of 1×10^{-15} erg cm^{-2} s^{-1} in the rovibrational 1-0 S(1) line at 2.1218 μm, and Rettig

et al. (2004) detected CO emission from TW Hya.

3.6. V819 Tau

V819 Tau shows no significant excess continuum emission at $\lambda < 12$ μm but exhibits strong excess emission at 12, 25, and 60 μm, which suggests the presence of a cold disk with a central dust hole (cf. Skrutskie et al. 1990; Wolk & Walter 1996). Bary et al. (2003) placed a flux upper limit of 3.0×10^{-15} erg cm^{-2} s^{-1} in the 1-0 S(1) line. The extinction of $A_V \sim 1.5$ mag to V819 Tau (Kenyon & Hartmann 1995; White & Ghez 2001) strongly attenuates any FUV emission. We do not discuss this star further.

3.7. V836 Tau

V836 Tau is typically classified as a WTTS, although it has a near-IR excess, indicating the presence of a disk (Mundt et al. 1983; Skrutskie et al. 1990; Skinner et al. 1991; Kenyon & Hartmann 1995; Wolk & Walter 1996). V836 Tau also has Hα emission with a variable equivalent width of $9-25$ Å (Skrutskie et al. 1990; Hartigan et al. 1995; White & Hillenbrand 2004) and an inverse P-Cygni profile (Wolk & Walter 1996), both indicative of accretion. We adopt $A_V \sim 0.6$ mag to V836 Tau (Kenyon & Hartmann 1995). White & Hillenbrand (2004) estimate a mass accretion rate of $\sim 10^{-8}$ $M_\odot$ yr^{-1}. At the time of our observation, we estimate a mass accretion rate of $\sim 10^{-9}$ $M_\odot$ yr^{-1} based on the measured C IV flux of 1.4×10^{-15} erg cm^{-2} s^{-1} and the relationship between $\dot{M}$ and C IV flux calculated by Johns-Krull et al. (2000).

3.8. V410 Tau

V410 Tau is a system with three WTTSs that are coronally active and have no detectable IR excess (Kenyon & Hartmann 1995). White & Ghez (2001) measured a separation of 0.″07 between the A and B components with an uncertain position angle, and a separation of 0.″29 between the A and C components with a position angle of 359°. Since they found that the primary dominates the U-band emission, we expect that it also dominates the FUV flux. Our FUV observation most likely includes both the A and B components but does not include V410 Tau C.

Kenyon & Hartmann (1995) estimated $A_V = 0.03$ mag, while White & Ghez (2001) calculated $A_V = 0.67$ mag. Although this disparity is large, it does not significantly impact

our analysis. Strong variability in the emission from V410 Tau has been well studied at radio to X-ray wavelengths (e.g., Stelzer et al. 2003; Fernández et al. 2004). Rydgren & Vrba (1983) first reported a 1.87 d period that has been attributed to stellar spots.

4. CHARACTERIZING THE H_2 EMISSION

Strong ($A_{ul} \sim 10^8$ s^{-1}) electronic transitions of H_2 occur throughout the FUV wavelength range. Cold H_2 can be excited by photons at $\lambda < 1120$ Å, while warmer H_2 can also be excited by photons at longer wavelengths. Lyman-band (B-X) transitions tend to occur at longer wavelengths than Werner-band (C-X) transitions because the B electronic state has a lower energy than the C electronic state. Once electronically excited, the H_2 molecule almost immediately decays to the ground (X) electronic state. The radiative decay from the B electronic state will occur by one of many different transitions that have similar branching ratios. Typically only a few transitions from the C electronic state have large branching ratios. The H_2 molecule in the B or C electronic state will dissociate by radiative decay to the ground vibrational continuum between 0–50% of the time, depending on the energy of the upper level.

Warm H_2 gas can absorb photons throughout the FUV. Therefore, a flat radiation field would excite a myriad of upper levels and produce a pseudo-continuum of densely-packed H_2 lines. However, the FUV emission from CTTSs is dominated by emission lines, in particular Lyα. Consequently, most of the detected H_2 lines are from one of the 10–25 different upper levels that are excited by transitions with wavelengths coincident with Lyα emission. Lyα-pumped H_2 fluorescent emission appears to be common to all CTTSs. The Lyα excitation and decay process for CTTSs is described in Herczeg et al. (2002). All lines discussed in this paper are Lyman-band lines, except where noted. The set of emission lines from a single upper level is termed a *progression*, and is referred to by the vibrational and rotational quantum number of the upper level, (v', J'). The amount of emission in a progression depends on the population of H_2 in the lower level of the transition, the oscillator strength of the pumping transition, and the radiation field at the transition wavelength. Table 3 lists the pumping transitions for the detected emission lines, together with the oscillator strength f, the energy E'' of the lower level of the pumping transition, the theoretical dissociation percentage P_{dis} from the upper level calculated by Abgrall et al. (2000), and the velocity of the pumping transition from Lyα line center. Table 4 lists the number of lines and the total observed flux from each upper level for every source.

Figure 2 shows the observed Lyα emission and locations of the pumping transitions for each source. For every source discussed here except TW Hya, most or all of the intrinsic

Lyα emission is attenuated by H I in the interstellar medium and stellar outflows. We do not detect any Lyα emission from T Tau, DG Tau, V836 Tau, or V410 Tau. We detect only weak Lyα emission located far from line center from DF Tau and RU Lupi. Only for TW Hya do we detect strong Lyα emission both longward and shortward of Lyα line center, because TW Hya is a weak accretor and isolated from molecular clouds that are typically associated with young stars. The strength and large width of the Lyα emission from TW Hya leads to a more extensive network of observed H_2 lines than from the other sources in our sample.

The observation of DF Tau obtained with the small aperture has lower S/N than that obtained with the large aperture, and shows fewer lines as a result. No significant differences in H_2 emission are detected between those two observations.

Several H_2 lines pumped by C IV from highly excited rovibrational levels in the ground electronic state are discussed in §4.3.

4.1. Identifying H_2 lines

The FUV spectra of the CTTSs TW Hya, DF Tau, RU Lupi, T Tau, and DG Tau, and the WTTS V836 Tau include many narrow H_2 emission lines. We do not detect any H_2 emission in the spectra of V819 Tau or V410 Tau. We identify H_2 lines using the linelist of Abgrall et al. (1993). Most of the lines are Lyman-band lines pumped by Lyα, because Werner-band lines pumped by Lyα are brightest at $\lambda < 1200$ Å, where the sensitivity of STIS is low. If one line from an upper level is present, then several other lines with large branching ratios from the same upper level should also be present. In order to positively identify a line as H_2, we require that several lines from a given upper level be present with relative fluxes consistent with branching ratios.

Based on models constructed for the H_2 fluorescence detected in the TW Hya spectrum (Herczeg et al. 2004, see also §4.2), we use observed fluxes from one or a few lines from an upper level to predict fluxes for all the lines in that progression. These models allow us to identify many weak emission features as H_2 lines. Figure 3 shows the observed and model fluxes of sixteen lines originating from $(v',J')=(2,12)$ in the DF Tau spectrum. We use the fluxes in the strongest lines in that progression, such as 2-8 P(13) at 1588.7 Å and 2-5 P(13) at 1434.5 Å, to identify and predict the fluxes of the weaker H_2 lines, such as 2-1 R(11) at 1185.2 Å and 2-3 P(13) at 1325.3 Å. These models provide a rigorous check on questionable line identifications because they predict the fluxes of all other possible lines from the same upper level.

In rare cases, we identify only one or two lines from a single upper level as Lyman-band H_2 lines when the following conditions are met: (i) the lines have an appropriate width and velocity shift, (ii) all other lines from the same upper level are either too weak to be detected or are obscured by wind absorption or other emission lines, and (iii) we expect emission in that progression based on the observed emission at wavelengths of possible pumping transitions. Generally only a few Werner-band lines from a single upper level have large branching ratios, and these lines preferentially occur at $\lambda < 1185$ Å, where STIS has low sensitivity. Therefore, we relax the requirement of detecting several lines from a single upper level for the identification of Werner-band H_2 lines.

H_2 emission lines were previously identified in the STIS spectra of TW Hya (Herczeg et al. 2002) and RU Lupi (Herczeg et al. 2005). In this paper, we identify H_2 lines from V836 Tau, T Tau, DG Tau, and two spectra of DF Tau, and expand the list of H_2 lines observed from TW Hya. Table 5 lists line identifications, fluxes, and branching ratios of observed Lyman-band H_2 emission lines that are pumped by Lyα from each star, sorted by progression. Table 6 lists the same properties for highly-excited H_2 emission lines that are pumped by C IV. Table 7 lists the blended H_2 lines. In some spectra, lines such as the 1455 Å blend are resolved into two separate lines, while in other spectra we were unable to discriminate between the two lines. Table 8 lists the Werner-band H_2 lines, most of which are also pumped by Lyα, although one Werner-band H_2 line from RU Lupi is pumped by strong emission in the O VI 1031 Å line. Outside of regions with strong lines such as C IV or O I, the H_2 linelist for TW Hya is complete for $\lambda > 1200$ Å down to a flux level of $\sim 4 \times 10^{-15}$ erg cm^{-2} s^{-1}, while the H_2 linelists for RU Lupi and DF Tau are complete down to $\sim 1 \times 10^{-15}$ erg cm^{-2} s^{-1}, and that of DG Tau and V836 Tau are complete down to $\sim 4 \times 10^{-16}$ erg cm^{-2} s^{-1}. The H_2 lines from T Tau are more difficult to identify because they are broad, which lowers the S/N in each pixel, and are weak relative to many other strong lines in the spectrum, which increases the likelihood of masking by other emission or wind absorption lines. As a result, our H_2 linelist for T Tau may not be complete.

Figures 4–7 present four spectral regions with strong H_2 lines. The strongest H_2 lines are transitions from the upper levels (v',J')=(1,4), (1,7), (0,1), (0,2), and (2,12). These lines are all pumped by transitions located between 0 and 600 km s^{-1} from Lyα line center (1215.67 Å). The pumping transitions typically have large oscillator strengths and H_2 lower levels with relatively low energies. The locations of the pumping transitions agree with results from Ardila et al. (2002), who detected only H_2 lines pumped on the red side of Lyα in GHRS spectra of several CTTSs. TW Hya, RU Lupi, DF Tau, DG Tau, and V836 Tau also exhibit weaker H_2 emission pumped shortward of Lyα line center. Many possible pumping transitions are present shortward of Lyα, and are all detected in the TW Hya spectrum. In the spectrum of DF Tau, we detect H_2 emission from only two levels that are pumped

shortward of Lyα, and both are pumped at $v < -300$ km s^{-1} relative to Lyα line center. However, some H_2 lines from DF Tau are pumped at $v = +1100$. Therefore, the H_2 lines from DF Tau and T Tau indicate that the centroid of the Lyα emission that irradiates the warm molecular gas is longward of line center.

As described above, the Lyα profile seen by the warm molecular gas differs from the observed Lyα emission because of H I attenuation in our line of sight to the star. Some Lyα emission may be attenuated by H I prior to irradiating the warm molecular gas. In principle, the H_2 gas may also see a different Lyα profile if geometrical effects result in anisotropic Lyα emission. The observed Lyα emission from RU Lupi, TW Hya, and DF Tau extends to 1219 Å, 1220 Å, and 1221 Å, respectively. Table 4 shows that the H_2 emission lines from DF Tau, but not from RU Lupi or TW Hya, are pumped at $\lambda > 1220$ Å. The H_2 lines pumped at $\lambda > 1218$ Å are also much stronger from TW Hya and DF Tau than from RU Lupi. DF Tau is viewed edge-on by both the observer and the H_2, but TW Hya and RU Lupi are observed face-on by the observer and edge-on by the H_2. Therefore, the presence or absence of the red wing in the Lyα emission profile appears to be independent of viewing angle.

The H_2 lines pumped at large velocities from Lyα line center are not detected in *IUE* spectra of HH 43 and HH 47 (Schwartz 1983; Curiel et al. 1995), or emission extended by up to 20″ from T Tau (Walter et al. 2003; Saucedo et al. 2003). Those spectra show H_2 emission from only the upper levels (1,4) and (1,7) that are pumped at +14 and +99 km s^{-1} from Lyα line center. The accretion processes associated with CTTSs produce much broader Lyα emission than is produced by shocks due to interactions between outflows and molecular clouds. Thus the pattern of H_2 fluorescence is a good diagnostic of whether accretion processes or shocks in the interstellar medium provide the Lyα pumping photons.

4.2. H_2 line fluxes

We fitted the H_2 lines with Gaussian profiles to measure the central wavelength, width, and flux. The H_2 lines from T Tau and RU Lupi both show significant asymmetric blueshifted emission. We fit each line from those two sources with one narrow, bright Gaussian component and a fainter broad component that is blueshifted. The width, velocity shift, and percent of the total flux in the weaker component were fixed based on fits to coadded emission lines (see §5.1). The H_2 lines from DF Tau also show a weak blueshifted asymmetry. By fitting single Gaussians to all of the lines from DF Tau, we may be underestimating the true flux by $\sim 5\%$. This fitting process assumes that the line profile does not depend on the upper level. This method is appropriate for RU Lupi but may result in underestimating the flux in lines originating from v',J'=(1,4) and (1,7) from T Tau and DF Tau (see §5.1).

Tables 5–8 list the H_2 lines from each star, sorted by upper level.

Wood et al. (2002) and Herczeg et al. (2004) constructed Monte Carlo models of H_2 fluorescence in a plane-parallel slab by computing on the optical depths of the various lines using the branching ratios calculated by Abgrall et al. (1993). Depending on the column density and excitation temperature of the H_2 emission region, large line opacities can occur when a low-energy lower level is heavily populated. Transitions from lower levels with large energies remain optically thin because those lower levels have negligible populations. This effect tends to weaken the lines at short wavelengths. These models have been used to probe the temperature T and column density $N(H_2)$ of the H_2 emission region. In this paper, we use the model with the best-fit parameters of $T = 2500$ K and $\log N(H_2)$=18.5 that Herczeg et al. (2004) found for the H_2 emission from TW Hya. We apply results from that model here to check our line identifications (§4.1) and to estimate fluxes in the undetected lines.

We scale the relative line fluxes predicted by the model to match the observed fluxes, after correcting for extinction. The predicted line fluxes are somewhat uncertain because the physical conditions and the geometry of the warm molecular gas could be different for stars with different emission sources (see §5.4). Nonetheless, these models explain most of the observed line fluxes successfully. Figures 3–7 compare the observed flux (solid line in Fig. 2 and shaded regions in Figs. 4–7) with the model flux (dashed lines). Tables 5–6 list estimates of the total emission from an upper level by correcting for lines that are unseen because they are outside of our wavelength range, are masked by strong emission lines, attenuated by wind absorption, or are too weak to be detected.

Although the relative line fluxes are weakly sensitive to extinction, we are unable to improve upon the existing extinction estimates because of the low S/N for lines at short wavelengths. The relative line fluxes are consistent with our adopted extinctions in all cases. The H_2 lines in the T Tau spectrum indicate $A_V < 1.0$ mag, which suggests that the lower extinction value toward T Tau of $A_V = 0.3$ mag adopted here is appropriate.

The observed H_2 fluxes from DF Tau are 2.5–3 times lower in our observation with the small aperture compared to the observation with the large aperture, but the Lyα emission was only 1.73 times smaller. Since H_2 is pumped by Lyα, the observed H_2 fluxes should be directly proportional to the strength of Lyα emission. However, we cannot draw any significant conclusions from this discrepancy because the large aperture contains both stars, while the $0\farcs2 \times 0\farcs06$ aperture contained only one star.

Table 9 lists the observed flux, not corrected for extinction, in strong FUV emission lines and in the strongest five H_2 progressions. The typical ratio of observed C IV to H_2 flux in the strongest progression is about 7:1. We therefore expect that between two to five

progressions from the WTTS V410 Tau should have fluxes $> 4 \times 10^{-15}$ erg cm^{-2} s^{-1}. We place flux upper limits of $1 - 2 \times 10^{-15}$ erg cm^{-2} s^{-1} in each progression from V410 Tau by finding flux upper limits for individual emission lines and then applying the models described above to calculate an upper flux limit in the entire progression. These upper limits are about a factor of two below the H_2 flux we crudely expect from the previously described correlation with C IV emission. We conclude that a significant reservoir of warm H_2 is probably not present around V410 Tau. Since a large extinction attenuates almost all of the FUV emission from the WTTS V819 Tau, the non-detection of H_2 from this star is not significant.

4.3. Highly Excited H_2

Most of the detected H_2 lines are photoexcited from lower levels in the ground electronic state with energies of $1 - 2$ eV. These levels are populated sufficiently with excitation temperatures of $T = 2000 - 3000$ K to explain the observed emission (Black & van Dishoeck 1987; Wood et al. 2002; Herczeg et al. 2004). Herczeg et al. (2002) detected emission from the (v',J')=(0,17) and (0,24) levels from TW Hya, yet these upper levels cannot be excited by Lyα. We confirm the presence of these lines in the spectra of both TW Hya and DF Tau. We also identify emission in lines from (1,14) in the spectrum of TW Hya. None of the transitions that could pump these levels are coincident with Lyα. These upper levels may be excited by C IV via 0-3 P(25) 1547.97 Å, 0-5 P(18) 1548.15 Å, and 1-7 R(13), respectively. The C IV 1548 Å resonance line is typically the second strongest line in FUV spectra of CTTSs, after Lyα, and the three possible pumping transitions have strong oscillator strengths. However, the lower levels (v'', J'')=(3,25), (5,18), and (7,13) have energies of 4.2, 3.8, and 3.8 eV, respectively, and cannot be thermally populated at temperatures where H_2 is present. These lower levels are also not directly populated by the fluorescence and subsequent decay into vibrationally excited levels of the ground electronic state. The fluorescence and subsequent decay increases the vibrational excitation without substantially changing the rotational excitation of H_2. Excitation of H_2 by FUV pumping and fluorescence therefore cannot explain the high rotational excitation seen here. Some non-thermal process, perhaps involving the formation of H_2, may also populate these highly energetic levels.

We investigated the excitation conditions required to produce this emission by forward modelling the H_2 spectrum. We constructed synthetic H_2 spectra by modelling a isothermal, plane parallel slab of H_2 following the procedure described by Wood et al. (2002) and Herczeg et al. (2004). The amount of emission absorbed by an H_2 transition, F_{H2}, is given by:

$$F_{H2} = \eta F_{pump} \int_{\lambda} [1 - e^{-\tau_{\lambda}(T, N(H_2))}] \mathrm{d}\lambda, \quad (1)$$

where F_{pump} is the flux at the pumping wavelength, η is the solid angle filling factor of H_2 as seen from the Lyα emission region, assumed to be 0.25 (Herczeg et al. 2004), T and $N(H_2)$ are the temperature and column density of the slab, and the integral is the effective equivalent width of the transition. The entire FUV spectrum is required to calculate the excitation of every upper level of H_2. We used the STIS spectrum of TW Hya to estimate the flux at $\lambda > 1187$ Å, and a *FUSE* spectrum of TW Hya to estimate the flux at $\lambda < 1187$ Å (Herczeg et al., in preparation). Among the many models run, we present results for synthetic spectra based on an H_2 layer with $\log N(H_2) = 18.5$ (units cm^{-2}) and $T = 2500$ K (our standard model), and that standard model with an additional layer of $\log N(H_2) = 17.0$ and $T = 2.5 \times 10^4$ K. Differences between the two model spectra are attributed to the small reservoir of highly excited gas. We also calculate spectra for models of gas that is irradiated by all FUV photons except for Lyα. Figure 8 compares the observed TW Hya spectrum to three of these models.

The H_2 lines from the (0,17), (0,24), and (1,14) upper levels are produced by photoexcitation by C IV in the highly excited layer of H_2. Lines in these three progressions are the strongest Lyman-band lines that are not pumped by Lyα. Based on these models, we find many other weak features in the spectrum that could also be attributed to pumping by C IV, C II, and several other strong emission lines. While the temperature and column density for this hot layer are poorly constrained at present, these results demonstrate the need for a thin layer of highly-excited H_2 to explain these lines.

With the presence of the highly excited H_2 layer, our models predict that many undetected H_2 lines should be much stronger than the weak lines from (0,17), (0,24), and (1,14). Since all of these undetected lines should be pumped by Lyα, we are forced to conclude that somehow Lyα photons are prevented from irradiating the bulk of the highly-excited H_2 gas. This observational result is unexpected and not easily explained. We therefore suggest a highly speculative possible explanation, although there may be other more physical explanations. In principle, the highly-excited H_2 could be mixed in with both the warm (~ 2500 K) H_2 layer and colder gas below. Scattering by H I in the warm surface layer could then increase the path length of Lyα photons, leading to preferential attenuation of Lyα emission by dust. In this case, the FUV radiation field that irradiates the gas beneath the thin surface layer may be dominated by emission in lines such as C IV. We caution the reader that this speculative scenario is outlined here only to describe the a process that could irradiate a surface with C IV but not Lyα emission.

The highly-excited H_2 emission is detected from two sources, TW Hya and DF Tau, that have strong FUV continuum emission, but is not detected from RU Lupi, which does not have a strong FUV continuum. Since the FUV continuum is likely produced by electron

excitation of H_2 (Bergin et al. 2004), it could be related to the highly-excited H_2. Electronic excitation of H_2, like FUV pumping, will result in significant vibrational excitation but not significant rotational excitation.. However, if the H_2 formation rate is sufficiently large, it could produce a population of H_2 in highly excited rovibrational levels. H_2 may form by many routes, including on grains in gas at $T < 500$ K, by associative detachment of H^-, or by dissociative recombination of H_3^+. These and other H_2 formation processes produces a population of highly excited H_2 (e.g. Takahashi et al. 1999; Bieniek & Dalgarno 1979; Kokoouline et al. 2001).

4.4. Variability of H_2 emission from T Tau

Walter et al. (2003) detected emission in the red wing of the Lyα line in two of three long-slit G140L spectra of T Tau obtained in our program, but no Lyα emission in the echelle spectrum of T Tau. Only this red wing is seen because the core is absorbed by interstellar H I, and any blueshifted emission is absorbed in the stellar winds. The non-detection of any Lyα emission in two of the four spectra is the result of either a variable Lyα line width or a variable H I column density in our line of sight. Walter et al. (2003) conclude that these changes are not caused by a different H I column density in our line of sight because the shape of the Lyα profile did not change, even though the detected Lyα line strength was different in the two observations. We confirm this result by relating the presence of emission in the red wing of Lyα to the relative flux in each progression.

Figure 9 shows the Lyα and 1400–1500 Å regions for our three long-slit spectra and our echelle spectrum, convolved to the spectral resolution of G140L ($R \sim 1000$). We scale the observed emission to equal the flux in every observation between 1495–1510 Å, a region dominated by several strong H_2 lines from (1,4) and (1,7). Based on the strength of the extended H_2 emission, at most 10% of the on-source emission in H_2 lines from (1,4) and (1,7) is related to the extended shocks seen in long-slit spectra. The relative flux of H_2 emission lines from the same upper level also remains constant during the four observations. A higher extinction in an observation would suppress lines at shorter wavelengths. We conclude that the extinction to T Tau remains constant during these observations.

When the redshifted Lyα emission disappears, the relative H_2 emission in lines from (0,1), (0,2), and (2,12) decreases substantially, relative to that from (1,4) and (1,7). The echelle observation shows the strongest emission in hot accretion lines such as C IV, H_2 lines from (1,4) and (1,7), and the continuum, but has no detectable redshifted Lyα emission and as a result shows the weakest absolute flux in H_2 lines from (0,1), (0,2), and (2,12). Since the lines from (0,1), (0,2), and (2,12) are pumped at +379, +487, and +551 km s^{-1}, respectively,

from Lyα line center, the strength of these lines probe the strength of the red wing of Lyα. The lines from (1,4) and (1,7), which are pumped at +99 and +14 km s^{-1}, depend on the emission near Lyα line center. The changes in the intrinsic Lyα profile are seen both directly in our observations and by the H_2 gas, even though we are viewing the system face-on while the H_2 is likely viewing the star with a large inclination.

5. CONSTRAINTS ON THE ORIGIN OF THE H_2 EMISSION

In this section, we analyze the spectral and spatial properties of the H_2 emission to identify the source of the H_2 emission. Strong lines within each progression are coadded for each star to improve the S/N in the spectral profiles. We consider only lines in the five strongest progressions, from (v',J')=(1,4), (1,7), (0,1), (0,2), and (2,12).

We group the lines from (1,4) and (1,7) together because these progressions are pumped at +99 and +14 km s^{-1} from Lyα line center, and consequently may be excited by a narrow Lyα emission line. The progressions from (0,1), (0,2), and (2,12) are grouped together because they are pumped by transitions between 380 to 550 km s^{-1} from Lyα line center, which requires broad Lyα emission.

5.1. Spectral Profiles of the H_2 Emission

Figure 10 shows the normalized spectral profiles of the coadded H_2 emission lines from (0,1), (0,2), and (2,12). Table 10 lists the parameters of Gaussian fits to these profiles, including the velocity relative to the star, the intrinsic FWHM deconvolved from the instrumental broadening, and the percent of flux in each component. These fits may not be unique. Much of the H_2 emission from each star occurs in a narrow profile, with an intrinsic FWHM ranging from 17.5–28.5 km s^{-1}. This narrow component of the H_2 emission detected from TW Hya, DF Tau, and V836 Tau is centered at the radial velocity of the star, but is shifted by −12, −12, and −27 km s^{-1} in the spectra of RU Lupi, T Tau, and DG Tau, respectively. The properties of this narrow component are presented in Table 11. Additionally, a strong broad component, blueshifted from the primary narrow component and extending to −100 km s^{-1}, is detected from RU Lupi and T Tau. Weak blueshifted emission extending to ~ -40 km s^{-1} is also detected in both FUV spectra of DF Tau, which were obtained with a PA that differed by 180°. Although the binarity of DF Tau may broaden the central profile, it cannot explain the broad blue wing.

All of the H_2 emission lines from TW Hya, RU Lupi, DG Tau, and V836 Tau appear

similar, regardless of the upper level. Figure 11 shows that the asymmetric blueshifted wing from DF Tau and T Tau is stronger from (1,4) and (1,7), relative to the flux in the narrow component, than it is from (0,1), (0,2), and (2,12). The lines from (1,4) and (1,7) from T Tau may also have additional redshifted emission. The Lyα emission profile that irradiates the the blueshifted gas around DF Tau and T Tau, like that from HH objects, is narrower than the Lyα emission profile that irradiates the bulk of the warm gas.

5.2. Spatial Profile of the H_2 Emission

Although the $0\farcs5 \times 0\farcs5$ and the $0\farcs2 \times 0\farcs06$ apertures used in our observations are narrow, the E140M echelle spectra yield some spatial information in the cross-dispersion direction. The pixels in the cross-dispersion direction are 29 mas wide, so each pixel corresponds to 4 AU at the 140 pc distance of the Taurus and Lupus star-forming regions and 1.7 AU at the 57 pc distance of TW Hya. These two apertures are large enough that we are not limited by spatial resolution, and small enough to minimize contamination by spatially extended gas associated with the parent molecular cloud.

The coadded H_2 lines from DF Tau, RU Lupi, and T Tau are strong enough to search for extended emission. We do not analyze the spatial profile of H_2 emission from DG Tau or V836 Tau because their H_2 lines are weak, and no atomic lines are strong enough to use for estimating the point-spread function. Herczeg et al. (2002) found that the H_2 and Lyα emission from TW Hya were not significantly spatially extended relative to the hot lines such as C IV.

For each observation, we extract the spatially-resolved spectrum at the wavelengths of strong H_2 lines and various other strong lines including the O I 1305 Å triplet, the C II 1335 Å doublet, the Si IV 1400 Å doublet, and the C IV 1550 Å doublet. We subtract the spatial profile of the background, which is measured from nearby spectral regions with continuum emission but no detectable line emission. The central position of the emission in the cross-dispersion direction depends on the echelle order and the horizontal position of the wavelength in that order and is automatically determined in the *calSTIS* data reduction program. When coadding the H_2 lines, we resample the emission profile in pixel space to account for sub-pixel differences.

The telescope thermal focus variations make the point-spread function of *HST* uncertain (see §2). The spatial profiles of the hot lines of C IV and Si IV are most likely produced at or near the accretion shock (Johns-Krull et al. 2000; Calvet et al. 2004) and should approximate the point-spread function. The strong lines produced in cooler gas, such as O I

and C II, are also not spatially extended and can be used as a proxy for the point-spread function. The point-spread function of STIS can depend on wavelength, particularly with the $0\farcs5 \times 0\farcs5$ aperture, so when possible we compare the spatial profile of lines located near each other. This method is sensitive to emission extended beyond the hot emission lines, but is not sensitive to reflection of FUV emission from a disk surface or nebulosity. Figure 12 shows the spatial distributions of various lines from DF Tau, T Tau, and RU Lupi. We also construct space-velocity diagrams to analyze the spatial distribution of co-added H_2 emission across the line profile.

5.2.1. DF Tau

We concentrate on the observation of DF Tau obtained with the $0\farcs5 \times 0\farcs5$ aperture, because the S/N in H_2 and other emission lines is higher than in the observation taken with the $0\farcs2 \times 0\farcs06$ aperture. All results are consistent with the observations that used the small aperture.

Figure 12 shows that the H_2 emission lines between 1270–1400 Å (top left) and 1500–1650 Å (bottom left) have a similar profile to the C II and C IV emission lines, respectively. The spatial profiles of this emission are well characterized by the combination of a narrow and a broad Gaussian profile. We measure an instrumental spatial resolution of $0\farcs10$ (3.6 pixels or 14.6 AU at the distance of DF Tau) and $0\farcs14$ (4.7 pixels or 19.0 AU) from the spatial profiles of C IV and C II emission, respectively. We identify weak asymmetric emission in the wings of several lines, including C II and C IV, offset from the emission peak by about $0\farcs17$. The spatial separation indicates that this emission is not directly associated with the secondary star. The disk of DF Tau is observed close to edge-on. Because dust strongly forward scatters FUV emission (Draine 2003), in principle one side of the disk could scatter such extended emission. This emission component may instead be an artifact from an asymmetric point spread function.

Figure 13 shows the space-velocity diagram for DF Tau for the observations obtained with the large aperture (left) and small aperture (right). The solid lines are contours of 0.2, 0.5, and 0.8 times the peak flux for emission from (0,1), (0,2), and (2,12). The shaded regions show the same contours for lines from (1,4) and (1,7). The lines pumped near Lyα line center, from (1,4) and (1,7), may be slightly more extended in the SW direction than the other H_2 lines.

5.2.2. RU Lupi

Figure 12 compares the spatial extent of H_2 emission from RU Lupi between 1270–1400 Å (top) and 1500–1650 Å (bottom) with that of Lyα, Si IV, and C IV. The H_2 and Lyα emission is extended to the SW. No other FUV emission lines, including Lyα-pumped Fe II emission, appear extended beyond a point source. Figure 14 shows a space-velocity diagram of coadded H_2 emission from RU Lupi. The shaded regions show contours of 0.2, 0.5, and 0.8 times the peak emission. The solid lines show contours of 0.2, 0.5, and 0.8 times the peak emission at each pixel in the spectra direction, and therefore indicate the spatial distribution of emission across the line profile. The dashed lines indicate the point-spread function measured from Si IV emission. The H_2 emission at ~ -15 km s^{-1} is extended in the SW direction but not in the NE direction. About 70% of this emission at ~ -15 km s^{-1} is produced on-source. We cannot discriminate between a second point-source or continuous H_2 emission in the SW direction, but some of the remaining 30% of the emission must be extended by at least 70 mas from the star. The H_2 emission at < -50 km s^{-1} is not extended beyond the C IV emission (FWHM=0.″1).

Figure 15 shows the spatial extent of Lyα emission across the line profile (solid line), smoothed by 75 km s^{-1}, compared to the spatial extent of Si IV emission (dashed lines). Like the H_2 emission at -15 km s^{-1}, the Lyα emission is spatially extended SW of the star but not NE of the star. The spatial extent of the detected Lyα emission does not depend on the velocity. Even off source, the optical depth in the Lyα line is large enough to produce emission at +800 km s^{-1} from line center.

5.2.3. T Tau

Figure 12 shows that the spatial profile of coadded H_2 emission from T Tau is slightly broader than the spatial profile of Si IV (top right) or C IV emission (bottom right). We coadd the H_2 lines from every upper level for this analysis to increase the S/N, even though the spectral profiles indicated that the lines pumped near line center of Lyα have stronger blueshifted emission than the other lines. The space-velocity diagram shown in Figure 16 indicates that the H_2 emission, particularly near $v = 0$ km s^{-1}, may be slightly more extended than the Si IV emission. The emission at $v = -50$ km s^{-1} may be slightly less extended than Si IV emission. We caution, however, that the S/N in the space-velocity diagram is low and that any conclusions drawn from the diagram may therefore be suspect.

5.3. Wind Absorption of H_2 Lines

Two strong H_2 lines, 0-4 R(0) and 0-4 R(1) at 1333.5 and 1333.8 Å, respectively, are located at -240 and -165 km s^{-1} from the C II 1334.5 Å resonance line. Those two H_2 lines may be attenuated by the stellar wind if the optical depth in this ground-state line is sufficiently large in the wind at those velocities.

Figure 17 shows the observed spectrum (shaded) and model H_2 emission (dashed lines) for the 1333–1336 Å spectral region for the six stars in our survey. Table 12 describes the wind properties and the attenuation of the 0-4 R(0) and 0-4 R(1) lines. We compare the maximum wind velocity (v_∞) in the C II 1334.5 Å line with that from the Mg II 2796 Å line. We also compare the observed flux in the two H_2 lines to the predicted flux, based on models described in §4.2.

Herczeg et al. (2002) found that the 0-4 R(1) 1333.8 Å line from TW Hya is weaker than expected from our models (see §4.2) because the wind absorption in the C II line extends to ~ -180 km s^{-1} in our line of sight. Both the 0-4 R(0) and the 0-4 R(1) lines from RU Lupi are attenuated by the optically thick wind, which extends to ~ -240 km s^{-1}. On the other hand, the observed flux in both lines from DF Tau is similar to the predicted flux, because the optically thick C II line in the wind of DF Tau only extends to ~ -140 km s^{-1}. Since the C II wind absorption from T Tau extends to ~ -180 km s^{-1} and the H_2 emission is shifted by -12 km s^{-1}, the optical depth of the wind at the 0-4 R(1) 1333.8 Å line is small. We detect C II emission between 1333.5–1333.8 Å, so some of the emission at 1333.8 Å is likely from C II. Assuming the presence of some C II emission, we infer that the 0-4 R(1) line in the T Tau spectrum is partially attenuated by the wind. The fluxes in both H_2 lines from V836 Tau are similar to the model flux, although we would not expect any optically thick wind absorption at -165 km s^{-1} because the winds of WTTSs are not nearly as optically thick at large velocities as winds from CTTSs. The 0-4 R(1) line at 1333.8 Å appears weaker than expected from DG Tau, but the 0-5 R(1) and 0-5 R(2) lines at 1394 Å and the blend of 0-6 R(1) and 0-6 R(2) at 1455 Å are also much weaker than expected. Therefore, we cannot conclude that any H_2 absorption is attenuated by the wind of DG Tau.

Several weaker H_2 lines also overlap with wind absorption features. The 0-4 R(3) line at 1335.1 Å line, located at -130 km s^{-1} from the C II 1335.7 Å line, may be detected from DF Tau but is not detected from TW Hya or RU Lupi because of wind absorption. We did not include this line from DF Tau in Table 5 because of the uncertain flux given the overlap with C II emission and low S/N. The red side of the 0-4 R(3) line does not appear in the T Tau spectrum, which strengthens our inference that the on-source H_2 emission from T Tau is attenuated by the wind. With better S/N than our data, several other lines are potentially useful for measuring attenuation of H_2 emission by the wind, such as 3-2 P(16) at 1305.663

Å located at -84 km s^{-1} from the strong O I 1306 Å line.

These observations demonstrate that the H_2 emission detected from TW Hya, RU Lupi, and T Tau is absorbed by the the stellar wind. Based on the similar patterns of H_2 emission, we infer that the H_2 emission would also be absorbed by the winds of DF Tau, DG Tau, or V836 Tau if their winds were optically thick in C II at larger velocities. This attenuation suggests that the H_2 emission is produced inside of any wind absorption, and as a result must be produced close to the central star.

5.4. Comparison to Previous Observations

Table 13 compares the fluxes, FWHM, and velocities of H_2 emission from DF Tau, RU Lupi, T Tau, and DG Tau in our *HST*/STIS spectra and corresponding data obtained with *HST*/GHRS of the same CTTSs, by Ardila et al. (2002). The *HST*/GHRS observations had $R = 20,000$, compared to $R = 25,000 - 45,000$ with STIS, and used a $2'' \times 2''$ aperture, compared to $0\farcs2 \times 0\farcs06$ and $0\farcs5 \times 0\farcs5$ with STIS. The absolute velocities are accurate to ~ 20 km s^{-1} for pre-COSTAR GHRS spectra and to ~ 3 km s^{-1} for STIS spectra. We compare H_2 lines pumped on the red side and near Lyα line center. Only a few line fluxes are co-added because the wavelength range of GHRS was limited to about 30 Å per exposure. We include the C IV flux as a rough proxy for the Lyα emission and mass accretion rate.

The centroid velocity of H_2 emission did not change significantly between the GHRS and STIS observations of RU Lupi, T Tau, and DF Tau. The FWHM of the H_2 emission from RU Lupi and T Tau is broader in the GHRS observation than in the STIS observation, which could be produced either by a real velocity dispersion or by spatially extended emission in the dispersion direction. The H_2 emission from the upper levels (1,4) and (1,7) from DG Tau, RU Lupi, and T Tau was much stronger relative to the C IV emission during the GHRS observation than the STIS observation. Because of the larger aperture used for the GHRS observations than the STIS observations, we infer that a reservoir of warm molecular gas extending beyond the star was present for RU Lupi, T Tau, and DG Tau.

The H_2 emission from DG Tau was more blueshifted in our STIS observation than in the GHRS observation, but the two observations could have sampled different gas. The GHRS observation of DG Tau exhibits strong C IV emission, which is not detected in our STIS spectra even though we would expect such emission based on the flux ratio of H_2 to C IV. The GHRS observations may have detected mostly extended emission in both H_2 and the other lines, including C IV. Güdel et al. (2005) detected extended X-ray emission from jets emanating from DG Tau. Hot gas traced by emission in C IV (Raymond et al. 1997) and

possibly O VI (Herczeg et al. 2005) has previously been detected in outflows from CTTSs. However, Walter et al. (2003) and Saucedo et al. (2003) did not detect any extended C IV emission from T Tau, despite the presence of extended X-ray emission (Güdel et al. 2004). Takami et al. (2004) found near-IR H_2 emission in several lines from DG Tau, including the 1-0 S(1) transition, which is blueshifted by ~ 15 km s^{-1} from the system velocity and offset from the source by $0\farcs2$. They used relative H_2 line fluxes to estimate a temperature of 2000 K, which is hot enough to produce Lyα-pumped H_2 emission in the FUV (e.g. Black & van Dishoeck 1987; Herczeg et al. 2004). Richter et al. (2002) estimated an upper flux limit of 3×10^{-14} erg cm^{-2} s^{-1} in the S(2) line at 12 μm from DG Tau.

Najita et al. (2003) detected fundamental CO emission from V836 Tau, but not from V410 Tau. Duvert et al. (2000) also detected weak CO $J = 2 - 1$ emission from V836 Tau. Bary et al. (2003) placed a flux upper limit of 9.4×10^{-16} erg cm^{-2} s^{-1} for the 1-0 S(1) line from V836 Tau. Our detection of H_2 emission from V836 Tau but not from V410 Tau is therefore consistent with previous studies that suggested that V836 Tau retains gas in its disk but that V410 Tau retains neither a gas nor a dust disk.

6. Discussion

Herczeg et al. (2002) found that the fluorescent H_2 emission from TW Hya is symmetric about the radial velocity of the star and is not spatially extended. They also found that the H_2 emission from TW Hya is attenuated by the wind, which constrains the origin of the emission to be close to the star. The only molecular gas known to be associated with TW Hya resides in its circumstellar disk. Therefore, the warm disk surface is a likely source for the H_2 fluorescence. However, the diverse spectral and spatial profiles of H_2 emission from other TTSs indicate that the source of H_2 emission depends on the target. Figure 2 shows no H_2 absorption against the observed Lyα emission from TW Hya, RU Lupi, or DF Tau. The Lyα emission from Mira B, which excites a similar pattern of H_2 fluoresence as seen here, shows several H_2 absorption because the warm H_2 is in our line of sight to the Lyα emission source (Wood et al. 2002). Thus, the warm H_2 is not in our line of sight to TW Hya, RU Lupi, or DF Tau. We note that TW Hya, T Tau, and RU Lupi have disks that are most likely viewed face-on, whereas DF Tau and DG Tau have disks that are viewed edge-on. Table 14 summarizes stellar properties and the properties of the H_2 fluorescence for each source.

The H_2 emission from T Tau, RU Lupi, and DG Tau is blueshifted by 10–30 km s^{-1}, which is similar to the blueshifts of H_2 emission from HH objects (Schwartz & Greene 2003) and indicates an outflow origin. The velocity of FUV H_2 emission from DG Tau is about

10 km s^{-1} larger than that of the IR H_2 emission, which is offset by 0.″2 from the star and clearly assosciated with an outflow (Takami et al. 2004). The blueshifted H_2 emission from T Tau and RU Lupi extends to -100 km s^{-1} and is not spatially extended. Detecting H_2 at such high velocities is surprising because a strong shock should destroy the H_2, given its dissociation energy of 4.5 eV. When produced in an outflow, the H_2 emission appears blueshifted regardless of whether the disk is observed edge-on or face-on. The asymmetic blueshifted emission, however, extends to a much larger velocity for the face-on CTTSs T Tau and RU Lupi than for the edge-on CTTS DF Tau. The absorption of H_2 emission by C II in the wind restricts the H_2 to be produced interior to optically thick wind absorption. Therefore, the H_2 emission from these sources is likely produced at or near the base of the outflow.

Figure 18 shows the space-velocity diagram of Hβ emission observed in our STIS G430L observation of RU Lupi. The blueshifted Hβ emission is spatially extended symmetrically about the star, as we would expect for emission from a stellar wind, a disk wind from a face-on star, or possibly from the disk itself. The SW extent of the H_2 and Lyα emission suggests that they are instead produced by a jet, possibly sweeping up nearby molecular material. Takami et al. (2001) used spectro-astrometry of RU Lupi to find that blueshifted Hα emission is displaced by 20–30 mas to the SW of the star, and blueshifted [O I] and [S II] emission is displaced by 30–300 mas to the SW of the star. Takami et al. (2001), however, also find redshifted Hα emission displaced by 30 km s^{-1} to the NE. Based on this detection, they infer that the edge-on disk of RU Lupi may have a central hole of 3–4 AU. This observational result is difficult to reconcile with the absence of either H_2 or Lyα emission extended NE from the star and the absence of any extended redshited Hβ emission.

Grady et al. (2005) found that the FUV emission from several CTTSs is extended by up to an arcsecond. This spatially extended emission may be produced either by extended H_2 gas, forward scattering by dust in a nearby nebulosity, or a jet interacting with nebulosity. In cases where only the H_2 emission from the CTTSs is extended, it is most likely related to the stellar outflows rather than the disk. The blueshifted H_2 emission may be produced where nearby nebulosity is shocked by outflows or in the dense outflows from CTTSs (e.g., Gomez de Castro & Verdugo 2001).

In their long-slit FUV spectra, Walter et al. (2003) and Saucedo et al. (2003) found that fluorescent H_2 emission is extended by at least 8″ from T Tau. This emission is most likely produced by the stellar outflows where they shock the surrounding molecular cloud. In the off-source spectrum, the only detected lines are from (v',J')=(1,4) and (1,7), which are pumped near Lyα line center, as is also the case for HH43 and HH47 (Schwartz 1983; Curiel et al. 1995). The presence of emission in these two progressions and absence of emission in

any other progression imply that the Lyα emission is relatively narrow when produced by outflows that shock the molecular gas. However, when $\log N(\mathrm{H\ I}) > 14.5$, the H I absorption at +14 km s^{-1} is optically thick. The Lyα emission that excites (1,7) must therefore be produced *in situ*. On the other hand, Walter et al. (2003) found in their long-slit spectra of T Tau that the on-source H_2 emission has a much richer spectrum, which we confirm with our echelle spectrum. The profile of the Lyα emission line that excites the on-source H_2 emission from T Tau must be broad and may be produced by accreting gas.

Like the extended emission from T Tau, we find excess blueshifted emission only in the lines from (1,4) and (1,7) in the on-source spectra of DF Tau and T Tau. The Lyα emission that irradiates this gas must be narrower than the Lyα emission that irradiates the bulk of the on-source molecular gas and may be produced in the accretion shock. The narrow Lyα emission associated with the outflow must also be produced close to the warm, blueshifted H_2 emission.

We do not detect any differences in the H_2 emission profiles from the various upper levels in the RU Lupi spectrum, even though the spatial extent of the H_2 and Lyα emission implies that they are produced in the outflow. The outflow of RU Lupi is sufficiently optically thick that extended Lyα emission is seen at +800 km s^{-1}. In contrast, the absence of spatially extended Lyα emission from TW Hya and DF Tau implies that the Lyα emission from those two sources is most likely produced by the accreting gas. Because RU Lupi has a high mass accretion rate, the accretion flow may be optically thick to Lyα emission, preventing us from detecting the Lyα emission produced by the accreting gas. Stassun et al. (2004) speculate that X-ray emission from strongly accreting CTTSs may be similarly attenuated by accreting gas. The strong outflow that produces Lyα emission from RU Lupi may also produce the blueshifted O VI 1035 Å and C III 977 Å emission detected in *FUSE* spectra, and could contribute to the complicated emission profiles of Si IV and C IV (Herczeg et al. 2005).

The bulk of the H_2 emission from DF Tau and V836 Tau is consistent with a disk origin, because the H_2 emission has the same radial velocity as the star and the bulk of the emission from DF Tau is not spatially extended. Our observations are unable to determine the spatial extent of H_2 emission from V836 Tau. The weak blueshifted H_2 emission from DF Tau is most likely associated with an outflow. The total H_2 flux from TW Hya, DF Tau, and V836 Tau is not an appropriate indicator of the total amount of H_2 present in circumstellar material, since the FUV H_2 emission is produced only in warm ($2000 - 3000$ K) molecular gas that is irradiated by a strong FUV emission source and that has a large filling factor around that source.

Irradiated by strong Lyα emission, the hot disk surface of CTTSs can produce the observed H_2 fluorescence. Therefore, it is surprising that very little if any H_2 emission in

the spectra of T Tau, RU Lupi, and DG Tau is produced at the stellar radial velocity, which suggests that fluorescent H_2 emission is not produced at the surface of their disks. T Tau, RU Lupi, DG Tau, and DF Tau all have large mass accretion rates, while TW Hya has a small mass accretion rate. V836 Tau retains a disk and may be weakly accreting. Ardila et al. (2002) found that the H_2 emission is not blueshifted from BP Tau and RY Tau, both of which have moderate mass accretion rates, or from RW Aur, which has a high mass accretion rate. The H_2 lines from the strongly accreting star DR Tau are blueshifted by 10 km s^{-1}. Moreover, the velocity shift of the H_2 emission does not appear to be correlated with dust settling or disk clearing, which is identified by the absence of excess NIR emission.

Mass loss rates from CTTSs scale with mass accretion rates (Hartigan et al. 1995). The H_2 emission from the strong accretors tend to be blueshifted, and may be produced by outflows sweeping up molecular gas that either surrounds the star or is located at the disk surface, or at the base of the wind. Most of the Lyα emission is likely produced by the accreting gas, but it may also be produced or scattered by outflows. The absence of H_2 emission from the disks of most of these strong accretors could result from the accretion flow being optically thick to the Lyα emission that is produced by the accreting gas.

Black & van Dishoeck (1987) calculated the FUV and IR H_2 emission produced by Lyα pumping of H_2. The FUV pumping of H_2 can change the level populations and, as a result, modulate the emission in IR H_2 lines. The models calculated by Black & van Dishoeck (1987) included a relatively narrow Lyα line because the *IUE* data from T Tau (Brown et al. 1981) and HH objects (Schwartz 1983) showed emission only in the H_2 lines pumped near line center. Although their generic description of the H_2 fluorescence from CTTSs is accurate, their specific results may not necessarily apply to the rich on-source H_2 emission spectra described here. Nomura & Millar (2005) revisited the relationship between FUV pumping and IR H_2 emission with a more realistic Lyα profile from TW Hya and a disk geometry to explain the emission in the strongest progressions. Their models predict H_2 excitation temperatures that are too low to explain the emission in several other progressions, but may be sufficient with additional heating by X-rays. These investigations also demonstrate that emission in IR lines from warm H_2 gas depend on the FUV emission.

7. CONCLUSIONS

We have analyzed H_2 fluorescence in high-resolution *HST*/STIS echelle spectra of the CTTSs TW Hya, RU Lupi, DF Tau, T Tau, DG Tau and the weakly accreting WTTS V836 Tau with the following results:

1. Between 41–209 H_2 lines are detected in each of these far-UV spectra. The H_2 emission is much brighter from TW Hya, RU Lupi, and DF Tau than from T Tau, DG Tau, and V836 Tau. The strength of H_2 emission depends on the amount of warm (2000–3000 K) H_2 gas in the environments around the various stars, the strength of Lyα emission, and the solid angle filling factor of H_2 around the Lyα emission. This emission does not trace the bulk of the gas in the disk, which is cold.

2. The H_2 lines are pumped from many different levels, with the strongest lines typically pumped by five transitions located between 0 to 550 km s^{-1} from Lyα line center. Several H_2 lines from all sources except T Tau are pumped by blueshifted Lyα emission, although those lines are weak in the spectra of DF Tau, RU Lupi, and V836 Tau. The H_2 lines from DF Tau and T Tau suggest that the Lyα emission irradiating the warm molecular gas around those stars is redshifted.

3. In the spectra of TW Hya and DF Tau, we find H_2 emission pumped by C IV from highly excited lower levels. This H_2 emission is consistent with $\sim 3\%$ of the warm gas having an excitation temperature of $\sim 2.5 \times 10^4$ K. The highly-excited gas could be related to the strong FUV continuum detected from TW Hya and DF Tau. RU Lupi shows neither a strong FUV continuum nor these highly excited lines. Surprisingly, many highly-excited H_2 lines that could be pumped by Lyα are not detected.

4. H_2 emission is detected from the WTTS V836 Tau, which retains a dust disk and is weakly accreting, but not from the WTTS V410 Tau, which no longer has a disk.

5. Walter et al. (2003) found that Lyα emission from T Tau is present in two G140L long-slit spectra but is absent in another long-slit spectrum and in the E140M echelle spectrum. We use the variability in H_2 lines from different upper levels to demonstrate that the width of the intrinsic Lyα profile changes, while the extinction and H I column density remain constant. We also find that the presence of H_2 emission pumped by the red wing of Lyα is correlated with Lyα emission at those wavelengths, even though our viewing angle is different than that seen by the fluorescing H_2 gas. We therefore conclude that the presence or absence of emission in the red wing of the Lyα emission profile is isotropic.

6. With the possible exception of DG Tau, the H_2 emission studied here must be produced close to the star because the bulk of the emission is not extended beyond a point source. The absorption of H_2 emission by C II in the wind requires that the H_2 emission is produced interior to the optically thick wind absorption. In cases where the Lyα is observed, the H_2 gas is not located in our line of sight to the Lyα emission region. The on-source H_2 fluorescence is excited by broad Lyα emission, in contrast to the spatially extended H_2 fluorescence detected from HH objects and the molecular complexes surrounding T Tau.

7. The H_2 lines show a diverse range of spatial and spectral profiles. The H_2 emission from RU Lupi, T Tau, and DG Tau is blueshifted, suggesting an outflow origin, while the emission from TW Hya, DF Tau and V836 Tau is centered at the radial velocity of the star, suggesting a disk origin. The H_2 lines from DF Tau, RU Lupi, and T Tau include a weak blueshifted component.

8. In the spectra of T Tau and DF Tau, the H_2 lines from the (v',J')=(1,4) and (1,7) upper levels, which are pumped near Lyα line center, have stronger excess blueshifted emission, relative to the flux in the narrow component, than the other H_2 lines pumped further from line center. The blueshifted component of these lines is likely produced in the outflow and may be pumped by Lyα emission produced *in situ* rather than in the accreting gas.

9. The H_2 and Lyα emission from RU Lupi are both extended to the SW relative to the emission in lines of C IV and Si IV, which are most likely produced by accreting gas. The H_2 and Lyα emission is presumably related to the blueshifted Hα, [O I], and [S II] emission also detected to the SW of the star by Takami et al. (2001). We speculate that the observed Lyα emission from RU Lupi, which pumps the H_2, may arise entirely in the outflow. The Lyα emission produced by the accreting gas could be absorbed by the accretion column.

10. Comparison of our STIS echelle spectra with the GHRS observations suggests that H_2 emission from T Tau, RU Lupi, and DG Tau is also extended, particularly from the levels (1,4) and (1,7), which are pumped near Lyα line center. Extended H_2 is likely produced by outflows that shock the surrounding molecular material.

11. We do not find any stellar property that reliably predicts whether the H_2 emission will be produced in the warm disk surface or the outflow. The presence or absence of blushifted H_2 emission does not appear to depend on disk evolution or environment. The absence of H_2 emission from a disk, however, tends to occur for the stars with higher mass accretion rates.

8. Acknowledgements

This research was funded in part by STScI programs GTO-7718, GTO-8041, and GO-8157 to the University of Colorado and to SUNY Stony Brook, and by the Swedish National Space Board. This paper is based on observations made by the NASA/ESA Hubble Space Telescope, obtained at the Space Telescope Science Institute, which is operated by the Association of Universities for Research in Astronomy, Inc., under NASA contract NAS5-26555. This research was also funded in part by the STScI program AR-9930 to the University of

Colorado and by NASA program S-56500-D to the University of Colorado.

We thank the anonymous referee for valuable suggestions. We also thank Ilya Ilyin, who obtained our *NOT* observations and reduced the spectrograms. GJH thanks Carol Grady for valuable discussion concerning the spatial distribution of emission from several other CTTSs, and Gail Schaefer for valuable discussion regarding the position of DF Tau in the aperture.

REFERENCES

Abgrall H., Roueff, E., Launay, F., Roncin, J. Y., & Subtil, J. L. 1993, A&AS, 101, 273

Abgrall H., Roueff, E., & Drira, I. 2000, A&AS, 141, 297

Anderson, J.M., Li, Z.-Y., Krasnopolsky, R., & Blandford, R.D. 2003, ApJ, 590, 107L

Ardila, D.R., Basri, G., Walter, F.M., Valenti, J.A., Johns-Krull, C.M. 2002, ApJ, 566, 1100

Ardila, D.R., Basri, G., Walter, F.M., Valenti, J.A., Johns-Krull, C.M. 2002, ApJ, 567, 1013

Bacciotti, F., Ray, T.P, Mundt, R., Eislöffel, J., & Solf, J. 2002, ApJ, 576, 222

Bary, J.S., Weintraub, D.A., & Kastner, J.H. 2003, ApJ, 586, 1136

Beck, T.L., Schaefer, G.H., Simon, M., Prato, L., Stoesz, J.A., & Howell, R.R. 2004, ApJ, 614, 235

Beckwith, S. V. W., Gatley, I., Matthews, K., & Neugebauer, G. 1978, ApJ, 223, L41

Bergin, E., et al. 2004, ApJ, 614, L133

Bertout, C., Robichon, N., & Arenou, F. 1999, A&A, 352, 574

Bieniek, R.J., & Dalgarno, A. 1979, ApJ, 228, 635

Black, J.H., van Dishoeck, E.F. 1987, ApJ, 322, 412

Bohlin, R.C., Savage, B.D., & Drake, J.F. 1978, ApJ, 224, 132

Bouret, J.-C., Martin, C., Deleuil, M., Simon, T., & Catala, C. 2003, A&A, 410, 175

Brittain, S.D., Rettig, T.W.; Simon, T., Kulesa, C., DiSanti, M.A., & Dello Russo, N. 2003, ApJ, 588, 535

Brown, A. Jordan, C., Millar, T. J., Gondhalekar, P., & Wilson, R. 1981, Nature, 290, 34

Calvet, N., D'Alessio, P., Hartmann, L., Wilner, D., Walsh, A., & Sitko, M. 2002, ApJ, 568, 1008

Calvet, N., Muzerolle, J., Briceno, C., Hernandez, J., Hartmann, L., Saucedo, J.L., & Gordon, K.D. 2004, AJ, 128, 1294

Cardelli, J. A., Clayton, G. C., & Mathis, J. S. 1989, ApJ, 345, 245

Carr, J.S., Tokunaga, A.T., & Najita, J. 2004, ApJ, 603, 213

Curiel, S., Raymond, J.C., Wolfire, M., Hartigan, O., Morse, J., Schwartz, R.D., & Nisenson, P. 1995, ApJ, 453, 322

D'Alessio, P., et al. 2005, ApJ, 621, 461

Duchene, G., Ghez, A.M., McCabe, C., & Ceccarelli, C. 2005, ApJ, accepted

Duvert, G., Guilloteau, S., Ménard, F., Simon, M., & Dutrey, A. 2000, A&A, 355, 165

Draine, B.T. 2003, ApJ, 598, 1017

Eislöffel, J., & Mundt, R. 1998, AJ, 115, 1554

Fernández, M., Stelzer, B., Henden, A., Grankin, K., Gameiro, J.F., Costa, V.M., Guenther, E., Amado, P.J., & Rodriguez, E. 2004, A&A, 427, 263

Furlan, E., et al. 2005, ApJ, 628, L65

Gahm G. F., Petrov, P. P., Stempels, H. C. 2005, in Proc. 13th Cambridge Workshop on Cool Stars, Stellar Systems and the Sun, eds. F. Favata, et al., p. 563

Giovannelli, F. et al. 1995, A&AS, 114, 341

Gizis, J.E., Shipman, H.L., & Harvin, J.A. 2005, ApJ, 630, L89

Glassgold, A.E., Najita, J., & Igea, J. 2004, ApJ, 615, 972

Gomez de Castro, A.I., & Verdugo, E. 2001, ApJ, 548, 976

Grady, C. et al. 2004, ApJ, 608, 809

Grady, C. et al. 2005, ApJ, submitted

Güdel, M., Audard, M., Skinner, S., & Smith, K. 2004, proceedings of *Cores, Disks, Jets, and Outflows 2004*

Güdel, M., Skinner, S.L., Briggs, K.R., Audard, M., Arzner, K., & Telleschi, A. 2005, ApJ, 626, L53

Gullbring, E., Hartmann, L., Briceno, C., & Calvet, N. 1998, ApJ, 492, 323

Gullbring, E., Calvet, N., Muzerolle, J., & Hartmann, L. 2000, ApJ, 544, 927

Hartigan, P., Edwards, S., & Ghandour, L. 1995, ApJ, 452, 736

Hartigan, P., & Kenyon, S.J. 2003, ApJ, 583, 334

Hartigan, P., Edwards, S., & Pierson, R. 2004, ApJ, 609, 261

Hartmann, L. & Stauffer, J.R. 1989, AJ, 97, 873

Herbig, G.H., Bell, K.R. 1988, Lick Observatory Bull., No. 1111

Herbst, T.M., et al. 1986, ApJ, 310, L71

Herbst, T.M., Beckwith, S.V.W., Glindemann, A., Tacconi Garman, L.E., Kroker, H., & Krabbe, A. 1996, AJ, 111, 2403

Herbst, T.M., Robberto, M., & Beckwith, S.V.W. 1997, AJ, 114, 744

Herczeg, G. J., Linsky, J. L., Valenti, J.A., Johns-Krull, C.M. 2002, ApJ, 572, 310 (Paper I)

Herczeg, G.J., Wood, B.E., Linsky, J.L., Valenti, J.A., Johns-Krull, C.M. 2004, ApJ, 607, 369

Herczeg, G.J.,et al. 2005, AJ, 129, 2777

Johns-Krull, C. M., Valenti, J. A., & Linsky, J. L. 2000, ApJ, 539, 815

Johns-Krull, C. M. & Valenti, J. A. 2001, ApJ, 561, 1060

Kastner, J.H., Zuckerman,B., Weintraub, D.A., & Forveille, T. 1997, *Science*, 277, 5322

Kenyon, S.J., & Hartmann, L. 1995, ApJS, 101, 117

Kokoouline, V., Greene, C.H., & Esry, B.D. 2001, Nature, 412, 891.

Koresko, C.D., Herbst, T.M., & Leinert, C. 1997, ApJ, 480, 741

Krist, J.E., et al. 1995, BAAS, 187, 4413

Krist, J. E., Stapelfeldt, K. R., Ménard, F., Padgett, D. L., & Burrows, C. J. 2000, ApJ, 538, 793

Lecavelier des Etangs, A. et al. 2001, *Nature*, 412, 706

Lecavelier des Etangs, A. et al. 2003, A&A, 407, 935

Leitherer, C., et al. 2001, STIS Instrument Handbook, Version 5.1 (Baltimore: STScI)

Lindler, D. 1999, CALSTIS Reference Guide (Greenbelt: NASA/LASP)

Liu, W. & Dalgarno, A. 1996, ApJ, 467, 446

Loinard, L., Mioduszewski, A.J., Rodríguez, L.F., González, R.A., Rodríguez, M.I., Torres, R.M. 2005, ApJ, 619, L179

Martin, C., Bouret, J.-C., Deleuil, M., Simon, T., & Catala, C. 2004, A&A, 416, L5

Martin-Zaïdi, C., Deleuil, M., Simon, T., Bouret, J.-C., Roberge, A., Feldman, P.D., Lecavelier des Etangs, A., & Vidal-Madjar, A. 2005, A&A, 440, 921

Mundt, R., Walter, F.M., Feigelson, E.D., Finkenzeller, U., Herbig, G.H., & Odell, A.P. 1983, ApJ, 269, 229

Najita, J., Carr, J.S., & Mathieu, R.D. 2003, ApJ, 589, 931

Nomura, H., & Millar, T.J. 2005, A&A, accepted

Qi, C., et al. 2004, ApJ, 616, 11L

Raymond, J. C., Blair, W. P., & Long, K. S. 1997, ApJ, 489, 314

Rettig, T.W., Haywood, J., Simon, T., Brittain, S.D., & Gibb, E. 2004, ApJ, 616, 163L

Richter, M.J., Jaffe, D.T., Blake, G.A., & Lacy, J.H. 2002, ApJ, 572, 161

Richter, M.J., Lacy, J.H., Greathouse, T.K., Jaffe, D.T., & Blake, G.A. 2004, astro-ph/0403349

Roberge, A., et al. 2001, ApJ, 551, L97

Roberge, A., et al. 2005, accepted by ApJL

Rydgren, A. E., & Vrba, F. J. 1983, ApJ, 267, 191

Sako, S., Yamashita, T., Kataza, H., Miyata, T., Okamoto, Y.K., Honda, M., Fujiyoshi, T., & Onaka, T. 2005, ApJ, 620, 347

Saucedo, J., Calvet, N., Hartmann, L., & Raymond, J.C. 2003, ApJ, 591, 275

Schwartz, R.D. 1983, ApJ, 268, L37

Schwartz, R.D., & Greene, T.P. 2003, AJ, 126, 399

Shaefer, G.H., Simon, M., Nelan, E., & Holfeltz, S.T. 2003, AJ, 126, 1971

Sheret, I., Ramsay Howat, S.K., & Dent, W.R.F. 2003, 343, L65

Simon, M., & Prato, L. 1995, ApJ, 450, 824

Skinner, S.L., & Brown, A. 1994, AJ, 107, 1461

Skinner, S.L., Brown, A., & Walter, F.M. 1991, AJ, 102, 1742

Skrutskie, M.F., Dutkevitch, D., Strom, S.E., Edwards, S., Strom, K.M., & Shure, M.A. 1990, AJ, 99, 1187

Solf, J., & Böhm, K.-H. 1999, ApJ, 523, 709

Stapelfeldt, K.R., et al. 1998, ApJ, 508, 736

Stassun, K.G., Ardila, D.R., Barsony, M., Basri, G., & Mathieu, R.D. 2004, AJ, 127, 3537

Stelzer, B., Fernández, M., Costa, V.M., Gameir, J.F., et al. 2003, A&A, 411, 517

Stempels H.C., & Piskunov, N. 2002, A&A, 391, 595

Stempels, H.C., Gahm, G.F., Petrov, P.P. 2005, A&A, accepted

Takahashi, J., Masuda, K., & Nagaoka, M. 1999, ApJ, 520, 724

Takami, M., Bailey, J., Gledhill, T.N., Chrysostomou, A., & Hough, J.H. 2001, MNRAS, 323, 177

Takami, M., Chrysostomou, A., Ray, T.P., Davis, C., Dent, W.R.F., Bailey, J., & Terada, H. 2004, A&A, 416, 213

Thi, W. F., et al., 2001, ApJ, 561, 1074

Trilling, D. E., Koerner, D. W., Barnes, J. W., Ftaclas, C., & Brown, R. H. 2001, ApJ, 552, 151

van Langevelde, H. J., van Dishoeck, E. F., van der Werf, P. P., & Blake, G. A. 1994, A&A, 287, L25

Valenti, J.A., Basri, G., & Johns, C.M. 1993, ApJ, 106, 2024

Valenti, J. A., Johns-Krull, C. M., & Linsky, J. L. 2000, ApJS, 129, 399

Walter, F.M., et al. 2003, AJ, 126, 3076

Walter, F.M. 2004, AN, 325, 241

Webb, R. A., Zuckerman, B., Patience, J., White, R. J., Schwartz, M. J., McCarthy, C., & Platais, I. 1999, ApJ, 512, L63

Weinberger, A. J., Becklin, E. E., Schneider, G., Chiang, E. I., Lowrance, P.J., Silverstone, M., Zuckerman, B., Hines, D. C. & Smith, B. A. 2002, ApJ, 566, 409

Weintraub, D. A., Kastner, J. H. & Bary, J. S. 2000, ApJ, 541, 767

White, R.J., & Ghez, A.M. 2001, ApJ, 556, 265

White, R.J., & Hillenbrand, L.A. 2004, ApJ, 616, 998

Wilkinson, E., Harper, G. H., Brown, A., & Herczeg, G. J. 2002, AJ, 124, 1077

Wilner, D. J., Ho, P. T. P., Kastner, J. H., & Rodriguez, L. F. 2000, ApJ, 534, L101

Wolk, S.J., & Walter, F.M. 1996, AJ, 111, 2066

Wood, B. E., Karovska, M. & Raymond, J. C. 2002, ApJ, 575, 1057

de Zeeuw, P.T., Hoogerwerf, R., de Bruijne, J.H.J, Brown, A.G.A., & Blaauw, A. 1999, AJ, 117, 354

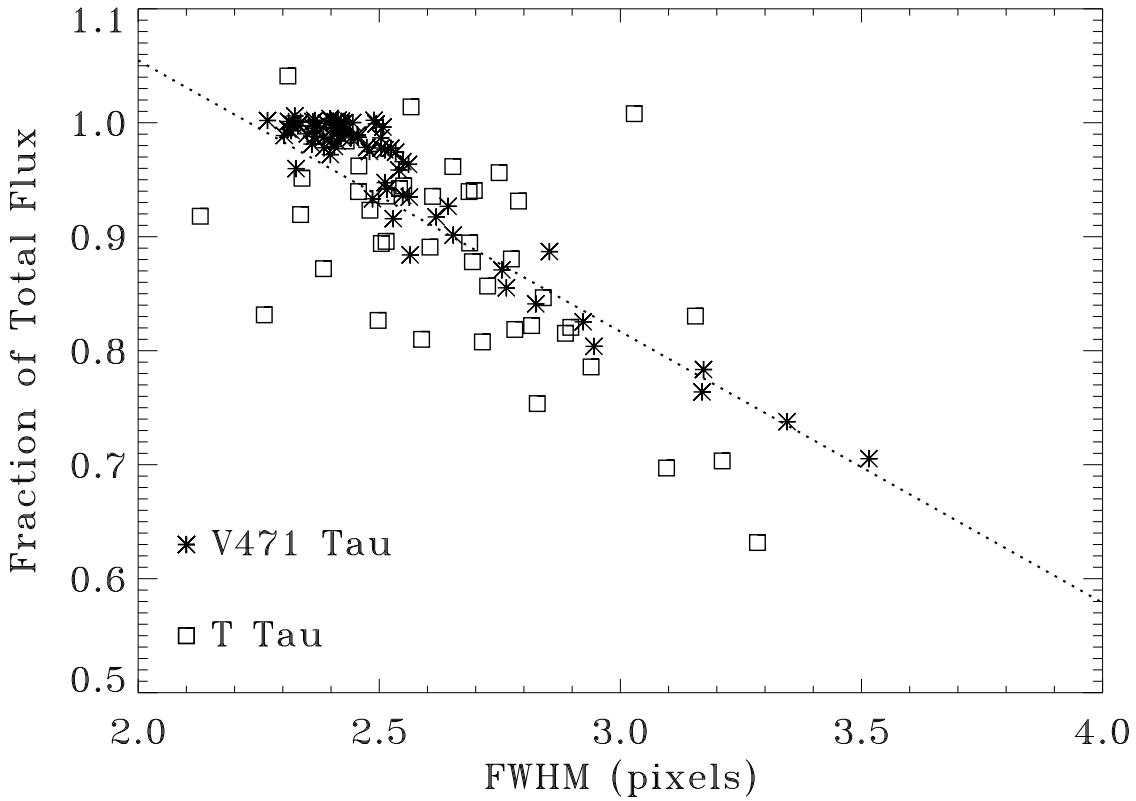

Fig. 1.— The dependence of count rate on the telescope focus. Changes in the telescope focus due to thermal variations alter the count rate in our observations of T Tau because the point-spread function may be wider than the aperture. We calibrate the observed flux by comparing the measured point-spread function and the flux in 300s time intervals. The point-spread function is the average of the point-spread functions measured in four spectral regions with strong emission lines in the T Tau spectrum (O I 1305 triplet, C II 1335 Å doublet, Si IV 1400 Å doublet, and C IV 1549 Å doublet). The FUV spectrum of V471 Tau is dominated by continuum emission from the white dwarf. We find the best-fit slope from the V471 Tau data and scale the T Tau data to calculate the total flux.

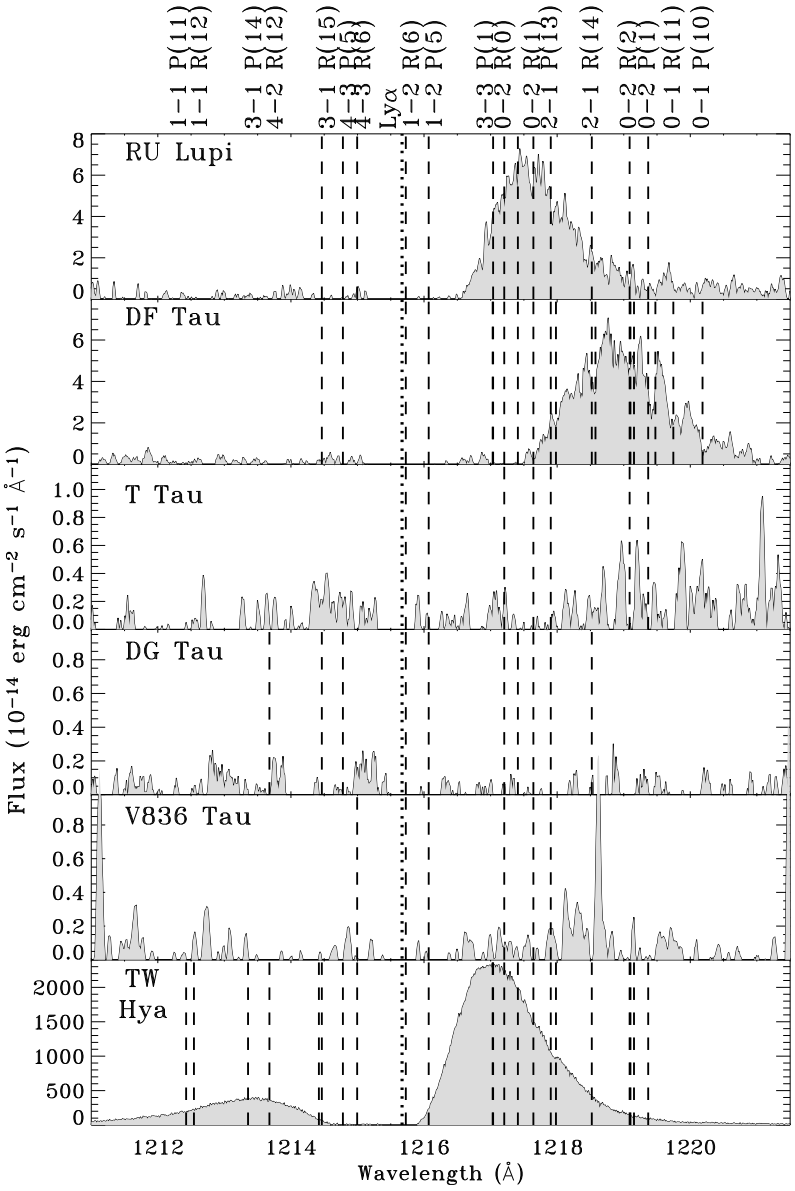

Fig. 2.— Observed Lyα emission from TTSs (shaded). The detected Lyα emission from TW Hya is strong because the H I column density in our line of sight is small. DF Tau and RU Lupi also show some Lyα emission, while the Lyα emission from T Tau, DG Tau, and V836 Tau is completely attenuated in our line of sight by H I in the wind and interstellar medium. The vertical dashed lines, most of which are labeled at the top, indicate the transitions that excite H_2 emission for each star. The broad Lyα emission from DF Tau pumps H_2 emission primarily in its red wing. Except for TW Hya, the stars show few or no H_2 lines pumped by emission shortward of Lyα line center.

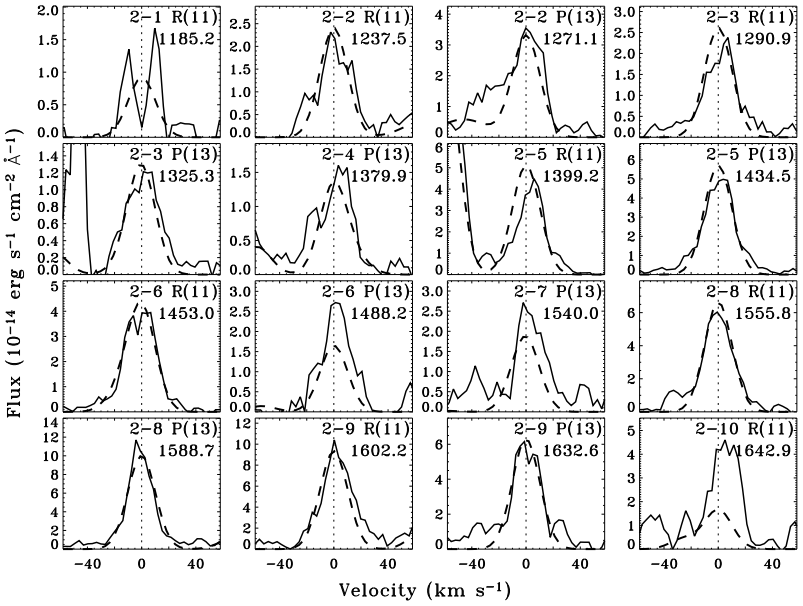

Fig. 3.— 16 H_2 lines from the upper level (v',J')=(2,12) in the STIS observation of DF Tau obtained with the $0\farcs5 \times 0\farcs5$ aperture. The predicted relative fluxes (dashed lines) described in §4.2 are scaled to the observed fluxes and fit the observed emission (solid lines) well. Several lines, such as the 2-1 R(11) line at 1185 Å, are weak and only identified as H_2 because the models predict the presence of emission at these wavelengths. The 2-10 R(11) line at 1642.9 Å may be blended with an Fe II line.

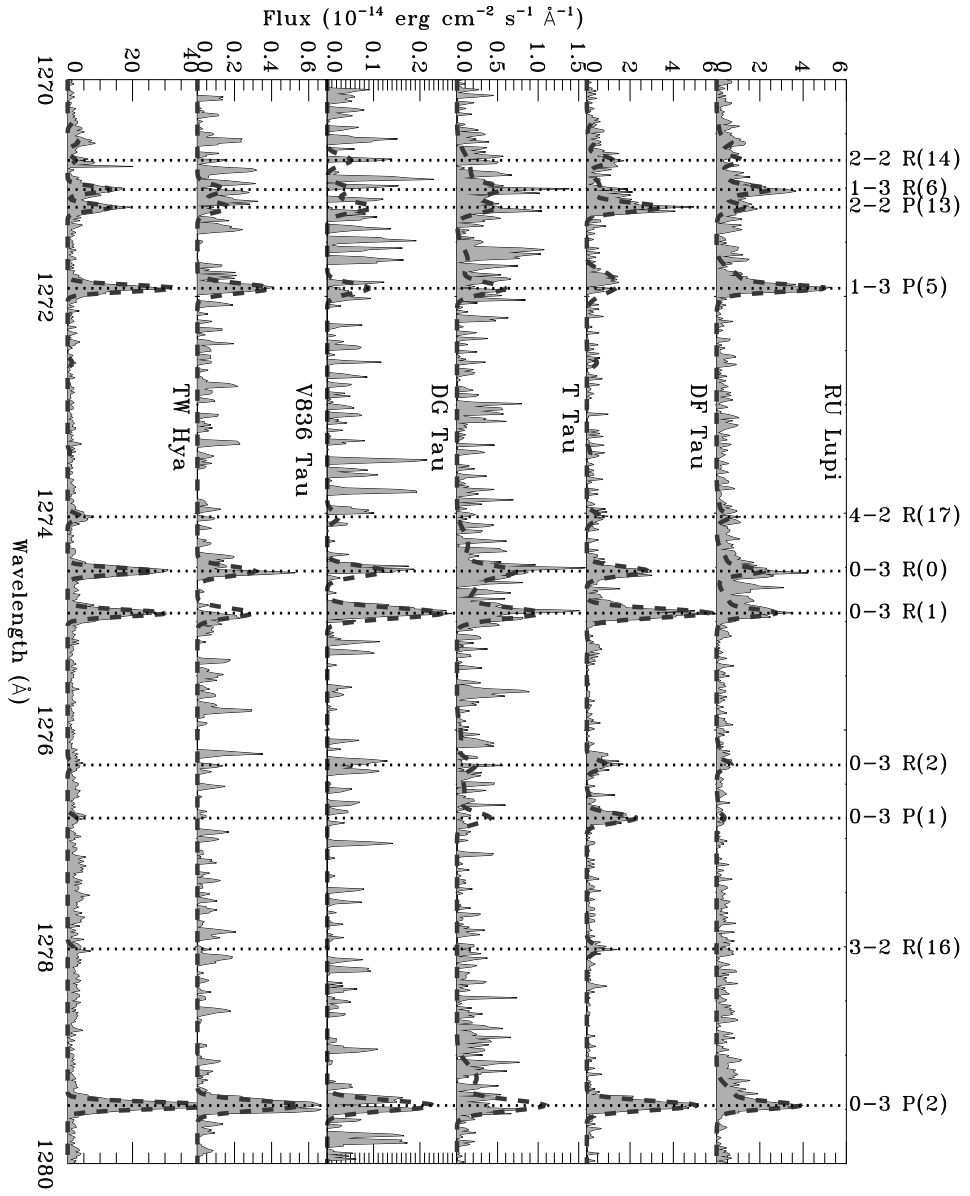

Fig. 4.— The spectral region from 1270–1276 Å for six stars. We display the observation of DF Tau obtained with the $0\farcs5 \times 0\farcs5$ aperture. The observed emission (shaded) is shifted in wavelength so that the H_2 lines occur at the theoretical wavelengths calculated by Abgrall et al. (1993). The model H_2 spectrum (dashed line), described in §4.2, well fits the observed H_2 lines, several of which are identified.

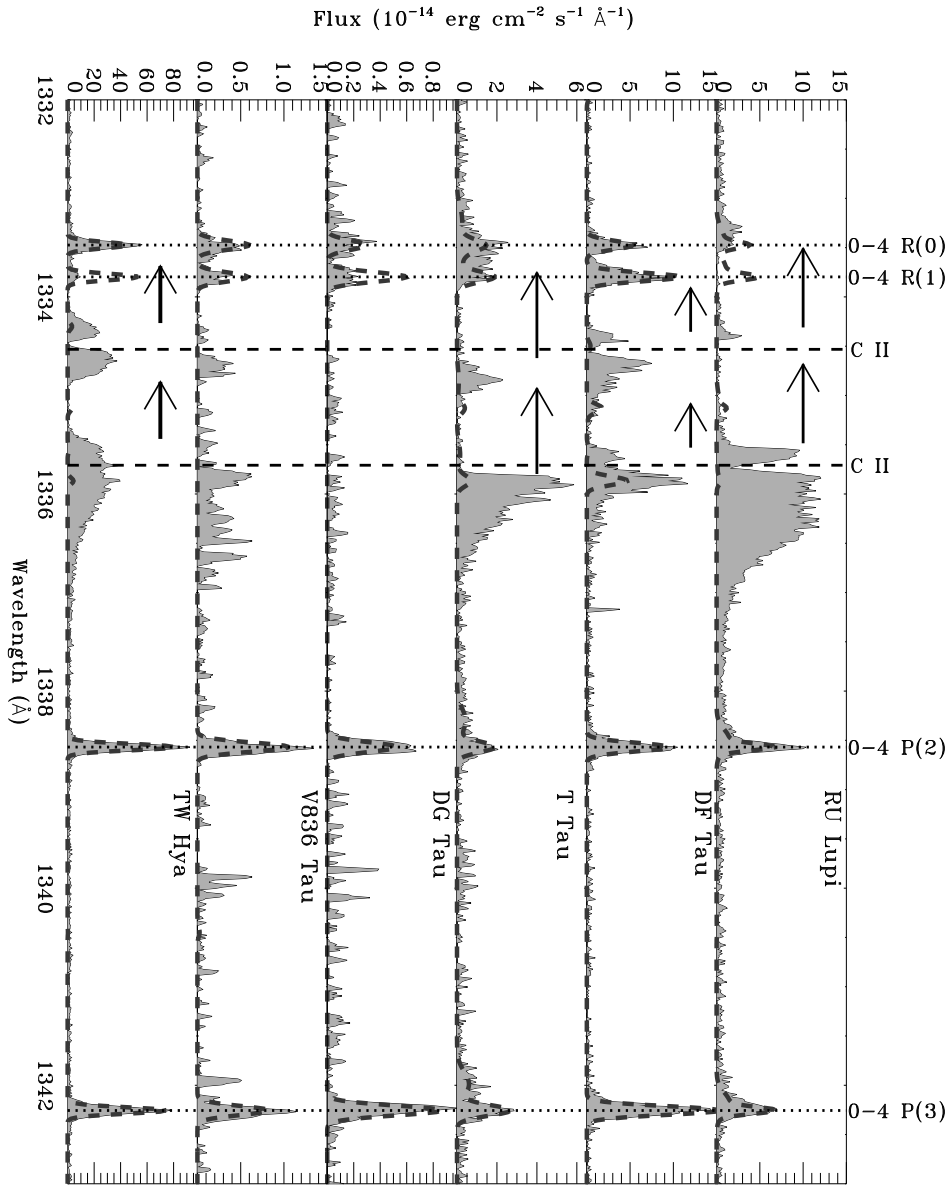

Fig. 5.— Same as Figure 4 for the spectral region 1332–1343 Å. This region is dominated by the C II doublet, as seen in strong redshifted emission and blueshifted absorption. The wavelength extent of wind absorption in both the C II 1334.5 and the C II 1335.7 Å lines is shown by the arrows. The narrow absorption feature near line center of C II is produced by the interstellar medium.

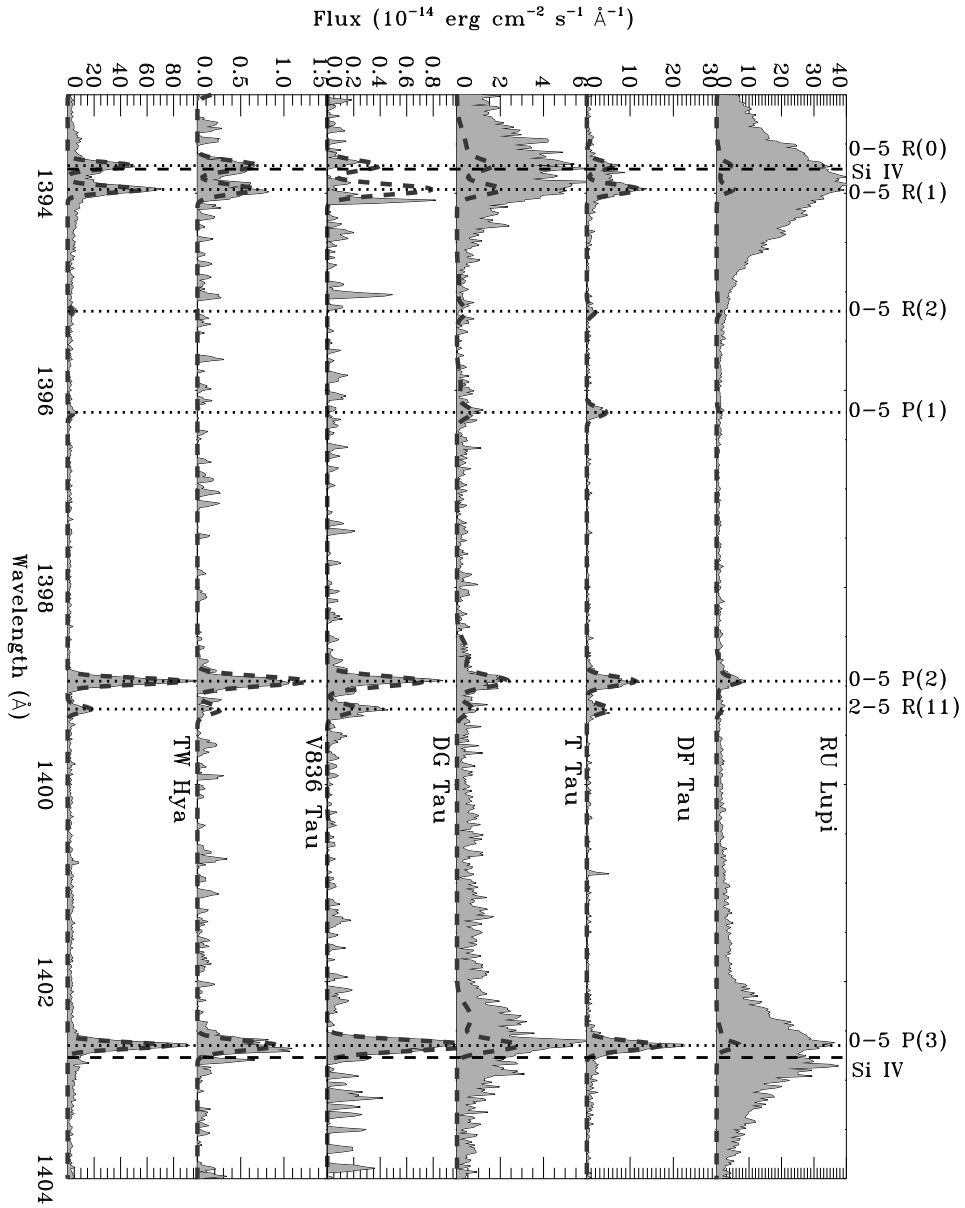

Fig. 6.— Same as Figure 4 for the spectral region 1393–1404 Å. The Si IV resonance doublet can be quite strong and mask several H_2 emission lines, as is seen in the RU Lupi and T Tau spectra. In the spectra of DF Tau and TW Hya, Si IV emission is weak and the region is instead dominated by strong H_2 lines.

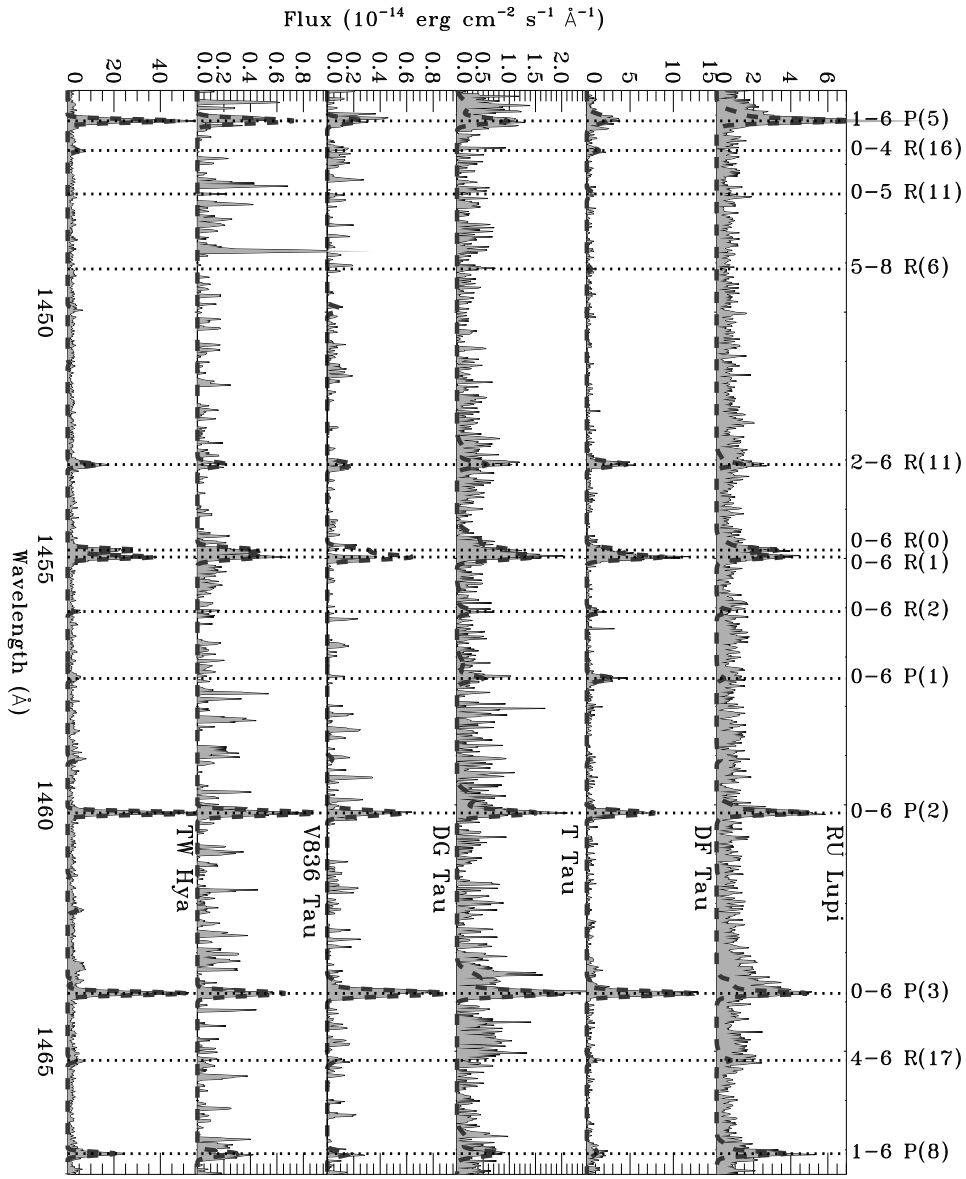

Fig. 7.— Same as Figure 4 for the spectral region 1453–1467 Å.

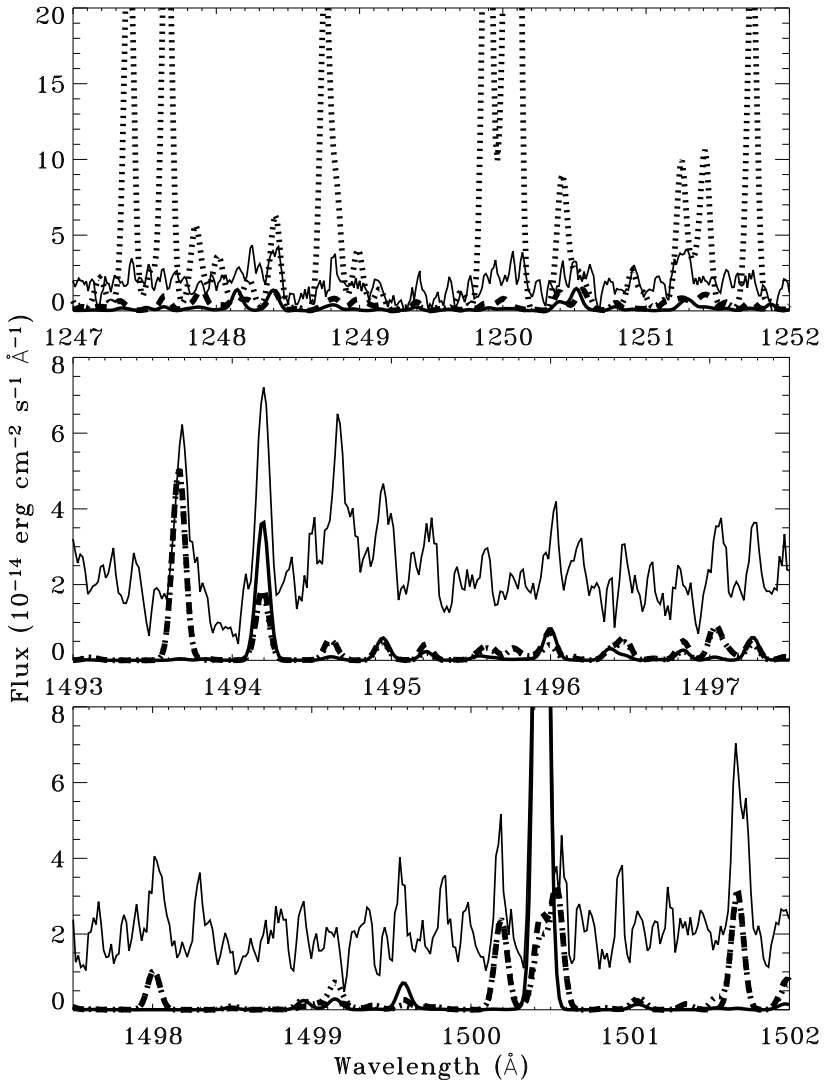

Fig. 8.— Synthetic H_2 emission spectra, estimated by calculating FUV pumping, compared to the observed spectrum of TW Hya (thin solid line). The synthetic spectra are calculated by simulating H_2 fluorescence in a plane-parallel slab of H_2 with $T = 2500$ K and $\log N(H_2)$=18.5 (thick solid line) and two models an additional layer of highly excited H_2 emission with $T = 2.5 \times 10^4$ K and $\log N(H_2)$=17 (dashed and dotted lines). All of the models include pumping throughout the FUV, although one model (dashed lines) does not include any pumping by Lyα. Lines at 1493.7, 1498.0, 1500.2, and 1501.7 require highly excited H_2 gas. However, if Lyα irradiates this highly excited gas, we would expect to see many lines that are not present in the data (dotted lines in top panel).

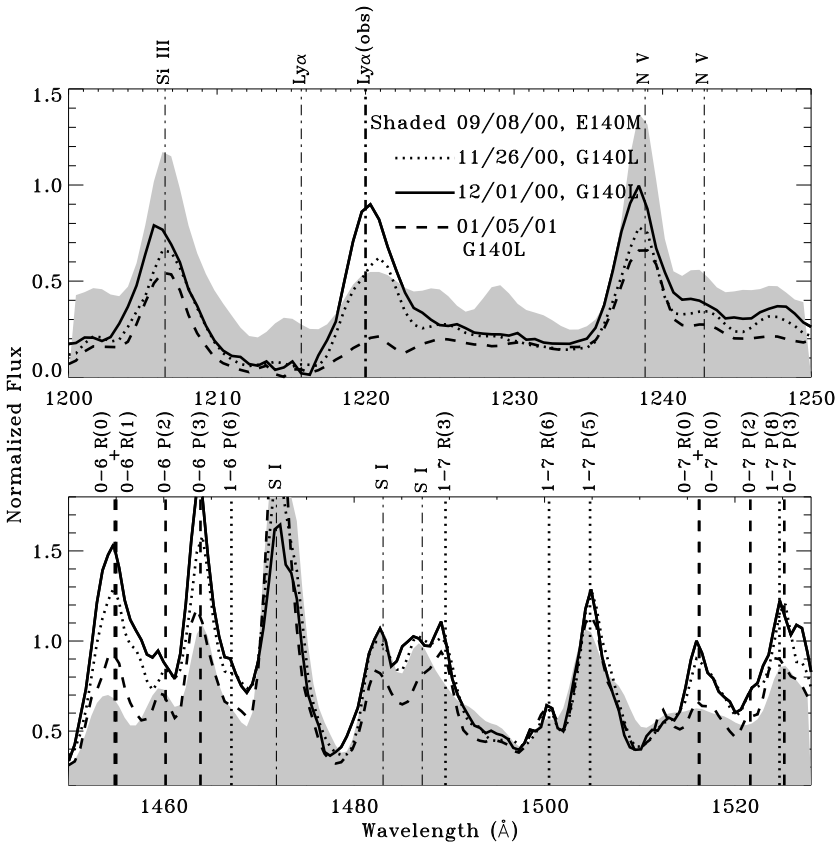

Fig. 9.— Lyα and H_2 emission in four spectra of T Tau, scaled by the flux between 1495–1510 Å. We previously obtained three long-slit G140L spectra of T Tau, with dates labeled (Walter et al. 2003). We convolve the E140M echelle spectrum (shaded) to the resolution of G140L ($R = 1000$). The Lyα emission is strong in the observations obtained on 11/26/00 and 12/01/00 but is not present in the echelle spectrum (the apparant bump at 1220 Å is noise, see Fig. 2) or the spectrum obtained on 01/05/01. As can be seen at 1455–1465 Å and 1515–1525 Å, when Lyα emission is not present the H_2 emission from (v',J')=(0,1) and (0,2), marked by dashed vertical lines are much weaker relative to the H_2 emission from (1,4) and (1,7), marked by the dotted vertical lines. Because lines from (0,1) and (0,2) are pumped by the red wing of Lyα, we infer that the intrinsic Lyα profile is narrower during those observations.

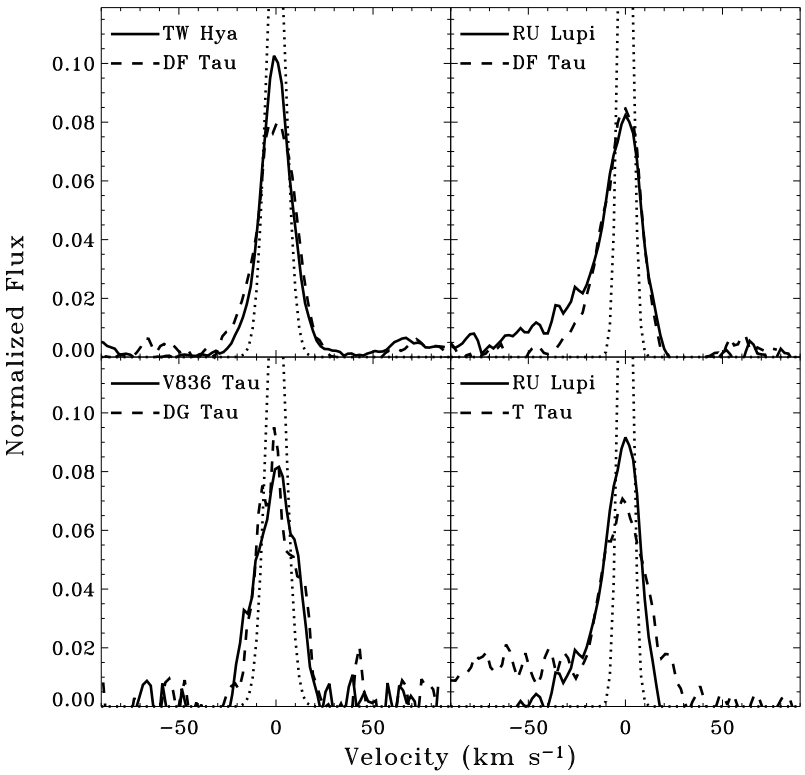

Fig. 10.— Spectral profiles of H_2 lines from upper levels (v',J')=(0,1), (0,2), and (2,12), shifted in velocity so that line center is at $v = 0$. The H_2 lines from RU Lupi, DF Tau, and T Tau all show a significant blueshifted component. Dotted lines indicate the instrumental line-spread function. The blueshift from DF Tau is evident in both observations, which had PA that differed by 180°, so the blueshift is real and not a spatial displacement of the secondary star in the dispersion direction.

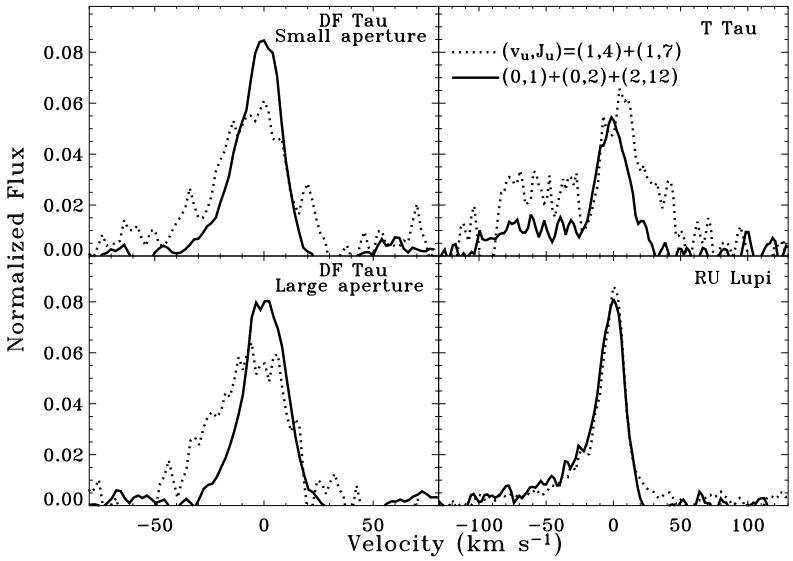

Fig. 11.— Spectral profiles of H_2 lines from upper levels (v',J')=(0,1), (0,2), and (2,12) (solid lines), which are pumped on the red wing of Lyα, compared with spectral profiles of H_2 emission from (1,4) and (1,7) (dotted lines), which are pumped near line center of Lyα. The lines pumped near Lyα line center, from (1,4) and (1,7), in the T Tau and DF Tau spectra show excess blueshifted emission, relative to the flux in the narrow component, than is seen in lines from (0,1), (0,2), and (0,12). The same lines from T Tau also show some excess redshifted emission. We do not detect any significant difference in emission line profiles for the different progressions in any other star, as illustrated here by RU Lupi.

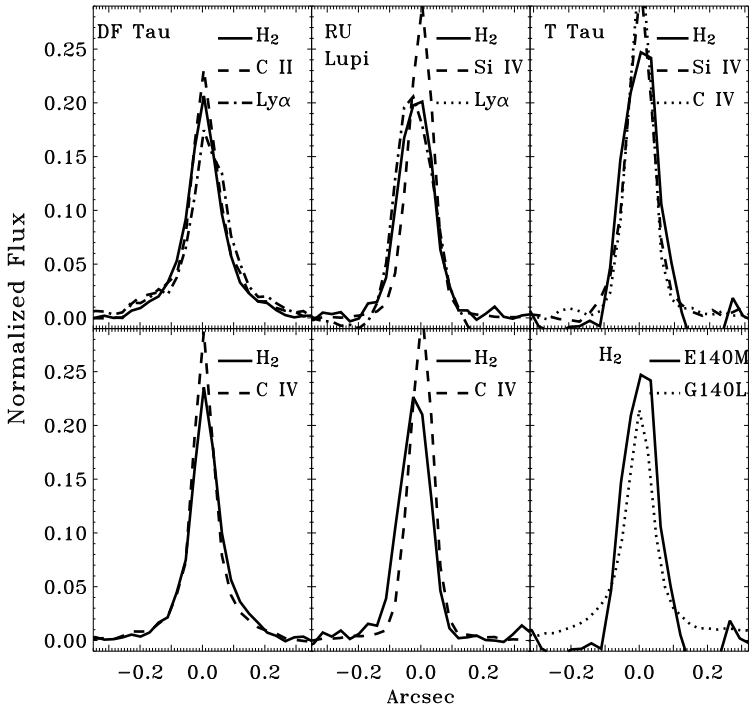

Fig. 12.— The spatial extent of selected emission lines in the cross-dispersion direction. The top left and center panels compare the spatial profiles of coadded H_2 lines between $1270 < \lambda < 1400$ Å with H I Lyα 1215.67 Å, the Si IV 1400 Å doublet, and the C II 1335 Å doublet, while the bottom left and center panels compare the spatial profiles of coadded H_2 lines between $1500 < \lambda < 1650$ Å with the C IV 1549 Å doublet. For T Tau (right panels), we coadd all H_2 lines for comparison with the other emission lines to increase S/N and because the point-spread function during that observation appears constant with wavelength. The H_2 emission from DF Tau is not significantly extended, while the H_2 and Lyα emission are clearly extended in one direction toward RU Lupi. The H_2 emission from T Tau may be slightly extended.

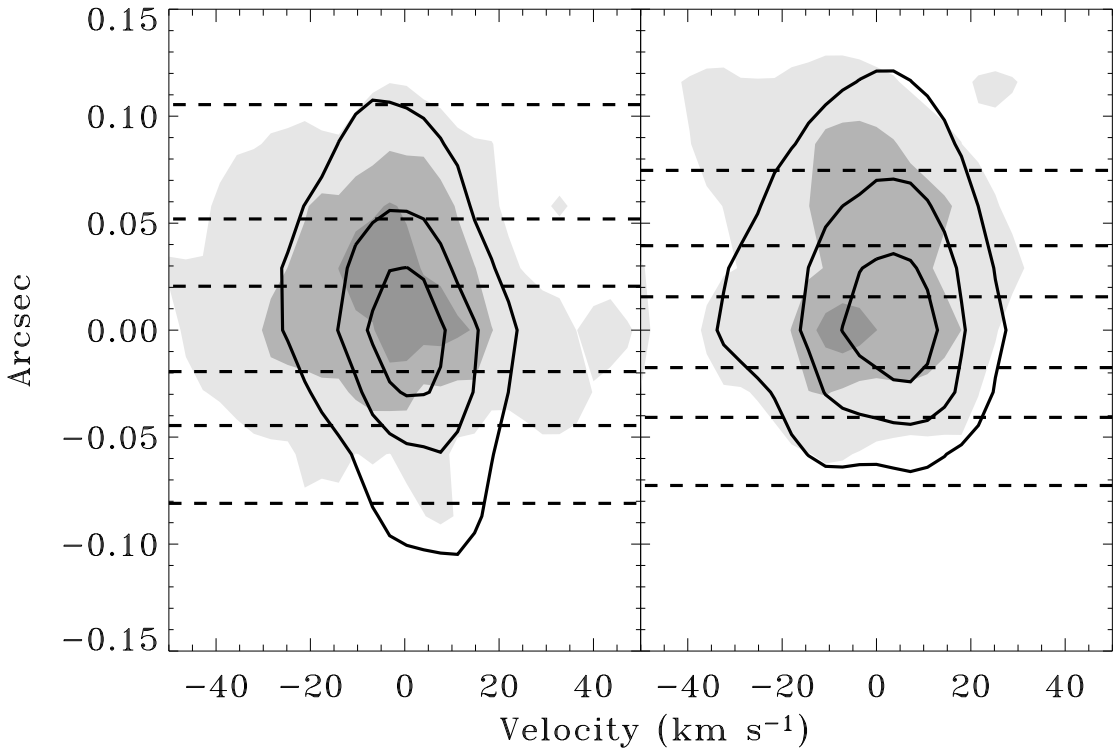

Fig. 13.— The space-velocity diagram of background-subtracted H_2 emission from DF Tau for the large (left) and small (right) aperture observations. The solid lines are contours of 0.2, 0.5, and 0.8 times the peak flux for H_2 lines from (v',J')=(0,1), (0,2), and (2,12), while the shaded regions are similar contours for (1,4) and (1,7). The background was calculated by coadding background regions nearby each of the H_2 lines. The contours of C II emission (dashed lines on left) and C IV emission (dashed lines on right) indicate the point-spread function during the two observations. The H_2 lines from the progressions pumped near line center [(1,4) and (1,7)] are clearly blueshifted, and also appear to be slightly extended to the SW (up in this figure).

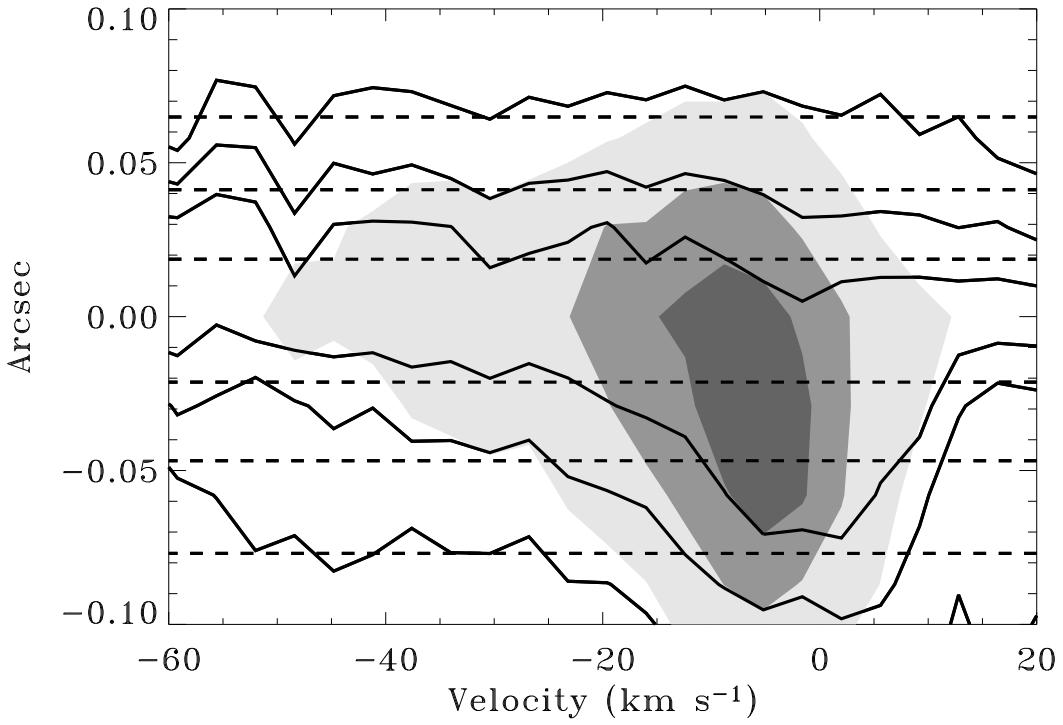

Fig. 14.— The space-velocity diagram of background-subtracted H_2 emission from RU Lupi. Flux contours of 0.2, 0.5, and 0.8 times the peak flux in any pixel (shaded regions) show where most of the H_2 emission occurs. The flux contours of 0.2, 0.5, and 0.8 times the peak flux in a pixel at that particular velocity (solid lines) display the spatial extent of emission across the line profile. The dashed lines represent the point-spread function measured from Si IV emission. These contours show that the H_2 emission at $v = -15$ km s^{-1} is spatially extended to the SW (down in this figure). However, the H_2 emission at $v < -25$ km s^{-1} is not extended beyond a point source. The spatial profile at $v = -15$ km s^{-1} is consistent with 70% of the H_2 originating on-source and 30% of the emission either being produced smoothly across the aperture or in a point source, located at ~ 70 mas from the star.

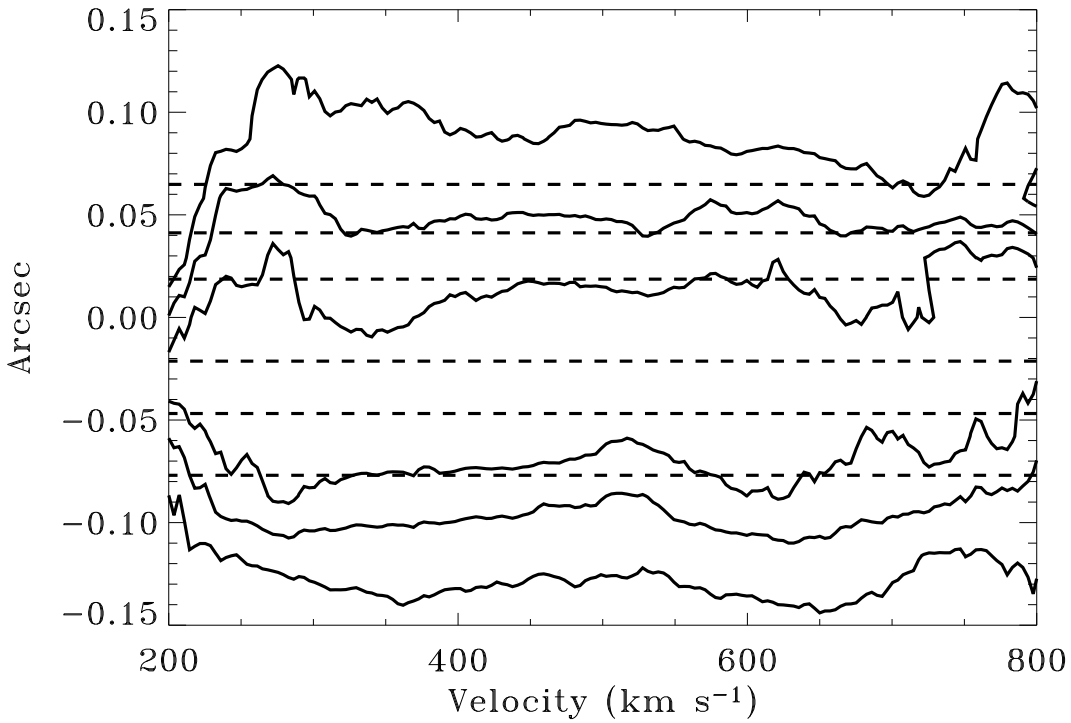

Fig. 15.— The spatial extent of Lyα emission toward RU Lupi, smoothed by 75 km s^{-1}. The solid lines show the flux contours of 0.2, 0.5, and 0.8 times the peak emission at that velocity. The dashed lines show the point-spread function of the observation, measured from Si IV emission. The Lyα emission is clearly extended in the SW direction (down in this figure), which matches the spatial extent of the H_2 emission. The amount of spatially extended emission does not depend on velocity from line center.

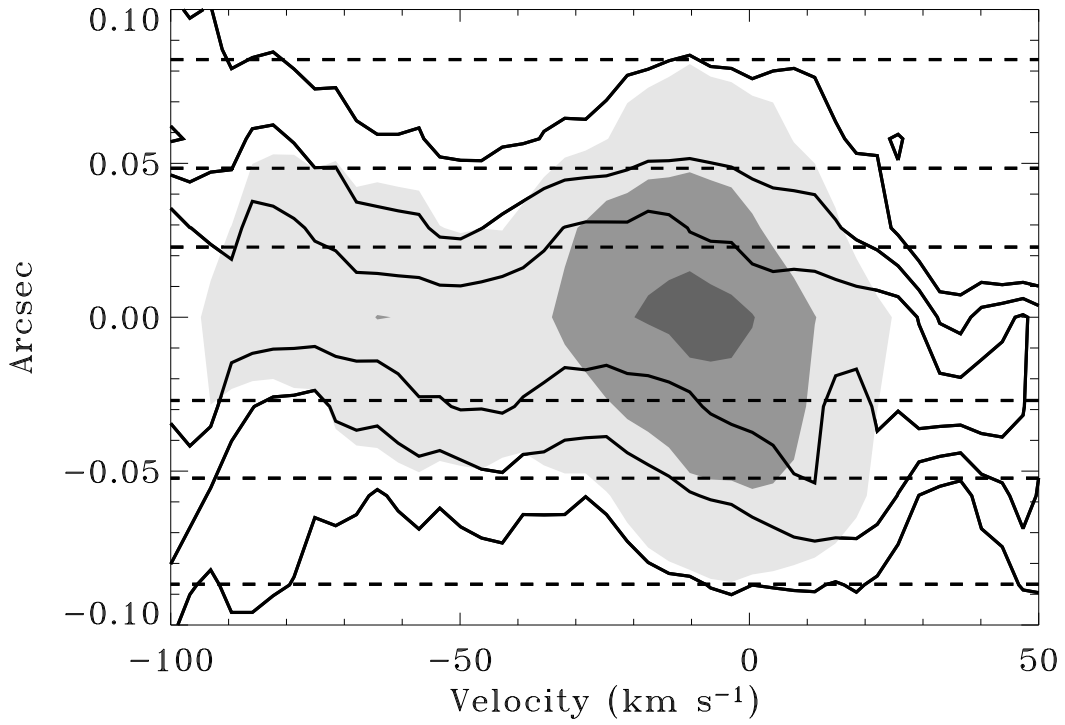

Fig. 16.— Same as Fig. 14, except for T Tau. The edge of the plot, particularly at $v = 40$ km s^{-1}, is dominated by noise and unreliable.

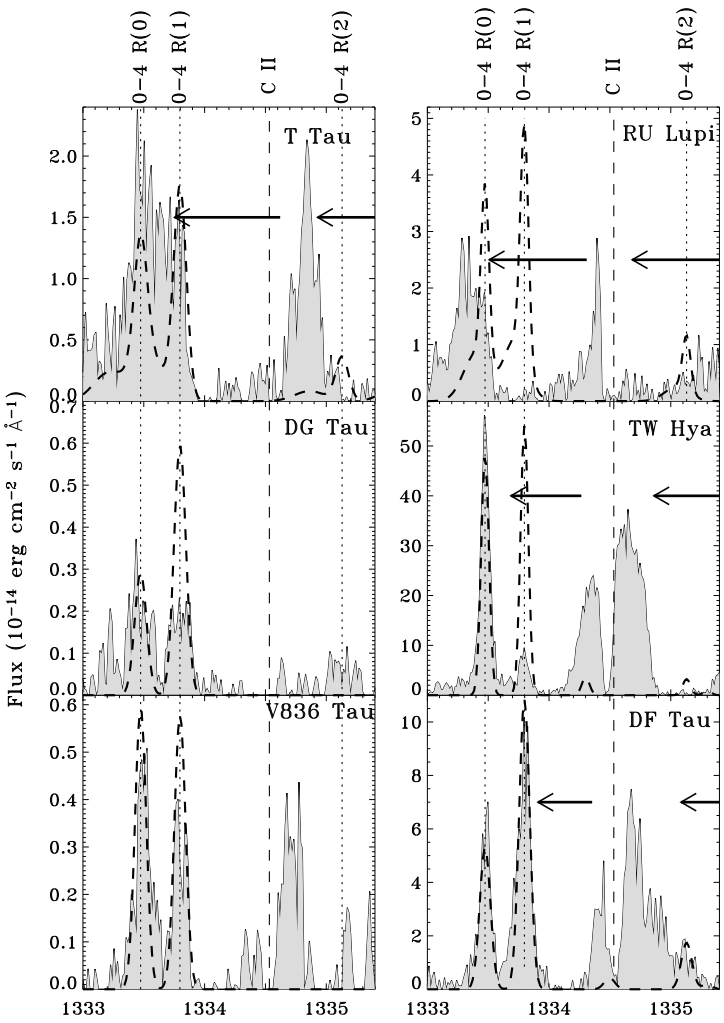

Fig. 17.— Same as Figure 4, except expanding a narrow spectral region. C II wind absorption from some sources, such as T Tau and RU Lupi, attenuates much of the otherwise strong C II emission and several H_2 lines. The 0-4 R(0), 0-4 R(1), and 0-4 R(2) lines from RU Lupi are not present, and the 0-4 R(1) and 0-4 R(2) lines from TW Hya are much weaker than expected because of wind absorption. The wind of DF Tau is not optically thick in C II at < -140 km s^{-1}, so both of these H_2 lines are as strong as predicted from our models (see §4.3). In the T Tau spectrum, the 0-4 R(1) line is weaker than predicted, assuming some C II emission at that wavelength, and the 0-4 R(2) line may also not be present because of wind absorption. The wind our line of sight to V836 Tau is not expected to be optically thick at the velocities of these H_2 lines. The 0-4 R(1) line to DG Tau appears weaker than expected, but several lines in the DG Tau spectrum (0-5 R(0) and 0-5 R(1) at 1394 Å, and 0-6 R(0) and 0-6 R(1) at 1455 Å) are unexpectedly weak for an unknown reason. As a result, we consider any attenuation of the line by the wind of DG Tau inconclusive.

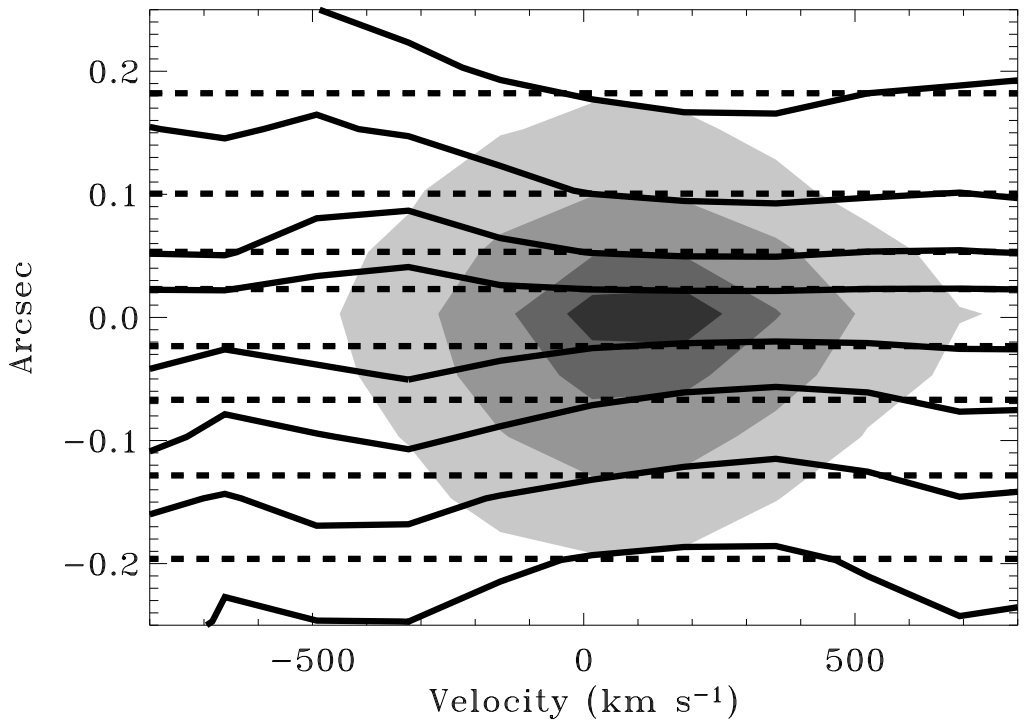

Fig. 18.— Same as Fig. 15 for Hβ in the low-resolution G430L spectrum of RU Lupi, with contours of 0.05, 0.2, 0.5, and 0.8. The point-spread function (dashed lines) is estimated from regions near Hβ that are dominated by the continuum. The bulk of the Hα emission may be produced by accreting gas, and appears redshifted presumably because of wind absorption, which is not detectable at our spectral resolution. The blueshifted Hβ emission may be produced by the stellar wind and is extended symmetrically about the star.

Table 1. LOG OF STIS OBSERVATIONS

Star	Date	Exp. Time(s)	Grating	Aperture	Bandpass (Å)	Spectral Res.	PA[a]
DF Tau[b]	9/18/99	72	G430L	$52'' \times 0''.2$	2850–5750	1500	215
DF Tau[b]	9/18/99	1670	E230M	$0''.2 \times 0''.2$	2130–2810	30000	215
DF Tau[b]	9/18/99	2320	E140M	$0''.5 \times 0''.5$	1170–1710	25000	215
DF Tau[c]	1/28/00	36	G430L	$52'' \times 0''.1$	2850–5750	1500	38
DF Tau[c]	1/28/00	9390	E140M	$0''.2 \times 0''.06$	1170-1710	45000	38
TW Hya[d]	5/7/00	72	G430L	$52'' \times 0''.2$	2850–5750	1500	43
TW Hya[d]	5/7/00	1670	E230M	$0''.2 \times 0''.2$	2130–2810	30000	43
TW Hya[d]	5/7/00	2320	E140M	$0''.5 \times 0''.5$	1170–1710	25000	43
RU Lupi[c]	7/12/00	60	G430L	$52'' \times 0''.1$	2850–5750	1500	41
RU Lupi[c]	7/12/00	12530	E140M	$0''.2 \times 0''.06$	1170-1710	45000	41
V819 Tau[c]	8/30/00	180	G430L	$52'' \times 0''.1$	2850–5750	1500	215
V819 Tau[c]	8/30/00	10390	E140M	$0''.2 \times 0''.06$	1170-1710	25000	215
T Tau[c]	9/8/00	120	G430L	$52'' \times 0''.1$	2850–5750	1500	216
T Tau[c]	9/8/00	12080	E140M	$0''.2 \times 0''.06$	1170-1710	45000	216
DG Tau[c]	10/22/00	120	G430L	$52'' \times 0''.1$	2850–5750	1500	230
DG Tau[c]	10/22/00	12295	E140M	$0''.2 \times 0''.06$	1170-1710	25000	230
V410 Tau[c]	1/30/01	120	G430L	$52'' \times 0''.1$	2850–5750	1500	32
V410 Tau[c]	1/30/01	9590	E140M	$0''.2 \times 0''.06$	1170-1710	25000	32
V836 Tau[c]	2/14/01	180	G430L	$52'' \times 0''.1$	2850–5750	1500	49
V836 Tau[c]	2/14/01	9390	E140M	$0''.2 \times 0''.06$	1170-1710	25000	49

[a]Position angle of cross-dispersion direction
[b]*HST* Program GTO-7718, P.I. J. Linsky
[c]*HST* Program GO-8157, P.I. F. Walter
[d]*HST* Program GTO-8041, P.I. J. Linsky

Table 2. Stellar Properties

Star	Sp. Type	Class	A_V (mag)	L_{acc} ($L_\odot$)	$\dot{M}_{acc}$ (10^{-8} $M_\odot$ yr^{-1})	v_r (km s^{-1})	$v \sin i$ (km s^{-1})	Incl. (°)	Mult. (#)
T Tau N	K0	CTTS	$0.3^a, z$	0.9^n	4^n	18^k	20 ± 5^k	15^b	3^b
DF Tau	M0	CTTS	$0.5^k, z$	0.24^k	$3, 0.2^k$	15^k	$\sim 15^k$	85^g	2
RU Lupi	K7	CTTS	$0.07^j, z$	0.35^j	3^j	-2^l	9.0 ± 0.9^l	23^m	$1–2^m$
DG Tau	K7	CTTS	1.6^c	0.22^k	3^k	17^g	37^g	90^g	3
V410 Tau	K4	WTTS	0.7^d	N/A	N/A	33^k	$\sim 40^k$	-	3
V836 Tau	K7	WTTS	0.6^d	-	0.1^k	17^k	$\sim 15^k$	-	1^f
V819 Tau	K7	WTTS	$1.5^{d,e}$	N/A	N/A	15^k	$< 10^k$	-	1^f
TW Hya	K7	CTTS	$0.0^i, z$	0.034^i	0.2^i	13^p	$< 6^g$	7 ± 1^h	1

[z]Calculated from N(H), assuming the interstellar relationship of Bohlin et al. (1978), with $R_V = 3.1$ (Cardelli et al. 1989).

[a]Walter et al. (2003)
[b]several references, see text
[c]Gullbring et al. (2000)
[d]Kenyon & Hartmann (1995)
[e]White & Ghez (2001)
[f]Simon & Prato (1995)
[g]Johns-Krull & Valenti (2001)
[h]Qi et al. (2004)
[i]Herczeg et al. (2004)
[j]Herczeg et al. (2005)
[k] This work
[l]Stempels & Piskunov (2002)
[m]Stempels et al. (2005)
[n]Calvet et al. (2004)
[p]Weintraub et al. (2000)

Table 3: Properties of H_2 Pumping Transitions

λ_{pump} (Å)	v_{trans} (km s^{-1})	band	v'	J'	v''	J''	f^a (10^{-3})	E''(eV)	P^b_{Dis}
1031.862[c]	-14	C–X	1	3	1	3	28.1	0.60	0.0
1212.426	-801	B–X	1	10	1	11	13.3	1.36	0.0
1212.543	-772	B–X	1	13	1	12	10.9	1.49	0.0
1213.356	-571	B–X	3	13	1	14	20.6	1.79	0.015
1213.677	-491	B–X	4	13	2	12	9.33	1.93	0.050
1214.421	-308	B–X	7	4	4	5	5.17	2.07	0.189
1214.465	-297	B–X	3	16	1	15	23.6	1.94	0.032
1214.566	-272	C–X	1	13	4	14	28.3	2.96	0.011
1214.781	-219	B–X	4	4	3	5	9.90	1.65	0.002
1214.995	-167	B–X	4	7	3	6	7.72	1.72	0.009
1215.726	14	B–X	1	7	2	6	34.8	1.27	0.0
1216.070	99	B–X	1	4	2	5	28.9	1.20	0.0
1216.988	325	C–X	1	4	5	5	7.1	2.46	0.016
1216.997	327	C–X	1	10	5	9	19.7	2.76	0.017
1217.031	336	B–X	3	3	3	2	1.24	1.50	0.0
1217.038	338	B–X	3	0	3	1	1.28	1.48	0.0
1217.205	379	B–X	0	1	2	0	44.0	1.00	0.0
1217.263	393	C–X	0	10	4	10	10.0	2.49	0.0
1217.410	429	B–X	4	18	0	19	9.28	2.20	0.417
1217.488	449	C–X	2	4	6	3	36.4	2.73	0.073
1217.643	487	B–X	0	2	2	1	28.9	1.02	0.0
1217.904	551	B–X	2	12	1	13	19.2	1.64	0.002
1217.982	571	B–X	3	17	0	18	6.64	2.02	0.189
1218.521	704	B–X	2	15	1	14	18.0	1.79	0.006
1218.575	717	B–X	5	7	3	8	12.9	1.89	0.040
1219.089	844	B–X	0	3	2	2	25.5	1.04	0.0
1219.101	847	B–X	2	10	2	9	31.8	1.56	0.0
1219.154	860	B–X	2	7	2	8	31.8	1.46	0.0
1219.368	913	B–X	0	0	2	1	21.4	1.02	0.0
1219.476	939	B–X	2	16	0	17	3.98	1.85	0.009
1219.745	1006	B–X	0	12	1	11	3.68	1.36	0.0
1220.184	1114	B–X	0	9	1	10	5.24	1.23	0.0
1547.971[d]	-42	B–X	0	24	3	25	57.1	4.19	0.008
1548.146[d]	-8	B–X	0	17	5	18	64.9	3.78	0.0
1549.512[d]	257	B–X	1	14	7	13	68.5	3.77	0.0

[a]Velocity from line center of the pumping transition (typically Lyα)

[a]Oscillator strength calculated from values of A_{ul} in Abgrall et al. (1993)

[b]Dissociation probability from upper level, calculated by Abgrall et al. (2000)

[c]Pumped by O VI emission. [d]Pumped by C IV emission.

Table 4. Fluxes in H_2 Progressions[a]

v'	J'	λ_{pump} (Å)	v_{trans} (km s^{-1})	DF Tau		DF Tau		RU Lupi		T Tau		DG Tau		V836 Tau		TW Hya	
				#	F_{obs}	#	F_{obs}	#	F_{obs}	#	F_{obs}	#	F_{obs}	#	F_{obs}	#	F_{obs}
1	10	1212.426	-801	-	-	-	-	-	-	-	-	-	-	-	-	9	4.2
1	13	1212.543	-772	-	-	-	-	-	-	-	-	-	-	-	-	5	1.6
3	13	1213.356	-571	-	-	-	-	-	-	-	-	-	-	-	-	8	4.7
4	13	1213.677	-491	-	-	-	-	-	-	-	-	4	0.10	-	-	8	2.4
7	4	1214.421	-308	-	-	-	-	-	-	-	-	-	-	-	-	3	0.85
3	16	1214.465	-297	4	0.52	-	-	7	0.97	-	-	6	0.19	-	-	13	14.9
4	4	1214.781	-219	5	0.76	2	0.25	9	1.8	-	-	3	0.099	-	-	12	8.9
4	7	1214.995	-167	-	-	-	-	6	0.82	-	-	-	-	2	0.21	9	2.6
1	7	1215.726	14	10	2.4	7	0.75	11	4.4	7	1.1	3	0.10	7	0.33	13	16.2
1	4	1216.070	99	10	4.3	7	1.3	13	8.1	5	1.4	7	0.34	9	0.66	16	36.0
3	3	1217.031	336	2	0.23	-	-	-	-	-	-	-	-	-	-	6	1.5
3	0	1217.038	338	3	0.38	1	0.037	4	0.61	-	-	-	-	-	-	6	3.5
0	1	1217.205	379	10	6.4	9	2.0	7	3.9	6	1.7	8	0.34	10	0.81	10	37.9
4	18	1217.410	429	6	0.69	6	0.30	4	0.54	-	-	3	0.028	-	-	9	3.7
0	2	1217.643	487	9	11.0	10	3.8	7	3.5	6	2.2	6	0.51	9	0.72	8	33.4
2	12	1217.904	551	16	8.7	15	3.1	11	2.6	9	1.7	8	0.46	6	0.34	14	18.4
3	17	1217.982	571	7	0.72	-	-	-	-	-	-	-	-	-	-	4	0.94
2	15	1218.521	704	13	3.0	8	0.55	1	0.33	-	-	8	0.27	-	-	10	3.1
5	7	1218.575	717	6	0.58	-	-	-	-	-	-	-	-	-	-	-	-
0	3	1219.089	844	8	1.5	8	0.54	3	0.43	3	0.26	-	-	-	-	8	2.1
2	10	1219.101	847	9	1.9	7	0.51	-	-	-	-	-	-	-	-	4	1.1
2	7	1219.154	860	7	0.81	8	0.63	-	-	-	-	-	-	-	-	2	0.87
0	0	1219.368	913	4	1.4	4	0.45	2	0.15	2	0.26	-	-	-	-	4	1.2
2	16	1219.476	939	7	0.93	-	-	-	-	-	-	-	-	-	-	-	-

Table 4—Continued

v'	J'	λ_{pump} (Å)	v_{trans} (km s^{-1})	DF Tau		DF Tau		RU Lupi		T Tau		DG Tau		V836 Tau		TW Hya	
				#	F_{obs}	#	F_{obs}	#	F_{obs}	#	F_{obs}	#	F_{obs}	#	F_{obs}	#	F_{obs}
0	12	1219.745	1006	6	0.60	-	-	-	-	-	-	-	-	-	-	-	-
0	9	1220.184	1114	4	0.35	-	-	-	-	-	-	-	-	-	-	-	-
0	24	1547.971	-42	4	0.59	-	-	-	-	-	-	-	-	-	-	3	1.2
0	17	1548.146	-8	5	0.78	-	-	-	-	-	-	-	-	-	-	5	1.6
1	14	1549.512	257	-	-	-	-	-	-	-	-	-	-	-	-	5	1.0

[a]Fluxes in 10^{-15} erg cm^{-2} s^{-1}.

Table 5. LYMAN-BAND H_2 LINES[a], LISTED BY PROGRESSION[b]

ID	λ_{calc} (Å)	f^c_{br}	TW Hya	DF[d] Tau	DF[e] Tau	RU Lupi	T Tau	DG Tau	V836 Tau
v'=1, J'=10, pumped by 1-1 P(11) at 1212.426 Å									
1-2 P(11)	1267.222	0.084	2.2	-	-	-	-	-	-
1-3 R(9)	1292.448	0.088	4.9	-	-	-	-	-	-
1-3 P(11)	1323.232	0.076	3.8	-	-	-	-	-	-
1-4 R(9)	1348.619	0.034	2.3	-	-	-	-	-	-
1-6 R(9)	1462.144	0.051	3.8	-	-	-	-	-	-
1-6 P(11)	1494.193	0.080	4.8	-	-	-	-	-	-
1-7 R(9)	1518.134	0.106	5.6	-	-	-	-	-	-
1-8 R(9)	1572.320	0.079	4.5	-	-	-	-	-	-
1-8 P(11)	1603.095	0.059	9.7	-	-	-	-	-	-
Total Observed Flux			41.6	-	-	-	-	-	-
Extinction Corrected Flux			41.6	-	-	-	-	-	-
Model Flux			50.8	- -	-	-	-	-	
v'=1, J'=13, pumped by 1-1 R(12) at 1212.543 Å									
1-2 P(14)	1303.254	0.082	1.7	-	-	-	-	-	-
1-3 R(12)	1321.249	0.096	3.0	-	-	-	-	-	-
1-4 R(12)	1376.780	0.045	4.0	-	-	-	-	-	-
1-6 P(14)	1525.790	0.086	4.9	-	-	-	-	-	-
1-7 R(12)	1541.060	0.112	2.8	-	-	-	-	-	-
Total Observed Flux			16.5	-	-	-	-	-	-
Extinction Corrected Flux			16.5	-	-	-	-	-	-
Model Flux			32.2	-	-	-	-	-	-
v'=3, J'=13, pumped by 3-1 P(14) at 1213.356 Å									
3-4 P(14)	1370.266	0.053	4.0	-	-	-	-	-	-
3-5 R(12)	1386.514	0.046	3.4	-	-	-	-	-	-
3-5 P(14)	1422.602	0.020	1.6	-	-	-	-	-	-
3-7 R(12)	1488.033	0.055	6.7	-	-	-	-	-	-
3-7 P(14)	1522.793	0.053	5.1	-	-	-	-	-	-
3-9 R(12)	1578.435	0.062	10.7	-	-	-	-	-	-
3-9 P(14)	1608.327	0.139	8.5	-	-	-	-	-	-
3-10 R(12)	1615.427	0.125	6.8	-	-	-	-	-	-
Total Observed Flux			46.9	-	-	-	-	-	-
Extinction Corrected Flux			46.9	-	-	-	-	-	-
Model Flux			57.3	-	-	-	-	-	-
v'=4, J'=13, pumped by 4-2 R(12) at 1213.677 Å									
4-3 P(14)	1298.480	0.029	2.7	-	-	-	-	-	-

Table 5—Continued

ID	λ_{calc} (Å)	f^c_{br}	TW Hya	DF[d] Tau	DF[e] Tau	RU Lupi	T Tau	DG Tau	V836 Tau
4-4 R(12)	1314.719	0.054	-	-	-	-	-	0.1	-
4-4 P(14)	1349.622	0.038	0.8	-	-	-	-	-	-
4-6 R(12)	1415.328	0.037	1.5	-	-	-	-	-	-
4-6 P(14)	1449.938	0.049	2.5	-	-	-	-	0.2	-
4-8 R(12)	1509.449	0.023	1.3	-	-	-	-	-	-
4-8 P(14)	1541.255	0.050	2.2	-	-	-	-	0.2	-
4-10 P(14)	1611.067	0.167	8.6	-	-	-	-	0.5	-
4-11 R(12)	1613.990	0.091	4.5	-	-	-	-	-	-
Total Observed Flux			24.0	-	-	-	-	1.0	-
Extinction Corrected Flux			24.0	-	-	-	-	51.8	-
Model Flux			27.3	-	-	-	-	116.3	-
v'=7, J'=4, pumped by 7-4 P(5) at 1214.421 Å									
7-6 P(5)	1311.344	0.018	1.5	-	-	-	-	-	-
7-13 R(3)	1575.747	0.085	3.7	-	-	-	-	-	-
7-13 P(5)	1581.820	0.148	3.4	-	-	-	-	-	-
Total Observed Flux			8.5	-	-	-	-	-	-
Extinction Corrected Flux			8.5	-	-	-	-	-	-
Model Flux			20.6	-	-	-	-	-	-
v'=3, J'=16, pumped by 3-1 R(15) at 1214.465 Å									
3-0 P(17)	1203.238	0.025	5.3	-	-	-	-	-	-
3-1 P(17)	1254.125	0.073	11.7	-	-	1.8	-	-	-
3-2 R(15)	1265.180	0.076	13.6	0.5	-	1.1	-	-	-
3-4 R(15)	1367.614	0.032	4.3	-	-	0.4	-	-	-
3-4 P(17)	1408.816	0.053	11.6	-	-	-	-	0.1	-
3-5 R(15)	1418.224	0.050	10.9	0.8	-	1.5	-	0.2	-
3-5 P(17)	1459.074	0.018	3.6	-	-	-	-	-	-
3-6 P(17)	1507.176	0.025	4.4	-	-	-	-	-	-
3-7 R(15)	1513.988	0.058	10.1	0.5	-	1.5	-	0.1	-
3-8 P(17)	1590.970	0.038	6.3	-	-	-	-	0.4	-
3-9 R(15)	1593.258	0.123	25.7	3.5	-	2.2	-	0.7	-
3-9 P(17)	1622.133	0.148	29.7	-	-	1.3	-	0.4	-
3-10 R(15)	1621.119	0.062	11.8	-	-	-	-	-	-
Total Observed Flux			149.0	5.2	-	9.7	-	1.9	-
Extinction Corrected Flux			149.0	17.9	-	11.7	-	89.3	-
Model Flux			163.5	30.4	-	15.8	-	123.9	-
v'=4, J'=4, pumped by 4-3 P(5) at 1214.781 Å									

Table 5—Continued

ID	λ_{calc} (Å)	f^c_{br}	TW Hya	DF[d] Tau	DF[e] Tau	RU Lupi	T Tau	DG Tau	V836 Tau
4-4 R(3)	1253.661	0.039	6.0	-	-	1.4	-	-	-
4-4 P(5)	1266.863	0.038	-	-	-	1.7	-	-	-
4-6 R(3)	1359.082	0.042	6.5	0.9	-	1.4	-	-	-
4-6 P(5)	1372.702	0.054	7.2	0.7	-	1.3	-	0.1	-
4-7 P(5)	1425.425	0.007	1.3	-	-	-	-	-	-
4-8 R(3)	1463.579	0.021	2.3	-	-	-	-	-	-
4-8 P(5)	1477.041	0.039	5.8	0.5	-	1.0	-	-	-
4-9 R(3)	1513.507	0.039	4.3	-	-	1.4	-	-	-
4-9 P(5)	1526.545	0.033	6.1	-	-	-	-	-	-
4-10 P(5)	1572.645	0.032	-	-	-	1.1	-	-	-
4-11 R(3)	1602.613	0.119	17.6	2.5	0.6	3.4	-	0.4	-
4-11 P(5)	1613.709	0.151	20.4	3.1	2.0	4.9	-	0.4	-
4-12 R(3)	1638.345	0.036	6.4	-	-	-	-	-	-
4-12 P(5)	1647.681	0.020	4.9	-	-	-	-	-	-
Total Observed Flux			88.7	7.6	2.5	17.6	-	1.0	-
Extinction Corrected Flux			88.7	25.8	8.2	21.0	-	47.3	-
Model Flux			111.6	45.5	27.9	29.8	-	117.9	-
v'=4, J'=7, pumped by 4-3 R(6) at 1214.995 Å									
4-3 P(8)	1235.863	0.035	1.4	-	-	-	-	-	-
4-4 R(6)	1266.566	0.046	3.7	-	-	1.0	-	-	-
4-4 P(8)	1287.913	0.036	2.2	-	-	0.6	-	-	-
4-6 R(6)	1371.098	0.041	1.4	-	-	0.7	-	-	-
4-6 P(8)	1392.949	0.051	1.2	-	-	-	-	-	-
4-8 P(8)	1494.948	0.042	2.9	-	-	1.2	-	-	-
4-9 R(6)	1522.005	0.041	2.1	-	-	-	-	-	-
4-11 R(6)	1606.284	0.133	4.4	-	-	2.0	-	-	1.3
4-11 P(8)	1622.909	0.134	7.1	-	-	2.7	-	-	0.9
Total Observed Flux			26.4	-	-	8.2	-	-	2.1
Extinction Corrected Flux			26.4	-	-	9.8	-	-	8.7
Model Flux			29.0	-	-	17.0	-	-	24.5
v'=1, J'=7, pumped by 1-2 R(6) at 1215.726 Å									
1-2 P(8)	1237.862	0.087	11.5	1.0	0.2	3.2	-	-	0.2
1-3 R(6)	1271.014	0.080	14.1	2.4	-	2.9	1.0	-	-
1-3 P(8)	1293.867	0.073	13.0	0.7	1.1	4.0	-	-	0.1
1-4 R(6)	1327.560	0.025	6.1	0.5	-	1.6	0.4	-	-
1-4 P(8)	1351.032	0.013	2.8	0.4	-	-	-	-	-

Table 5—Continued

ID	λ_{calc} (Å)	f^c_{br}	TW Hya	DF[d] Tau	DF[e] Tau	RU Lupi	T Tau	DG Tau	V836 Tau
1-5 P(8)	1408.959	0.011	2.2	-	-	-	-	-	-
1-6 R(6)	1442.860	0.056	11.3	-	-	5.1	1.3	-	-
1-6 P(8)	1467.079	0.080	17.6	3.8	1.1	4.3	1.9	-	0.4
1-7 R(6)	1500.443	0.101	19.7	4.1	1.1	6.1	1.7	0.3	0.4
1-7 P(8)	1524.648	0.111	23.5	4.6	1.7	6.1	3.0	0.4	0.5
1-8 R(6)	1556.860	0.074	17.0	4.8	1.4	4.7	2.0	0.4	1.1
1-8 P(8)	1580.666	0.065	17.5	1.5	1.0	3.3	-	-	0.6
1-9 R(6)	1610.946	0.024	-	-	-	2.7	-	-	-
1-9 P(8)	1633.833	0.015	5.5	-	-	-	-	-	-
Total Observed Flux			161.8	23.6	7.5	44.1	11.4	1.0	3.3
Extinction Corrected Flux			161.8	85.3	26.7	52.9	24.3	50.4	14.8
Model Flux			169.6	79.8	32.9	56.1	34.6	115.8	15.7
v'=1, J'=4, pumped by 1-2 P(5) at 1216.070 Å									
1-1 P(5)	1161.814	0.049	6.2	-	-	-	-	-	-
1-2 R(3)	1202.449	0.078	11.3	-	-	3.0	-	-	-
1-3 R(3)	1257.828	0.069	18.1	1.4	0.6	6.0	-	-	-
1-3 P(5)	1271.925	0.074	20.5	2.0	0.5	5.4	0.6	-	0.4
1-4 R(3)	1314.613	0.017	12.2	1.2	0.2	2.0	-	-	0.2
1-4 P(5)	1329.137	0.012	7.5	-	-	1.1	-	-	-
1-5 R(3)	1372.490	0.005	3.2	-	-	-	-	-	-
1-5 P(5)	1387.362	0.012	7.1	0.5	-	2.1	-	0.1	0.2
1-6 R(3)	1431.010	0.058	29.0	4.9	-	8.3	-	0.2	0.8
1-6 P(5)	1446.118	0.083	44.2	8.7	2.7	15.7	3.8	1.1	0.6
1-7 R(3)	1489.564	0.094	48.2	7.9	3.1	9.4	2.5	0.4	0.9
1-7 P(5)	1504.751	0.115	57.5	9.4	3.6	13.9	4.0	0.9	1.9
1-8 R(3)	1547.334	0.067	35.3	-	-	-	-	0.4	0.7
1-8 P(5)	1562.389	0.071	37.2	5.5	2.1	10.2	2.6	0.2	0.9
1-9 R(3)	1603.249	0.022	11.2	1.6	-	1.7	-	-	-
1-9 P(5)	1617.886	0.020	11.6	-	-	2.0	-	-	-
Total Observed Flux			360.3	42.9	12.9	80.7	13.5	3.4	6.6
Extinction Corrected Flux			360.3	153.1	45.6	96.8	28.7	181.8	30.1
Model Flux			382.3	192.9	61.1	110.5	41.1	189.6	38.9
v'=3, J'=3, pumped by 3-3 R(2) at 1217.031 Å									
3-4 P(4)	1281.047	0.061	1.9	-	-	-	-	-	-
3-5 R(2)	1324.652	0.023	1.2	-	-	-	-	-	-
3-7 R(2)	1434.097	0.050	1.5	-	-	-	-	-	-

Table 5—Continued

ID	λ_{calc} (Å)	f^c_{br}	TW Hya	DF[d] Tau	DF[e] Tau	RU Lupi	T Tau	DG Tau	V836 Tau
3-7 P(4)	1445.182	0.066	3.1	0.8	-	-	-	-	-
3-10 R(2)	1589.142	0.101	4.6	1.5	-	-	-	-	-
3-11 R(2)	1633.621	0.046	2.9	-	-	-	-	-	-
Total Observed Flux			15.0	2.3	-	-	-	-	-
Extinction Corrected Flux			15.0	7.7	-	-	-	-	-
Model Flux			36.5	32.7	-	-	-	-	-
v'=3, J'=0, pumped by 3-3 P(1) at 1217.038 Å									
3-4 P(1)	1270.577	0.108	3.1	-	-	0.6	-	-	-
3-5 P(1)	1325.056	0.041	1.8	-	-	0.8	-	-	-
3-7 P(1)	1435.048	0.117	4.0	1.1	0.4	-	-	-	-
3-9 P(1)	1541.768	0.072	3.5	0.5	-	-	-	-	-
3-10 P(1)	1591.310	0.232	14.4	2.2	-	1.9	-	-	-
3-11 P(1)	1636.328	0.098	7.8	-	-	2.7	-	-	-
Total Observed Flux			34.7	3.8	0.4	6.1	-	-	-
Extinction Corrected Flux			34.7	12.8	1.3	7.3	-	-	-
Model Flux			32.7	21.9	8.0	10.3	-	-	-
v'=0, J'=1, pumped by 0-2 R(0) at 1217.205 Å									
0-2 P(2)	1221.955	0.072	9.1	1.6	-	-	-	-	0.2
0-3 R(0)	1274.534	0.067	27.4	2.6	1.6	3.2	1.4	0.1	0.2
0-3 P(2)	1279.464	0.134	39.2	5.3	1.7	4.1	1.3	0.2	0.9
0-4 R(0)	1333.474	0.084	42.8	6.8	2.1	-	-	0.5	0.8
0-4 P(2)	1338.568	0.166	73.1	12.1	4.0	11.8	4.0	1.0	1.4
0-5 R(0)	1393.719	0.073	35.3	9.4	1.3	-	-	-	0.9
0-5 P(2)	1398.951	0.141	73.8	12.6	3.7	10.0	4.0	0.8	1.2
0-6 R(0)	1454.829	0.044	20.8	3.5	1.6	2.5	-	-	0.5
0-6 P(2)	1460.165	0.083	41.6	7.3	3.1	5.3	4.2	0.5	1.4
0-7 P(2)	1521.587	0.032	16.2	2.6	1.0	2.0	1.5	-	0.5
Total Observed Flux			379.4	63.8	20.1	38.9	16.6	3.1	8.1
Extinction Corrected Flux			379.4	247.5	77.8	47.0	36.9	246.5	41.2
Model Flux			423.3	270.1	91.4	65.7	57.0	355.9	41.8
v'=4, J'=18, pumped by 4-0 P(19) at 1217.410 Å									
4-1 R(17)	1224.914	0.089	6.4	-	0.5	-	-	-	-
4-2 R(17)	1274.033	0.047	5.0	1.1	0.6	0.9	-	0.1	-
4-3 P(19)	1366.120	0.025	2.5	1.0	0.5	-	-	-	-
4-4 R(17)	1372.061	0.056	4.9	1.3	0.6	0.9	-	0.1	-
4-4 P(19)	1414.696	0.039	4.6	0.8	0.5	-	-	-	-

Table 5—Continued

ID	λ_{calc} (Å)	f^c_{br}	TW Hya	DF[d] Tau	DF[e] Tau	RU Lupi	T Tau	DG Tau	V836 Tau
4-5 R(17)	1419.687	0.006	1.2	-	-	-	-	-	-
4-6 R(17)	1465.186	0.039	5.2	1.3	-	1.5	-	0.1	-
4-6 P(19)	1505.162	0.042	3.9	-	-	2.1	-	-	-
4-7 P(19)	1544.199	0.008	-	-	0.3	-	-	-	-
4-8 R(17)	1544.254	0.038	3.6	1.3	-	-	-	-	-
Total Observed Flux			37.2	6.9	3.0	5.4	-	0.3	-
Extinction Corrected Flux			37.2	25.8	12.2	6.5	-	21.6	-
Model Flux			44.5	42.0	19.4	13.4	-	49.3	-
v'=0, J'=2, pumped by 0-2 R(1) at 1217.643 Å									
0-2 P(3)	1225.535	0.064	-	-	0.6	1.3	-	-	-
0-3 R(1)	1274.922	0.080	24.6	5.2	2.1	4.8	2.2	0.3	0.2
0-3 P(3)	1283.111	0.120	28.0	8.3	3.5	5.0	3.0	0.3	0.6
0-4 R(1)	1333.797	0.101	7.9	12.3	3.5	-	-	-	0.5
0-4 P(3)	1342.256	0.148	64.9	16.9	7.3	11.0	5.2	1.2	1.4
0-5 R(1)	1393.961	0.088	52.4	15.3	3.6	-	-	-	1.3
0-5 P(3)	1402.648	0.126	73.1	20.6	7.9	-	4.5	1.5	1.4
0-6 R(1)	1454.971	0.053	30.9	10.2	3.3	5.2	-	-	0.5
0-6 P(3)	1463.826	0.074	42.1	14.9	4.7	6.2	4.8	1.3	0.8
0-7 P(3)	1525.153	0.029	17.9	6.9	1.7	1.1	2.7	0.6	0.6
Total Observed Flux			333.9	110.5	38.1	34.6	22.3	5.1	7.2
Extinction Corrected Flux			333.9	420.9	146.9	41.9	50.0	363.8	35.9
Model Flux			422.2	473.4	162.3	73.5	86.0	624.8	35.0
v'=2, J'=12, pumped by 2-1 P(13) at 1217.904 Å									
2-1 R(11)	1185.224	0.059	-	1.6	-	-	-	-	-
2-2 R(11)	1237.536	0.088	8.7	2.5	1.2	1.2	0.8	-	-
2-2 P(13)	1271.177	0.073	13.5	3.2	2.0	2.0	1.1	-	-
2-3 R(11)	1290.897	0.038	9.1	2.6	1.4	1.2	1.0	0.3	0.2
2-3 P(13)	1325.342	0.015	3.3	1.6	0.5	-	-	-	-
2-4 P(13)	1379.982	0.015	2.3	1.9	1.1	1.3	-	-	-
2-5 R(11)	1399.234	0.054	12.1	4.7	2.2	2.0	-	0.5	-
2-5 P(13)	1434.533	0.066	15.6	6.6	2.2	2.3	2.6	0.4	0.4
2-6 R(11)	1453.093	0.049	15.4	5.6	2.3	2.1	1.5	0.2	-
2-6 P(13)	1488.239	0.021	6.8	3.3	1.4	-	-	-	-
2-7 P(13)	1540.094	0.020	6.9	3.0	1.2	-	-	-	-
2-8 R(11)	1555.880	0.077	20.1	8.3	2.8	2.0	2.9	0.6	0.7
2-8 P(13)	1588.793	0.119	24.1	12.7	3.7	5.6	1.7	0.7	0.4

Table 5—Continued

ID	λ_{calc} (Å)	f^c_{br}	TW Hya	DF[d] Tau	DF[e] Tau	RU Lupi	T Tau	DG Tau	V836 Tau
2-9 R(11)	1602.264	0.111	28.7	14.1	4.0	5.2	2.4	1.1	0.8
2-9 P(13)	1632.608	0.076	17.5	9.0	2.9	-	3.1	0.9	0.8
2-10 R(11)	1642.936	0.024	-	6.3	2.1	1.2	-	-	-
Total Observed Flux			183.9	86.8	30.9	26.1	17.1	4.6	3.4
Extinction Corrected Flux			183.9	306.2	110.6	31.2	36.4	239.0	14.4
Model Flux			195.5	300.6	107.3	37.6	43.9	258.8	21.3
v'=3, J'=17, pumped by 3-0 P(18) at 1217.982 Å									
3-1 R(16)	1227.422	0.075	-	0.9	-	-	-	-	-
3-1 P(18)	1268.840	0.073	1.4	0.5	-	-	-	-	-
3-2 R(16)	1278.020	0.079	-	0.8	-	-	-	-	-
3-2 P(18)	1320.200	0.045	1.7	-	-	-	-	-	-
3-4 R(16)	1379.721	0.031	-	0.3	-	-	-	-	-
3-4 P(18)	1422.364	0.053	-	0.9	-	-	-	-	-
3-8 P(18)	1597.418	0.069	2.0	1.7	-	-	-	-	-
3-9 R(16)	1597.207	0.150	4.3	2.1	-	-	-	-	-
Total Observed Flux			9.4	7.2	-	-	-	-	-
Extinction Corrected Flux			9.4	27.1	-	-	-	-	-
Model Flux			22.3	35.8	-	-	-	-	-
v'=2, J'=15, pumped by 2-1 R(14) at 1218.521 Å									
2-0 P(16)	1205.106	0.014	-	0.4	-	-	-	-	-
2-1 P(16)	1257.394	0.060	2.7	1.2	0.4	-	-	0.2	-
2-2 R(14)	1270.744	0.092	6.2	1.3	0.4	-	-	-	-
2-2 P(16)	1310.547	0.078	4.1	1.9	0.9	-	-	0.1	-
2-3 R(14)	1323.669	0.049	2.1	1.6	0.1	-	-	0.1	-
2-3 P(16)	1364.168	0.019	-	0.6	-	-	-	-	-
2-4 P(16)	1417.708	0.013	-	0.7	-	-	-	-	-
2-5 R(14)	1429.706	0.051	-	-	-	-	-	0.2	-
2-5 P(16)	1470.441	0.067	1.9	2.4	0.6	-	-	0.3	-
2-6 R(14)	1481.418	0.051	1.9	1.7	0.5	-	-	-	-
2-6 P(16)	1521.390	0.016	1.7	-	-	-	-	-	-
2-7 P(16)	1569.281	0.039	3.1	2.2	-	-	-	-	-
2-8 R(14)	1576.873	0.100	-	6.8	1.6	3.3	-	0.5	-
2-8 P(16)	1612.381	0.138	3.6	4.8	1.0	-	-	0.6	-
2-9 R(14)	1617.414	0.103	4.1	4.3	-	-	-	0.9	-
Total Observed Flux			31.4	30.0	5.5	3.3	-	2.7	-
Extinction Corrected Flux			31.4	106	20.2	3.9	-	150.9	-

Table 5—Continued

ID	λ_{calc} (Å)	f^c_{br}	TW Hya	DF[d] Tau	DF[e] Tau	RU Lupi	T Tau	DG Tau	V836 Tau
Model Flux			36.5	115	22.2	32.2	-	143.8	
v'=5, J'=7, pumped by 5-3 P(8) at 1218.575 Å									
5-5 R(6)	1299.087	0.019	-	1.0	-	-	-	-	-
5-6 P(8)	1371.027	0.020	-	0.5	-	-	-	-	-
5-8 R(6)	1449.124	0.041	-	0.7	-	-	-	-	-
5-10 R(6)	1539.097	0.043	-	0.6	-	-	-	-	-
5-12 R(6)	1608.170	0.144	-	2.2	-	-	-	-	-
5-12 P(8)	1620.906	0.093	-	0.8	-	-	-	-	-
Total Observed Flux			-	5.8	-	-	-	-	-
Extinction Corrected Flux			-	20.3	-	-	-	-	-
Model Flux			-	38.0 -	-	-	-	-	
v'=0, J'=3, pumped by 0-2 R(2) at 1219.089 Å									
0-2 P(4)	1230.089	0.061	-	-	0.3	-	-	-	-
0-3 R(2)	1276.322	0.085	2.6	1.5	0.3	0.8	-	-	-
0-3 P(4)	1287.731	0.114	2.0	1.3	0.8	0.6	0.7	-	-
0-4 P(4)	1346.908	0.141	3.8	2.3	0.6	-	-	-	-
0-5 R(2)	1395.197	0.096	2.4	1.8	0.6	-	-	-	-
0-5 P(4)	1407.286	0.120	3.0	3.3	1.4	3.2	1.3	-	-
0-6 R(2)	1456.075	0.059	2.1	1.6	0.6	-	0.5	-	-
0-6 P(4)	1468.387	0.070	3.4	2.3	0.7	-	-	-	-
0-7 P(4)	1529.557	0.027	1.9	1.2	-	-	-	-	-
Total Observed Flux			21.2	15.4	5.4	4.6	2.4	-	-
Extinction Corrected Flux			21.2	58.3	21.1	5.6	5.4	-	-
Model Flux			25.5	74.2	23.0	18.3	16.2	-	-
v'=2, J'=10, pumped by 2-2 R(9) at 1219.101 Å									
2-2 P(11)	1248.145	0.071	-	1.4	-	-	-	-	-
2-4 P(11)	1357.497	0.016	-	1.0	-	-	-	-	-
2-5 R(9)	1381.954	0.056	1.5	0.7	0.4	-	-	-	-
2-5 P(11)	1412.812	0.066	2.6	1.7	0.5	-	-	-	-
2-6 R(9)	1436.806	0.045	1.9	1.6	0.6	-	-	-	-
2-8 R(9)	1543.057	0.070	5.1	2.7	0.6	-	-	-	-
2-8 P(11)	1572.687	0.108	-	4.0	1.0	-	-	-	-
2-9 R(9)	1592.189	0.108	-	2.8	0.7	-	-	-	-
2-9 P(11)	1620.093	0.089	-	2.6	1.2	-	-	-	-
Total Observed Flux			11.2	18.6	5.1	-	-	-	-
Extinction Corrected Flux			11.2	65.3	17.2	-	-	-	-

Table 5—Continued

ID	λ_{calc} (Å)	f^c_{br}	TW Hya	DF[d] Tau	DF[e] Tau	RU Lupi	T Tau	DG Tau	V836 Tau
Model Flux			29.6	62.4	21.6 -	-	-	-	
v'=2, J'=7, pumped by 2-2 P(8) at 1219.154 Å									
2-5 R(6)	1361.629	0.058	-	1.6	0.7	-	-	-	-
2-5 P(8)	1384.772	0.068	3.1	1.3	0.7	-	-	-	-
2-6 R(6)	1417.506	0.038	-	0.7	0.6	-	-	-	-
2-6 P(8)	1440.875	0.024	-	0.7	0.5	-	-	-	-
2-8 R(6)	1527.382	0.066	-	1.5	-	-	-	-	-
2-8 P(8)	1550.289	0.098	-	-	0.5	-	-	-	-
2-9 R(6)	1579.405	0.102	5.6	1.2	0.6	-	-	-	-
2-9 P(8)	1601.399	0.100	-	-	2.3	-	-	-	-
2-10 R(6)	1627.672	0.039	-	1.2	0.4	-	-	-	-
Total Observed Flux			8.7	8.1	6.3	-	-	-	-
Extinction Corrected Flux			8.7	28.7	21.9	-	-	-	-
Model Flux			37.2	51.7	23.9 -	-	-	-	
v'=0, J'=0, pumped by 0-2 P(1) at 1219.368 Å									
0-3 P(1)	1276.813	0.201	2.0	2.2	0.7	-	-	-	-
0-4 P(1)	1335.868	0.249	3.4	-	1.0	-	-	-	-
0-5 P(1)	1396.223	0.213	3.3	4.5	1.5	0.7	1.7	-	-
0-6 P(1)	1457.435	0.126	3.7	5.5	1.3	0.8	1.0	-	-
0-7 P(1)	1518.894	0.050	-	2.2	-	-	-	-	-
Total Observed Flux			12.4	14.4	4.5	1.5	2.7	-	-
Extinction Corrected Flux			12.4	53.6	17.2	1.7	5.8	-	-
Model Flux			14.4	72.8	19.8	3.7	13.0	-	-
v'=2, J'=16, pumped by 2-0 P(17) at 1219.476 Å									
2-2 P(17)	1324.805	0.079	-	0.9	-	-	-	-	-
2-3 P(17)	1378.122	0.020	-	0.4	-	-	-	-	-
2-5 R(15)	1440.837	0.051	-	0.3	-	-	-	-	-
2-5 P(17)	1483.021	0.067	-	2.0	-	-	-	-	-
2-7 P(17)	1578.867	0.051	-	0.7	-	-	-	-	-
2-8 R(15)	1583.881	0.113	-	2.9	-	-	-	-	-
2-8 P(17)	1619.484	0.141	-	2.1	-	-	-	-	-
Total Observed Flux			-	9.3	-	-	-	-	-
Extinction Corrected Flux			-	32.0	-	-	-	-	-
Model Flux			-	44.0	-	-	-	-	-
v'=0, J'=12, pumped by 0-1 R(11) at 1219.745 Å									
0-3 R(11)	1331.955	0.081	-	0.4	-	-	-	-	-

Table 5—Continued

ID	λ_{calc} (Å)	f^c_{br}	TW Hya	DF[d] Tau	DF[e] Tau	RU Lupi	T Tau	DG Tau	V836 Tau
0-4 R(11)	1389.584	0.123	-	1.4	-	-	-	-	-
0-4 P(13)	1427.005	0.130	-	1.3	-	-	-	-	-
0-5 R(11)	1447.602	0.127	-	0.9	-	-	-	-	-
0-5 P(13)	1485.416	0.117	-	0.8	-	-	-	-	-
0-6 R(11)	1505.325	0.087	-	1.2	-	-	-	-	-
Total Observed Flux			-	6.0	-	-	-	-	-
Extinction Corrected Flux			-	21.8	-	-	-	-	-
Model Flux			-	28.1 -	-	-	-	-	
v'=0, J'=9, pumped by 0-1 P(10) at 1220.184 Å									
0-4 R(8)	1363.521	0.121	-	0.9	-	-	-	-	-
0-4 P(10)	1393.453	0.129	-	0.7	-	-	-	-	-
0-5 R(8)	1422.546	0.118	-	0.9	-	-	-	-	-
0-6 R(8)	1481.817	0.078	-	1.0	-	-	-	-	-
Total Observed Flux			-	3.5	-	-	-	-	-
Extinction Corrected Flux			-	12.8	-	-	-	-	-
Model Flux			-	23.1	-	-	-	-	-

[a]Flux in 10^{-15} erg cm^{-2} s^{-1}

[b]The total flux in a progression, here termed model flux, may be larger than the extinction-corrected observed flux because of unseen lines.

[c]Branching ratio, including dissociation percentage

[d]Data obtained with the $0\farcs5 \times 0\farcs5$ aperture

[e]Data obtained with the $0\farcs2 \times 0\farcs06$ aperture

Table 6: HIGHLY EXCITED H_2 LINES[a], LISTED BY PROGRESSION[b]

ID	λ_{calc} (Å)	f^c_{br}	TW Hya	DF Tau
v'=0, J'=24, pumped by 0-3 P(25) at 1547.971 Å				
0-2 P(25)	1498.007	0.049	2.9	1.0
0-4 R(23)	1542.241	0.168	4.0	1.3
0-4 P(25)	1594.059	0.180	5.4	2.1
0-5 R(23)	1586.688	0.168	-	1.5
Total Observed Flux			12.3	5.9
Extinction Corrected Flux			12.3	19.6
Model Flux			24.0	26.0
v'=0, J'=17, pumped by 0-5 P(18) at 1548.146 Å				
0-2 P(18)	1381.413	0.040	2.4	0.5
0-3 P(18)	1437.781	0.094	1.6	0.5
0-4 R(16)	1446.719	0.127	4.4	1.8
0-5 R(16)	1501.674	0.142	3.8	2.7
0-6 R(16)	1554.849	0.098	4.3	2.3
Total Observed Flux			16.5	7.8
Extinction Corrected Flux			16.5	27.1
Model Flux			30.0	44.5
v'=1, J'=14, pumped by 1-7 R(13) at 1549.512 Å				
1-2 R(13)	1277.587	0.075	2.0	-
1-3 R(13)	1332.310	0.098	1.1	-
1-6 R(13)	1497.031	0.049	1.9	-
1-6 P(15)	1536.976	0.089	2.5	-
1-7 P(15)	1588.183	0.115	2.6	-
Total Observed Flux			10.1	-
Extinction Corrected Flux			10.1	-
Model Flux			19.8	-

[a]Flux in 10^{-15} erg cm^{-2} s^{-1}

[b]The total flux in a progression, here termed model flux, may be larger than the extinction-corrected observed flux because of unseen lines.

[c]Branching ratio, including dissociation percentage

[d]Data obtained with the $0\farcs5 \times 0\farcs5$ aperture

[e]Data obtained with the $0\farcs2 \times 0\farcs06$ aperture

Table 7. IDENTIFICATION AND FLUXES[a] OF BLENDED H_2 LINES

λ	ID1	ID2	TW Hya	DF[b] Tau	DF[c] Tau	RU Lupi	T Tau	DG Tau	V836 Tau
1266.9	4-4 P(5)	4-1 P(19)	13.1	1.3	0.40	-	-	-	-
1320.2	3-2 P(18)	5-7 P(8)	-	2.2	-	-	-	-	-
1408.8	1-5 P(8)	3-4 P(17)	-	-	-	1.8	-	-	-
1429.7	2-5 R(14)	3-5 R(16)	4.6	1.5	-	-	-	-	-
1454.9	0-6 R(0)	0-6 R(1)	-	-	-	-	4.0	0.51	-
1493.7	0-4 P(18)	0-3 R(23)	4.7	0.8	-	-	-	-	-
1516.2	0-7 R(0)	0-7 R(1)	22.0	5.4	1.7	3.7	1.3	0.59	-
1522.8	3-7 P(14)	3-7 R(16)	5.2	-	-	-	-	-	-
1572.7	4-10 P(5)	2-8 P(11)	8.3	-	-	-	-	-	-
1576.9	2-8 R(14)	0-8 R(0)[d]	15.1	-	-	-	-	-	-
1585.8	4-10 P(8)	0-8 P(3)	7.4	3.9	-	-	-	-	-
1586.8	4-10 P(12)	0-5 P(23)	10.8	-	-	-	-	-	-

[a]Flux in 10^{-15} erg cm^{-2} s^{-1}
[b]Data obtained with the $0\farcs5 \times 0\farcs5$ aperture
[c]Data obtained with the $0\farcs2 \times 0\farcs06$ aperture
[d]Also 0-8 R(1)

Table 8. IDENTIFICATION AND FLUXES[a] OF WERNER-BAND H_2 LINES

λ	ID	TW Hya	DF[b] Tau	RU Lupi	Pump
1154.910	1-3 P(11)	12.3	-	-	1-5 R(9) 1216.997 Å
1172.0[c]	1-4 R(5)	7.5	2.9	-	1-5 P(5) 1216.988 Å
1174.4[d]	1-3 R(9)	-	5.6	-	1-5 R(9) 1216.997 Å
1186.226	1-4 R(12)	4.9	-	-	1-4 P(14) 1214.566 Å
1208.932	1-5 Q(3)	-	-	2.2	1-1 Q(3) 1031.862 Å
1228.406	2-6 P(5)	-	1.3	-	2-6 P(3) 1217.488 Å
1255.507	1-5 P(14)	5.x8	-	-	1-4 P(14) 1214.566 Å

[a]Flux in 10^{-15} erg cm^{-2} s^{-1}.
[b]Data obtained with the $0\farcs5 \times 0\farcs5$ aperture
[c]Also 0-3 Q(10), pumped by 0-4 Q(1) 1217.263 Å
[d]Also 2-5 R(1), pumped by 2-6 R(1) 1217.298 Å, and
1-4 Q(7), pumped by 1-5 Q(7) 1218.508 Å

Table 9. Fluxes in Strong Lines and H_2 Progressions[a]

Star	C IV 1549 Å	Si IV 1400 Å	C II 1335 Å	O I 1305 Å	He II 1640 Å	H_2 (1,4)	H_2 (1,7)	H_2 (0,1)	H_2 (0,2)	H_2 (2,12)
TW Hya	284	11	11	95	1.4	38	17	41	43	19
RU Lupi	70	69	11	26	7.6	9.2	4.7	5.4	6.1	3.1
DF Tau (large)	33	2.5	4.3	5.6	8.1	5.2	2.2	7.0	12.3	8.4
DF Tau (small)	2.9	0.38	0.78	1.6	0.82	1.6	0.89	2.4	4.2	3.0
T Tau	22.6	5.6	2.5	25	5.5	1.8	1.6	2.5	3.8	2.0
DG Tau	< 0.08	< 0.05	< 0.04	0.09	< 0.07	0.30	0.19	0.48	0.86	0.46
V836 Tau	1.4	0.13	0.38	0.44	0.84	3.9	1.6	4.2	3.5	2.1
V410 Tau	2.8	0.88	1.2	1.1	1.7	< 0.3	< 0.16	< 0.08	< 0.2	< 0.2
V819 Tau	< 0.2	< 0.2	< 0.1	< 0.2	< 0.08	< 0.2	< 0.2	< 0.07	< 0.2	< 0.2

[a] 10^{-14} erg cm^{-2} s^{-1}, not corrected for extinction

Table 10. Multiple components of H_2 Emission

Star	(v', J')	Component[a]	v_{H2}	FWHM	Flux Fraction[e]
DF Tau[b]	(0,1);(0,2);(2,12)	1	-1	23	N/A
DF Tau[b]	(1,4);(1,7)	1	-8	41	N/A
DF Tau[c,d]	(0,1); (0,2); (2,12)	1	6	19	0.70
	(0,1); (0,2); (2,12)	2	-8	30	0.30
DF Tau[c,d]	(0,1); (0,2); (2,12)	1	3	24	N/A
DF Tau[c]	(1,4);(1,7)	1	0	36	N/A
RU Lupi	all	1	-12	18	0.57
	all	2	-30	53	0.43
T Tau	(0,1); (0,2)	1	-12	28	0.64
	(0,1); (0,2)	2	-72	65	0.36
T Tau	(1,4); (1,7)	1	-2	30	0.49
	(1,4); (1,7)	2	-65	69	0.51

[a]Component of fit, if the fit used multiple Gaussians.
[b]Large Aperture [c]Small Aperture
[d]Lines fit as both a single and double Gaussian.
[e]Fraction of flux in a component, where applicable

Table 11. Global Properties of H_2 Emission

Star	v^a_{H2} (km s^{-1})	FWHM[a] (km s^{-1})	# Upper Levels	# Lines[b]	F^c_{obs}	F^c_{ext}	F^c_{mod}
DF Tau[d]	-1	23.2	22	164	51.0	188	210
DF Tau[e]	6	18.6	13	94	14.4	53.5	62.1
RU Lup	-12	17.6	13	88	28.5	34.3	48.3
T Tau	-12	28.4	7	41	9.26	20.2	29.2
DG Tau	-27	26.1	10	58	2.55	152[f]	210
V836 Tau	0	24.3	6	45	3.13	14.8	17.7
TW Hya	0	18.2	24	209	217	217	244

[a]Velocity with respect to the star and FWHM are for narrow component only.
[b]Several blends from each star are counted as a single line.
[c]Observed flux, flux corrected for extinction, and model flux in 10^{-14} erg cm^{-2} s^{-1}.
[d]Large apeture [e]Small aperture
[f]Extinction to H_2 emission from DG Tau is very uncertain.

Table 12. Attenuation of H_2 lines by the wind

Star	v_∞^a (C II 1334.5 Å) km s^{-1}	v_∞^a (Mg II 2796 Å) km s^{-1}	v_{H2} km s^{-1}	0-4 R(0), -240 km s^{-1} Model[b]	0-4 R(0), -240 km s^{-1} Obs.[b]	0-4 R(1), -165 km s^{-1} Model[b]	0-4 R(1), -165 km s^{-1} Obs.[b]
DF Tau[c]	-190	-130	-1	6.0	6.8	12.2	12.3
TW Hya	-205	180	0	36.9	42.8	42.7	7.9
RU Lupi	-350[d]	-265	-12	4.7	< 2.1	6.1	< 0.2
T Tau	-300[d]	-180	-12	2.0	< 3.0	3.6	< 2.7
DG Tau	-330[d]	-	-27	0.4	0.5	0.8	~ 0.4[f]
V836 Tau	-	> -190[e]	0	0.7	0.8	0.7	0.5

[a]Maximum velocity of wind absorption
[b]Flux, 10^{-15} erg cm^{-2} s^{-1}
[c]Obtained with large aperture
[d]From Ardila et al. (2002)
[e]Inferred from H_2 lines.
[f]Flux estimate unreliable.

Table 13. Comparisons to previous observations

	STIS					GHRS[a]				
Star	v^b_{H2}	FWHM[b]	$F^{c,d}_{red}$	$F^{c,e}_{cen}$	F(C IV)[c]	v^b_{H2}	FWHM[b]	$F^{c,d}_{red}$	$F^{c,e}_{cen}$	F(C IV)[c]
DF Tau[f]	-1	23	46.3[g]	5.5[h]	330	-1	27	52[g]	4[h]	498
RU Lupi	-12	18	-	14.9[i]	700	-17	37	-	26[i]	146
T Tau	-12	28	16.1[j]	12.8[k]	230	-9	52	33[j]	98[k]	166
DG Tau	-27	26	1.9[l]	1.0[m]	< 0.8	-11	41	19[l]	8[m]	44

[a]From Ardila et al. (2002). DF Tau and RU Lupi were observed with GHRS before COSTAR was installed, leading to a ~ 20 km s^{-1} uncertainty in the absolute velocity scale. T Tau and DG Tau were observed after COSTAR was installed, and have velocities measured to ~ 3 km s^{-1}.

[b]km s^{-1} [c]Flux in various lines, 10^{-15} erg cm^{-2} s^{-1}

[d]F_{red}: lines from (v',J')=(0,1),(0,2), and (2,12) pumped on the red wing of Lyα

[e]F_{cent}: lines from (v',J')=(1,4) and (1,7) pumped near Lyα line center)

[g]Fluxes from observation obtained with $0\farcs5 \times 0\farcs5$ aperture

[g]Coadded flux in 0-4 P(2), 0-5 P(2), 0-4 P(3), and 2-5 R(11) lines

[h]Flux in 1-8 P(5) line

[i]Flux in 1-8 R(6) and 1-8 R(5) lines

[j]Flux in 0-4 P(2), 0-5 P(2), 0-4 P(3), and 2-8 R(11) lines

[k]Flux in 1-7 R(3), 1-7 P(5), 1-8 P(5), 1-7 R(6), and 1-8 R(6)

[l]Flux in 0-5 P(2), 2-5 R(11), and 2-8 R(11)

[m]Flux in 1-8 R(3), 1-8 P(5), and 1-8 R(6)

Table 14. Summary of stellar and H_2 emission line properties

Star	Class	A_V^a (mag)	i^a (°)	$\dot{M}_{acc}^a$ ($10^{-8} M_\odot$ yr^{-1})	Origin (D/W)[e]	v_{pump} range[b] (km s^{-1})	v_{H2}^c (km s^{-1})	v_{blue}^d (km s^{-1})	Extended? Y/N
TW Hya	CTTS	0.0	7	0.2	D	-801 to 913	0	N/A	No
DF Tau	CTTS	0.5	85	3,0.2	D,W	-297 to 1114	2.5	-35	No
RU Lupi	CTTS	0.07	23	3	W	-297 to 913	-12	-100	Yes
T Tau	CTTS	0.3	15	4	W	14 to 913	-12	-100	No
DG Tau	CTTS	1.6	90	3	W	-491 to 704	-27	N/A	Yes?
V836 Tau	WTTS[f]	0.6	?	0.1	D	-167 to 551	0	N/A	?
V410 Tau	WTTS	0.7	-	0	Possibly significant non-detection of H_2 emission				
V819 Tau	WTTS	1.5	-	0	Insignificant non-detection of H_2 emission				

[a] See Table 2 for references

[b] Range of velocities for pumping transitions, measured from Lyα line center.

[c] Velocity of narrow component of H_2 emission

[d] Maximum velocity of asymmetric blueshifted wing on H_2 emission profiles

[e] Disk (D) or Wind (W)

[f] Classified as WTTS, but is a weak accretor with a disk.